6. SITE 865[1]

Shipboard Scientific Party[2]

HOLE 865A

Date occupied: 27 March 1992

Date departed: 2 April 1992

Time on hole: 5 days 15 hr

Position: 18°26.410′N, 179°33.339′W

Bottom felt (rig floor, m; drill-pipe measurement): 1529.1

Distance between rig floor and sea level (m): 10.68

Water depth (drill-pipe measurement from sea level, m): 1518.4

Total depth (rig floor, m): 2400.0

Penetration (m): 870.9

Number of cores (including cores with no recovery): 94

Total length of cored section (m): 870.9

Total core recovered (m): 131.57

Core recovery (%): 15.1

Oldest sediment cored:
Depth (mbsf): 837.6
Nature: Clayey limestone
Age: late Albian
Measured velocity(km/s): 2.25–5.17

Hard rock:
Depth (mbsf): 870.9
Nature: Basalt
Measured velocity(km/s): 2.93–4.5

HOLE 865B

Date occupied: 2 April 1992

Date departed: 4 April 1992

Time on hole: 1 day 2 hr 15 min

Position: 18°26.415′N, 179°33.349′W

Bottom felt (rig floor, m; drill-pipe measurement): 1527.0

Distance between rig floor and sea level (m): 10.78

Water depth (drill-pipe measurement from sea level, m): 1516.2

Total depth (rig floor, m): 1692.5

Penetration (m): 165.5

Number of cores (including cores with no recovery): 19

Total length of cored section (m): 165.5

Total core recovered (m): 123.66

Core recovery (%): 74.7

Oldest sediment cored:
Depth (mbsf): 165.5
Nature: Wackestone
Age: late Albian
Measured velocity(km/s): Not measured

HOLE 865C

Date occupied: 4 April 1992

Date departed: 4 April 1992

Time on hole: 12 hr 45 min

Position: 18°26.425′N, 179°33.339′W

Bottom felt (rig floor, m; drill-pipe measurement): 1528.2

Distance between rig floor and sea level (m): 10.78

Water depth (drill-pipe measurement from sea level, m): 1517.4

Total depth (rig floor, m): 1664.5

Penetration (m): 136.3

Number of cores (including cores with no recovery): 15

Total length of cored section (m): 136.3

Total core recovered (m): 114.11

Core recovery (%): 83.7

Oldest sediment cored:
Depth (mbsf): 136.3
Nature: Foraminifer-nannofossil ooze
Age: Paleocene
Measured velocity(km/s): Not measured

Principal results: Site 865 (proposed Site All-A) is located on the summit of Allison Guyot in the western Mid-Pacific Mountains. The site was drilled for the following goals:

1. Determining the timing of inception of the reefal complex,
2. Documenting the history of subsidence and reef growth,
3. Developing a picture of the facies anatomy of the reef and adjacent lagoonal environments,
4. Identifying the timing and magnitude of relative sea-level fluctuations,
5. Constraining the timing and causes of the demise and drowning of the carbonate platform, including
6. Identifying and characterizing possible subaerial exposure events,
7. Developing a model of seismic stratification for comparison with other guyots, and
8. Examining the post-drowning sedimentary history of the guyot summit.

Although our pre-cruise plan had been to drill a single hole to a depth of about 500 meters below seafloor (mbsf), ending midway through the section of expected lagoonal facies limestones, excellent drilling conditions and scientific results spurred the drilling of three holes at Site 865, with the deepest penetrating to 870.9 mbsf. Hole 865A was the deep hole, drilled with the RCB. It was terminated in alternating limestone and basalt because the hole had already surpassed its goals and there were no clear indications that true volcanic basement was near. Hole 865A was drilled

[1] Sager, W.W., Winterer, E.L., Firth, J.V., et al., 1993. *Proc. ODP, Init. Repts.*, 143: College Station, TX (Ocean Drilling Program).
[2] Shipboard Scientific Party is as given in list of participants preceding the contents.

with the RCB rather than beginning with the APC/XCB bottom-hole assembly (BHA), following the usual ODP procedure used in pelagic sediments, because of fear that the APC might smash into a hard chert layer and be bent, thus terminating the hole. Instead, the first hole showed that the pelagic cap contained a unique, expanded, and intact Paleogene section that had no chert layers. Holes 865B and 865C were primarily APC holes designed to recover a duplicated set of relatively undisturbed cores through the Paleogene section for paleoceanographic study. Hole 865B also penetrated approximately 27 m into the top of the shallow-water limestones to obtain additional samples of the limestone/pelagic sediment interface.

Using combined microfossil and macrofossil biostratigraphies, visual core descriptions (augmented with smear-slide and thin-section data, physical properties data, and downhole logging data), four principal stratigraphic units were distinguished (see "Lithostratigraphy" section, this chapter). In stratigraphic order (from the bottom upward), these are as follows:

1. Unit IV (870.9–621.9 mbsf). Late Albian clayey organic wackestone-packstone with decreasing amounts of clay and organic matter upward. Limestone layers contain a varied biota of benthic foraminifers, ostracods, snails, bivalves, solitary corals, sponges, and dasycladacean and red algae. Mudstone beds are commonly extensively burrowed. Pyrite is common in dark-colored clay layers, and gypsum has been identified in several clay layers. Carbonaceous fragments of land plants are common, particularly near the bottom of the hole, and decrease in abundance upward. The lowest 30 m of the drilled section contains basalt that is thought to be one or more sills that intruded into the sediments, rather than volcanic basement. Good core recovery in the unit allowed us to recognize depositional shallowing-upward cycles, which were repeated on a scale of about 0.5 m. These cycles could be seen exceptionally well in the formation microscanner (FMS) logs, which could be matched satisfactorily with the cores themselves in many intervals.

2. Unit III (621.9–207.3 mbsf). Late Albian white limestones of several facies: peloidal mudstone, wackestone, packstone, and rare grainstone with molds of formerly aragonitic mollusks. High-spired gastropods, small bivalves, sponges, and large sponge spicules are common; benthic foraminifers are relatively abundant; and ostracods and dasycladacean algae are scattered. Rudists and corals occur in a few layers. Induration is variable, and the limestone ranges from chalky to hard. Dissolution has removed most molluscan shells. Episodic subaerial exposure is suggested by the occurrence of erosional surfaces, reddish stains, and brecciated well-indurated wackestones. The FMS logs show a continuation of the cyclic alternations seen in Unit IV.

3. Unit II (207.3–139.7 mbsf). Phosphatized, karstified limestone, riddled in the upper 40 m with internal cavities encrusted with phosphatic pelagic limestone and manganese oxyhydroxides. The cavities are partly filled with geopetal sediment that contains nannofossils and planktonic foraminifers of Late Cretaceous age. This unit is genetically like Unit III below it, except for the mineralization. The unit is silicified at the very top and shows concentrations of uranium in the downhole logs.

4. Unit I (139.7–0 mbsf). Middle Paleocene to Quaternary foraminiferal nannofossil ooze and foraminiferal sand. Approximately 90% of this section is of middle Paleocene to late Eocene age and probably formed as the guyot drifted beneath the equatorial high productivity zone. These sediments generally contain a large fraction of sand-sized foraminifers, which suggests winnowing by currents.

The pelagic sections of Site 865 holes had good recovery, averaging 61%, 90%, and 84% for Holes 865A, 865B, and 865C, respectively. Core recovery in the shallow-water limestones of Holes 865A and 865B was disappointing for some intervals, particularly in Units II and III, where values of 1% to 2% were typical (see "Lithostratigraphy" section, this chapter). In Unit IV of Hole 865A, recovery improved in basalts and clayey limestones and ranged from 7% to 100% in the deepest 200 m of the hole.

Despite the overall low core recovery, it was possible to reconstruct the lithologic sequence by comparing the cored material with a suite of geophysical, geochemical, and FMS logs (see "Downhole Measurements" section, this chapter). These logs, taken together with the measurements of sonic velocity and density in cored specimens, allowed for satisfactory correlation to be made between the reflectors seen in seismic profiles at the site and the observed sequence of strata drilled at the site.

Data from Site 865 are consistent with a classic Darwinian picture of carbonate atoll evolution from early formation to final drowning, although there is no direct evidence for a reef rim. The deepest recovered sediments (Subunit IVD) contain abundant oysters and evidence of intense burrowing, suggesting a restricted, shallow, lagoonal environment. Abundant plant remains imply a nearby shoreline and marshy conditions. The presence of pyrite with associated organic matter indicates bacterial sulfate reduction in anoxic sediments, but the water must have been oxygenated well enough for shallow infaunal activity. Early diagenetic dolomite occurs in some layers and may be caused by seasonally evaporative conditions. Basaltic dikes intruded the sediments, probably at shallow depths. This event may represent late-stage volcanics or a rejuvenation of volcanism.

Subunit IVC shows periods of more open-marine conditions. Land-derived organic matter wanes through this sequence and disappears at the top of this subunit. Dolomite is not found above Subunit IVB, and clay disappears by the top of Subunit IVA, implying that the shoreline gradually retreated. Episodic clay seams in these subunits suggest cyclic variations in water depth, either by autocyclic processes such as sedimentary-lobe switching or allocyclic mechanisms such as irregular subsidence of the seamount foundations, or eustatic sea-level fluctuations, or combinations of all these.

The facies of Unit III suggest a quiet-water lagoonal environment. The degree of faunal diversity is not high, but the occurrence of rudists and corals higher in the section indicates conditions evolving from more restricted (Subunit IIIB) to open marine (Subunit IIIA). Winnowed carbonate sands in this unit suggest sporadic storm activity, whereas scattered reddish stains attest to periods of subaerial exposure. Evidence for prolonged emergence occurs at the top of the shallow-water carbonates in Unit II. Although these limestones are genetically the same as those in Unit III, they display mineralization, dissolution, and infilling of cavities by fine, possibly aeolian sediments as well as by Late Cretaceous pelagic sediments. High gamma-ray log readings imply concentrations of uranium, either from aeolian deposits or from association with phosphorite. The high uranium values suggest that the thickness of the exposed layer is approximately 68 m. Shipboard biostratigraphic data suggest that the carbonate bank evolved and died quickly: the entire 731-m drilled section of shallow-water limestones appears to have been deposited within the last half of the Albian stage.

Following exposure near the end of the Albian, the carbonate bank drowned. The oldest pelagic fossils, in the cracks and cavities, are between mid-Turonian and late Coniacian age. Sometime during the 5 to 10 m.y. interval between emergence and installation of pelagic conditions over the guyot, the emergent bank subsided below sea level, but without re-establishment of reefs. Because the seamount was probably located in low southern latitudes during all this time (Winterer et al., in press; Sager et al., in press), unusual conditions are required; for example, a rapid and substantial rise in sea level, such as the rise postulated for Cenomanian/Turonian boundary time (Suess, 1906; Hancock and Kauffman, 1979; Schlanger, 1986).

During the remainder of the Cretaceous, after the bank drowned, the environment was mainly nondepositional, leaving only a thin veneer of sediments. It is not yet clear whether later Cretaceous sediments were simply not deposited, or whether they were removed by subaerial erosion.

During the Paleogene, the guyot rode the Pacific Plate northward across the equator. As it passed beneath the equatorial high-productivity zone, it acquired a substantial pelagic cap that consisted mainly of late Paleocene and early- to middle-Eocene-age nannofossil and foraminiferal oozes and sand. Currents swirling around the summit eroded some of the cap and produced winnowed foraminiferal sands. Neogene sedimentation was slow and produced only a thin frosting that appears to rest unconformably on top of the thick Paleogene pile.

Biostratigraphic studies of the pelagic cap show that the Paleogene section is relatively complete and spans nannofossil zones NP21 through NP4 and foraminiferal Zones P17 through P2 (early Oligocene to early

Paleocene). This section is rare, not only because it contains sediments from an epoch (the Paleocene) that is rarely cored in Pacific pelagic sediments, but also because the guyot was near the equator, and its summit was in depths of only about 1000 m. What is more, the section appears to contain the Paleocene/Eocene boundary, a transition of considerable interest to paleoceanographers studying the shift of climate from warm in the Cretaceous to cold in the late Tertiary.

As expected, organic geochemistry measurements showed that the percentage of $CaCO_3$ in the cored material from Site 865 is generally high, typically greater than 95%. A small percentage of lower values (as low as 27% $CaCO_3$) were found in clay-rich intervals in Unit IV. Despite the abundance of plant remains in the lowest sedimentary unit, total organic-carbon (TOC) values were typically very low to low (less than 0.5%). Moderate to high percentages (as much as 35.4%) were found in Unit IV in small, organic-rich beds. Analyses of inorganic compounds in interstitial waters showed values consistent with seawater throughout all holes at the site. This suggests that both the pelagic cap and the limestones have a high permeability and are essentially open to circulation of seawater. With the exception of samples from the very bottom of the hole, sulfate concentrations stay relatively constant and imply that sulfate reduction is not occurring quickly enough to deplete sulfate concentrations. A slight decrease in sulfate deep in Hole 865A suggests a small amount of reduction.

Physical properties show a discontinuity from the pelagic cap to limestone: porosities decrease from >60% to about 10 to 20% and bulk densities jump from 1.6 to 1.7 g/cm^3 to 2.3 to 2.7 g/cm3. Furthermore, seismic velocities increase sharply in the limestones with values >4 km/s from 140 to 400 mbsf and decrease to typically 2.0-3.5 km/s below 500 mbsf. Downhole physical logs give similar trends in bulk density, but show that the shipboard velocity readings are biased to the high side by the selective recovery of the harder layers. In the limestone between 140 and 350 mbsf, the sonic log displays large variations in velocity, from about 2.0 to 4.5 km/s, apparently from alternating hard and soft layers. Velocities below 350 mbsf are more consistent, but average from about 2.9 to 3.5 km/s, with short excursions to higher values. Overall, both the sonic log and physical properties measurements demonstrate that the velocities used to calculate depths to seismic reflectors during pre-cruise planning, based mainly on plateau carbonate sediments, are significantly too low.

Other logs yielded valuable information about the structure and composition of the shallow-water limestones. The gamma-ray log showed significantly higher counts in the upper 68 m of the shallow-water limestone. This is possibly a result of scavenging of uranium by phosphorite. Resistivity logs give numerous short-wavelength variations probably owing to thin beds. Finally, the FMS gave a unique view of the structure of the limestone section. In the bottom part of Hole 865A, it is possible to make a detailed correlation of beds in the cores and imaged beds in the borehole wall. Moreover, in many intervals, structures such as vugs are visible in the FMS recording. Clearly, low recovery in the cores has biased the limestone samples, but the FMS data will allow us to place these samples into perspective by comparing them with the borehole images.

BACKGROUND AND SCIENTIFIC OBJECTIVES

Site 865 (proposed Site All-A) is located at 18°26.41′N, 179°33.34′W, at a water depth of 1518.4 m atop Allison Guyot (Fig. 1) in the central Mid-Pacific Mountains (see "Introduction and Scientific Objectives" chapter, this volume). Allison is typical of Mid-Pacific Mountain guyots because it has a thick limestone cap with a seismic reflection signature that has been interpreted as a sequence of ponded lagoonal sediments enclosed by a perimeter reef. In addition, the limestones are surmounted by a thick cap of pelagic sediments which provide a post-drowning history.

Site-survey seismic profiles showed several prominent and many minor reflectors beneath the surface of the guyot (see "Site Geophysics" and "Seismic Stratigraphy" sections, this chapter). Strong reflections at two-way traveltimes of 0.168 and 0.627 s below the seafloor were thought to represent the top of shallow-water limestone and volcanic basement, respectively. Depth to these interfaces was estimated at 151 and 574 m using acoustic wave velocities of 1.8 and 2.5 km/s for pelagic sediments and limestones, respectively. Between these reflectors lies a series of lesser seismic horizons that may have resulted from sea-level oscillations, and beneath the "basement" reflector can be seen several additional weak returns that suggested layered volcanics, or interlayered sediments and volcanics.

The location of Site 865, between the center and south rim of the guyot, was chosen so that drilling would

1. Commence where the pelagic cap was thick enough to support the entire BHA;
2. Penetrate the oldest pelagic sediments post-dating the shallow-water limestone, to constrain the time of reefal drowning; and
3. Penetrate the oldest and deepest lagoonal sediments. Farther to the south, seismic cross sections show scattered acoustic energy, suggesting perimeter reef material, whereas to the north, a buried basement high can be seen in the center of the guyot (see "Site Geophysics" section, this chapter). Because of time constraints, pre-leg 143 plans included drilling a single hole only about 500 mbsf at Site 865; however once actual drilling had reached a few hundred meters below the seafloor, good hole conditions and fast rates of penetration enticed us to deepen the hole until basalt was encountered. A uniquely thick and relatively undissolved Paleogene pelagic sequence cored in Hole 865A further enticed us to drill two additional holes to core the pelagic cap with the APC and to obtain samples for paleoceanographic study of this important part of the stratigraphic column.

Drilling Objectives

Drilling at Site 865 had the following goals:

1. To develop a history of Cretaceous reef growth and evolution by determining the lithologic, biostratigraphic, isotopic, and seismic stratigraphic successions within the limestone cap, for use in:
   a. Direct correlation with other guyots drilled during Legs 143 and 144;
   b. Correlations through reflection seismology among guyots in the northwestern Pacific;
   c. Comparisons of the timing and magnitude of relative sea-level changes recorded in the guyot limestones with sea-level curves developed elsewhere in the world;
2. To provide constraints on the timing and cause(s) of reef platform drowning;
3. To examine the timing and extent of the karst event(s) evident in the morphology and in seismic-reflection profiles of Allison and other western Pacific guyots;
4. To compare the shallow-water reef biotic assemblages with others of similar age elsewhere as a clue to migration patterns;
5. To gather pore-water samples from the pelagic cap and lagoonal sediments, to infer residence times and chemical evolution of interstitial waters; and
6. To examine pelagic sediments, deposited above the CCD atop the guyot, for Late Cretaceous and Paleogene stable isotope and biostratigraphic data, as well as additional constraints on the timing of platform drowning.

Objectives Accomplished

As detailed in the relevant sections of this site report, preliminary shipboard study of the samples and downhole logs collected at the site suggests that the main objectives can be met through further post-cruise study of the data and samples. Core recovery was relatively low, but study of downhole logs suggests that the recovered material is fairly representative of the rocks penetrated.

The first objective was addressed by detailed shipboard examination of the textures, structures, compositions, and fossil content of

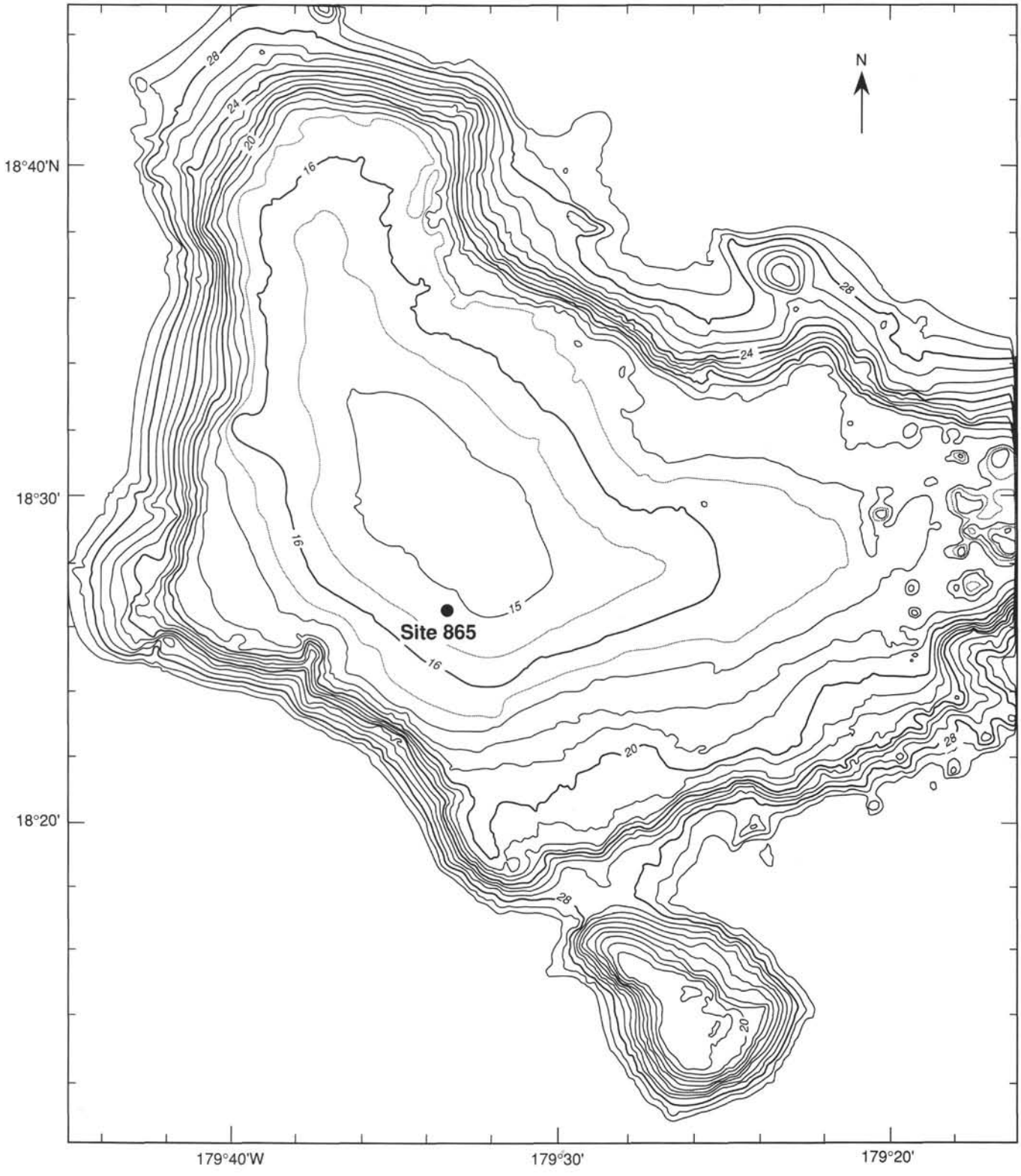

Figure 1. Bathymetry of Allison Guyot summit. Values are shown in hundreds of meters. Bathymetric contours at 100 m intervals above 3000 m are shown; heavy contours at 400-m intervals. Supplementary 50-m contours on the guyot summit are shown in gray. Bathymetric data were obtained with the SeaBeam multibeam echo-sounder in 1988 during Leg 10 of the Roundabout Expedition of the *Thomas Washington* of Scripps Institution of Oceanography.

cored limestones. Shipboard age data from macrofossil and microfossil studies are preliminary, but place strong constraints on the age of the limestones. Additional age constraints should become available through post-cruise strontium-isotope measurements from samples collected. Downhole logs were an invaluable aid when reconstructing the limestone stratigraphy, because they provided a continuous record of physical and chemical properties to be used as a framework into which the recovered samples could be fitted.

Objectives 2 and 3 were pursued by studying the sediments and fossils that bracketed the contact between pelagic cap and shallow-water limestone. Detailed structural and chemical analyses of the highest shallow-water limestones were used to infer the extent of karst and the processes that led to the demise of the carbonate platform. Once again, downhole geochemical logs were an important tool because they provided a record of mineralization in the reef top limestones. Paleontological studies and strontium-isotope measurements will yield age constraints.

Objective 4 has been and will be addressed by studying the species of fossils recovered in the cores and comparing them with the known distribution of Cretaceous reef biota.

Objective 5 was accomplished by analyzing interstitial waters squeezed from whole-round samples taken from the pelagic cap sections of Holes 865A and 865B. Two additional water samples were obtained using the water sampler temperature probe (WSTP) in Hole 865B.

Two additional holes, 865B and 865C, were added to the proposed drilling program primarily to double-APC the pelagic cap in pursuit of objective 6. Detailed biostratigraphic, magnetic, and stable isotope studies are being conducted with these cores to construct a high-resolution record of the Paleogene sediments.

OPERATIONS

Transit from Honolulu to Site 865

The last mooring line in Honolulu was pulled aboard the ship at 0100 hr UTC, 23 March 1992, and we headed west toward Site 865, streaming a magnetometer and making soundings with the 12- and 3.5-kHz echo sounders. About halfway to the site, reflection profiling began, to obtain seismic records across previously unprofiled guyots near the ship's track. Speeds between 10 and 11.5 kt were maintained en route.

Approach to Site 865

At a position about 12 nmi (22 km) east of Site 865, near the eastern end of Allison Guyot, the ship slowed to about 6 kt to obtain better seismic reflection records, and a course was steered to bring the ship across the proposed site (Fig. 2). We deployed an expendable sonobuoy while steaming on this line to obtain wide-angle reflection and refraction data and to estimate the acoustic velocity structure of the guyot summit. Unfortunately, recording problems prevented the collection of useful seismic refraction data.

Immediately after crossing the proposed site, the ship turned south for about 4 nmi (7.4 km) to the edge of the flat-topped surface of the guyot, then steamed west to turn onto seismic-reflection and 3.5-Khz lines previously made by the *Thomas Washington* during a site survey in 1988 (see "Site Geophysics" section, this chapter). The *Resolution* followed this line back to the proposed site, and an acoustic beacon was dropped at 1921 hr UTC, 27 March, at a position judged to be within a few hundred meters of the proposed site location.

Coring of Hole 865A

An RCB was used in this hole, and the BHA included a monel-metal drill collar to allow for magnetic core orientation. After lowering the BHA and drill string near the seafloor estimated from the PDR record as 1526.4 m below the dual elevator stool (DES) or 1515.7 mbsl, the bit was slowly lowered until the needle on the driller's weight dial indicated contact with the bottom, at 1531 mbrf.

Pelagic Sediments

Core 143-865A-1R was punched, with no pipe rotation and very slow water circulation, from 1529.1 to 1534.8 mbrf where we recovered soupy foraminiferal ooze of Quaternary age. The seafloor depth was accepted as 1529.1 mbrf, or 1518.4 mbsl. Coring continued in the same mode with no difficulty through Oligocene and Eocene ooze, to a depth of 1610.9 m (81.8 mbsf), with average recovery rates of about 46%. Owing to a plugged bit in the interval from 1610.9 to 1639.9 m (81.8-110.8 mbsf) recovery was only about 1%, in the same type of ooze as above. The plug was cleared with an "unplugger" tool, and recovery was good down to 1668.8 m (139.7 mbsf), in Paleocene ooze.

Shallow-water Limestone

From the core catcher of Core 143-865A-16R, a chunk of very hard, manganese-stained, phosphatic limestone was recovered. This marks the top of the shallow-water Cretaceous limestone beneath the pelagic sediments. In the limestone, in spite of repeated efforts to improve recovery by changing the style of coring (rate of pipe rotation, water-circulation rates, etc.), recovery rates decreased to an average of only about 2%, with a few cores recovering as much as 15%.

Moderately hard, shelly limestone was recovered as chunks, typically 1 to 4 cm wide. Virtually no shells are preserved; rather, only molds remain to mark their former presence. Taken together with evidence of internal veinlets of calcite cutting across some pieces, we suppose that as the button inserts on the coring bit cones hammer the irregular honeycomb structure of the limestone during coring, the limestone breaks up into crumbs and chunks, rather than being smoothly cut as a continuous cylindrical core. The larger chunks may then block the bottom of the core barrel so as to prevent new core from entering. Alternatively, harder limestone may constitute only scattered layers, with the bulk of the sediments consisting of limestone too weakly cemented to core using the coring tools available. Recovery was best in intervals having the least moldic porosity.

At a depth of about 625 mbsf, in Core 143-865A-68R, faint greenish tints in the limestone mark the highest occurrence of clayey limestone, and from this level downward clay content increases, but clayey limestone intervals alternate with nearly clay-free limestone. Rates of core recovery gradually improved in the more clayey strata, and averaged about 5% between 622 and 786 mbsf (Cores 143-865A-68R to -84R). As clayey limestone increased in proportion in the cores, the rate of penetration of the core bit slowed (Fig. 3).

From about 786 to 841 mbsf, in Cores 143-865A-85R to -90R, clayey and silty burrowed and shelly limestone is the dominant lithology, and core recovery averaged about 53%, while penetration rates continued to decrease.

Basalt was cored in the bottom 4 to 5 m of Core 143-865A-90R, but because of pervasive alteration, it cored at the same rate as the clayey limestone immediately above or below. From here to the total depth of 870.9 mbsf, vesicular, amygdaloidal basalt alternated with greenish clayey limestone and reddish, hydrothermally altered and veined greenish and red-brown claystone, siltstone, and volcanic sandstone. Recovery averaged about 63%, but coring rates slowed still further (Fig. 3).

The sonic core monitor (SCM) device and the "tensor" core orientation tool were tried first in Core 143-865A-91R, along with the core scribing tool, but with no success. The batteries on the SCM malfunctioned, so the scribed pieces could not be monitored as they entered the barrel. The tensor tool vibrated so much in the barrel that consistent azimuth readings could not be obtained. The same tools were tried again in Core 143-865A-94R.

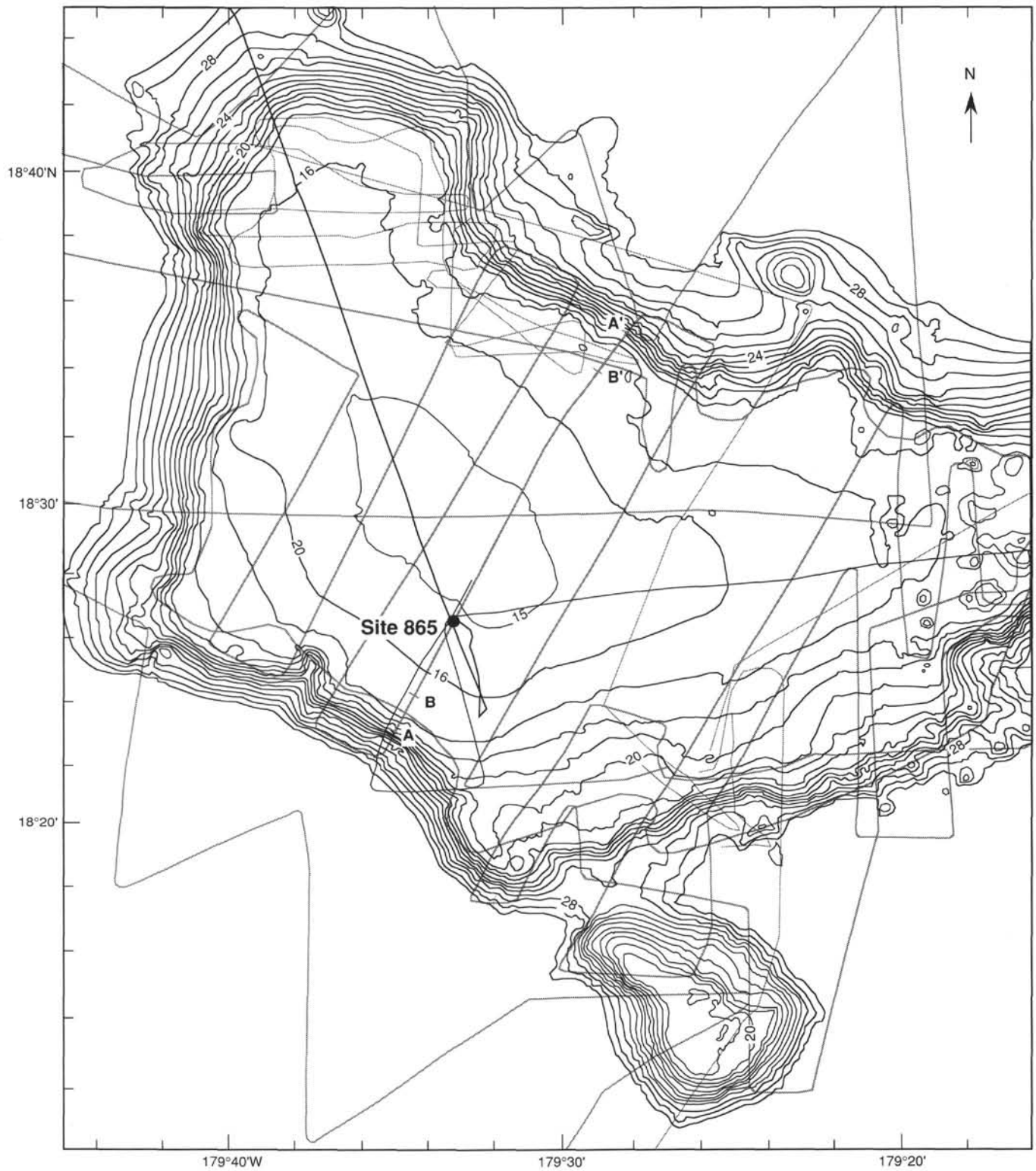

Figure 2. Bathymetry of Allison Guyot and ship's geophysical track lines. Contours are shown at 100-m intervals (labeled in hundred of meters) with a heavy contour every 400 m. Most contours have been derived from an extensive SeaBeam multibeam echosounder survey. Grayed lines represent ship's tracks of the Roundabout Leg 10 site-survey cruise. The dark ship's track is the path of the *JOIDES Resolution* on approach and exit from Site 865. A-A′ mark the ends of the seismic-reflection profile shown in Figure 4. B-B′ mark the ends of the 3.5-kHz profile shown in the "Seismic Stratigraphy" section (this chapter, Fig. 56).

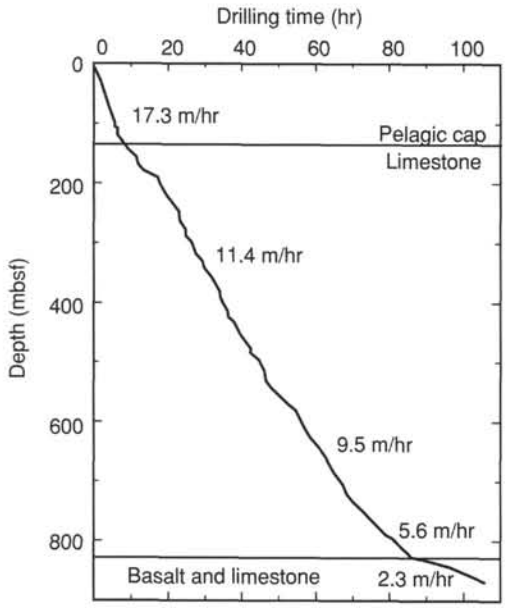

Figure 3. Plot of penetration vs. time, Hole 865A. Penetration rates for linear sections of the curve are indicated.

Coring was halted at a total depth (TD) of 870.9 mbsf because we had exceeded the allotted time for the site, and because there seemed little certainty, either from the evidence of the cores or from the seismic-reflection profile, that the solid volcanic basement, underlying all sediments, was close beneath the level attained.

Hole 865A Logging

Logging operations in Hole 865A (Table 1) began at 1400 hr UTC, 1 April 1992, with a mud sweep, wiper trip, and release of the bit. At 0000 UTC, 2 April, the drill pipe was pulled up to a depth of 102.5 mbsf for logging.

The heave compensator was used during all runs, and it was turned on and off at 149 mbsf. The first run was with the geophysical tool string (spectral gamma ray, neutron porosity, lithodensity, sonic, resistivity, and Lamont temperature tools). The sonic tool did not work and was changed out. The second sonic tool also did not work and was removed from the tool string before proceeding downhole. Down-going logs were recorded with the gamma ray and resistivity tools from 102.5 to 848.5 mbsf. The Schlumberger computer malfunctioned while the tool string was at 426 mbsf and was not repaired until 494 mbsf. Data thus were not recorded between these depths. The tool string malfunctioned again at the bottom of the hole and had to be pulled back to the surface for inspection. The problem was diagnosed as a leak in both the cable head and the cable. Both were re-wired before the next Schlumberger tool string run.

The second logging run was with the Japanese magnetometer. The tool was rigged up with the Gearhart-Owen cable head and lowered to 500 mbsf. Data were recorded onto an internal computer from 500 to 867 mbsf on both the down-going and up-going runs as the tool was being run at a speed of 1000 m/hr.

A modified geophysical tool string was run next that had the gamma-ray, sonic, neutron porosity, and lithodensity tools, but no resistivity tool. The tool string was run from 861.3 to 102.5 mbsf.

The fourth logging run was made with the geochemical tool string (spectral gamma-ray, aluminum clay, and geochemical tools). On the first pass, data were recorded from 853.0 to 102.5 mbsf. The second pass recorded data from 241 to 102.5 in open hole, and from 102.5 to 64.6 mbsf in drill pipe.

Table 1. Well logs recorded from Hole 865A.[a]

Log type	Depth (mbsf)
Resistivity	102.5–848.5
Bulk density	102.5–861.3
Neutron porosity	102.5–859.3
Sonic velocity	102.5–848.5
[b]Gamma-ray/U-Th-K	64.6–838.5
[b]Aluminum	64.6–850.2
[b]Geochemistry	64.6–853.0
Caliper	102.5–858.5
Formation microscanner	102.5–846.1
Lamont temperature	102.5–869.5

[a] Assumes seafloor at 1529.1 m and with all logs correlated and depths shifted to the gamma-ray log from the resistivity tool string.
[b] These logs were recorded in pipe from 102.5 to 64.6 mbsf.

The FMS tool string (gamma-ray, GPIT, and FMS tools) was rigged up and lowered to total depth. Data were recorded with only one pass of the tool string from 847.0 to 102.5 mbsf. This last tool string was run up to the rig floor and rigged down at 0900 UTC on April 3, 1992, which ended logging operations at Hole 865A. The entire logging operation, including conditioning the hole, took 43.5 hr.

Coring of Hole 865B

After pulling out of Hole 865A, the ship was moved about 20 m north and Hole 865B was spudded, using the APC/XCB BHA. Fourteen APC cores were taken to a depth of 132.0 mbsf (Table 2). A water/temperature sample probe (WSTP) was attempted at 122.5 mbsf but failed. A successful WSTP sample was taken at 132.0 mbsf.

From 132.0 mbsf, we elected to use the XCB corer, fearing to smash the APC against the hard limestone near 138 mbsf. At the top of Core 143-865A-16X, we struck very hard limestone, and continued to core in limestone to the TD of 165.5 mbsf.

Because the Eocene–Paleocene pelagic sediments were thick, well preserved, and from a rarely preserved time interval, we moved the ship over slightly again to core Hole 865C. Our aim was to provide a set of intact cores of Paleogene age for sampling by the large community of paleoceanographers and to fill in the coring gaps in Hole 865B.

Coring of Hole 865C

After raising the BHA above the seafloor and moving the ship, a set of 15 APC cores was taken, to a depth of 136.3 mbsf, and after splitting the cores and making nondestructive measurements of physical properties, descriptions of the lithology, and passing the core halves through the magnetometer, the cores were stored for future sampling. The drill string was pulled out of the hole, and the ship departed for Site 866 at 0115 UTC, 5 April, 1992. Reflection-profile and wide-angle refraction surveys using an expendable sonobuoy were conducted while steaming away from the site.

SITE GEOPHYSICS

Few geophysical data were available from Allison Guyot before the 1988 Roundabout Leg 10 site-survey cruise. A single seismic-reflection profile across the guyot was published by Heezen et al. (1973; their "Navoceano" Guyot), who noted that it showed a thick sequence of ponded sediments contained within a summit depression and surmounted by a thick pelagic cap. Work on dredged (Hamilton, 1956) and drilled (Winterer, Ewing, et al., 1973) samples from other Mid-Pacific Mountain seamounts indicated that the depressions were drowned atoll lagoons surrounded by perimeter reef rock (Winterer and Metzler, 1984).

Table 2. Coring summary for Holes 865A, 865B, and 865C.

Core no.	Date (1992)	Time (UTC)	Depth (mbsf)	Length cored (m)	Length recovered (m)	Recovery (%)
Hole 865A						
1R	28 March	0400	0.0–5.7	5.7	5.69	99.8
2R	28 March	0435	5.7–14.7	9.0	5.55	61.6
3R	28 March	0520	14.7–24.2	9.5	2.03	21.3
4R	28 March	0550	24.2–33.7	9.5	4.21	44.3
5R	28 March	0620	33.7–43.2	9.5	5.94	62.5
6R	28 March	0650	43.2–52.7	9.5	3.15	33.1
7R	28 March	0720	52.7–62.3	9.6	5.07	52.8
8R	28 March	0750	62.3–71.8	9.5	2.63	27.7
9R	28 March	0820	71.8–81.8	10.0	3.64	36.4
10R	28 March	0845	81.8–91.5	9.7	0.23	2.4
11R	28 March	0915	91.5–101.2	9.7	0.01	0.1
12R	28 March	1015	101.2–110.8	9.6	0.17	1.8
13R	28 March	1040	110.8–120.5	9.7	9.60	98.9
14R	28 March	1125	120.5–130.1	9.6	7.48	77.9
15R	28 March	1155	130.1–135.1	5.0	9.62	192.0
16R	28 March	1240	135.1–139.7	4.6	7.24	157.0
17R	28 March	1335	139.7–144.7	5.0	0.08	1.6
18R	28 March	1430	144.7–149.4	4.7	0.18	3.8
19R	28 March	1520	149.4–159.1	9.7	0.13	1.3
20R	28 March	1600	159.1–168.8	9.7	0.01	0.1
21R	28 March	1700	168.8–178.4	9.6	0.02	0.2
22R	28 March	2100	178.4–188.0	9.6	0.13	1.4
23R	28 March	2200	188.0–197.7	9.7	0.25	2.6
24R	28 March	2245	197.7–207.3	9.6	0.07	0.7
25R	28 March	2345	207.3–217.0	9.7	0.08	0.8
26R	29 March	0030	217.0–226.6	9.6	0.01	0.1
27R	29 March	0130	226.6–236.3	9.7	0.03	0.3
28R	29 March	0230	236.3–245.9	9.6	1.44	15.0
29R	29 March	0300	245.9–255.6	9.7	0.04	0.4
30R	29 March	0340	255.6–265.2	9.6	0.08	0.8
31R	29 March	0430	265.2–274.9	9.7	0.15	1.5
32R	29 March	0500	274.9–284.6	9.7	0.08	0.8
33R	29 March	0545	284.6–294.2	9.6	0.10	1.0
34R	29 March	0650	294.2–303.5	9.3	0.96	10.3
35R	29 March	0720	303.5–313.1	9.6	0.12	1.3
36R	29 March	0820	313.1–322.8	9.7	0.25	2.6
37R	29 March	0925	322.8–332.4	9.6	0.13	1.4
38R	29 March	1005	332.4–341.9	9.5	0.11	1.2
39R	29 March	1115	341.9–351.6	9.7	0.36	3.7
40R	29 March	1200	351.6–361.2	9.6	0.25	2.6
41R	29 March	1310	361.2–370.8	9.6	0.14	1.5
42R	29 March	1350	370.8–380.5	9.7	0.12	1.2
43R	29 March	1430	380.5–390.1	9.6	0.04	0.4
44R	29 March	1520	390.1–399.9	9.8	0.08	0.8
45R	29 March	1600	399.9–409.6	9.7	0.10	1.0
46R	29 March	1645	409.6–419.2	9.6	0.06	0.6
47R	29 March	1730	419.2–428.9	9.7	0.05	0.5
48R	29 March	1815	428.9–438.3	9.4	0.05	0.5
49R	29 March	1900	438.3–448.0	9.7	0.00	0.0
50R	29 March	2000	448.0–457.6	9.6	0.11	1.1
51R	29 March	2100	457.6–467.3	9.7	0.10	1.0
52R	29 March	2200	467.3–477.0	9.7	0.09	0.9
53R	29 March	2315	477.0–486.6	9.6	0.04	0.4
54R	30 March	0015	486.6–496.3	9.7	0.03	0.3
55R	30 March	0115	496.3–505.9	9.6	0.06	0.6
56R	30 March	0215	505.9–515.5	9.6	0.30	3.1
57R	30 March	0245	515.5–525.2	9.7	0.10	1.0
58R	30 March	0330	525.2–534.8	9.6	0.17	1.8
59R	30 March	0415	534.8–544.5	9.7	0.08	0.8
60R	30 March	0550	544.5–554.2	9.7	0.12	1.2
61R	30 March	0720	554.2–563.9	9.7	0.05	0.5
62R	30 March	0940	563.9–573.6	9.7	0.00	0.0
63R	30 March	1035	573.6–583.1	9.5	0.00	0.0
64R	30 March	1150	583.1–592.8	9.7	0.10	1.0
65R	30 March	1240	592.8–602.5	9.7	0.04	0.4
66R	30 March	1330	602.5–612.2	9.7	0.35	3.6
67R	30 March	1415	612.2–621.9	9.7	0.05	0.5
68R	30 March	1515	621.9–631.5	9.6	0.32	3.3
69R	30 March	1645	631.5–641.0	9.5	0.06	0.6
70R	30 March	1800	641.0–650.8	9.8	0.03	0.3
71R	30 March	1900	650.8–660.4	9.6	0.12	1.3
72R	30 March	1945	660.4–670.1	9.7	0.25	2.6
73R	30 March	2045	670.1–679.7	9.6	0.67	7.0
74R	30 March	2145	679.7–689.4	9.7	0.85	8.8
75R	30 March	2245	689.4–699.1	9.7	0.82	8.5
76R	30 March	2345	699.1–708.7	9.6	0.75	7.8
77R	31 March	0040	708.7–718.3	9.6	0.08	0.8
78R	31 March	0145	718.3–728.1	9.8	0.75	7.7
79R	31 March	0300	728.1–737.7	9.6	0.40	4.2
80R	31 March	0445	737.7–747.4	9.7	0.32	3.3
81R	31 March	0600	747.4–757.1	9.7	1.30	13.4
82R	31 March	0745	757.1–766.8	9.7	1.12	11.5
83R	31 March	0910	766.8–776.5	9.7	0.16	1.7
84R	31 March	1030	776.5–786.2	9.7	0.69	7.1
85R	31 March	1225	786.2–795.8	9.4	1.95	20.7
86R	31 March	1420	795.8–805.4	9.6	3.53	36.8
87R	31 March	1600	805.4–815.1	9.7	2.32	23.9
88R	31 March	1745	815.1–824.8	9.7	2.44	25.1
89R	31 March	2100	824.8–831.8	7.0	7.30	104.0
90R	01 April	0030	831.8–841.1	9.3	6.81	73.2
91R	01 April	0505	841.1–847.2	6.1	6.20	101.0
92R	01 April	0730	847.2–853.4	6.2	4.88	78.7
93R	01 April	1020	853.4–863.1	9.7	2.73	28.1
94R	01 April	1350	863.1–870.9	7.8	4.97	63.7
Coring totals				870.9	131.57	15.1
Hole 865B						
1H	03 April	1800	0.0–8.5	8.5	8.51	100.0
2H	03 April	1915	8.5–18.0	9.5	8.43	88.7
3H	03 April	2000	18.0–27.5	9.5	9.89	104.0
4H	03 April	2030	27.5–37.0	9.5	8.15	85.8
5H	03 April	2105	37.0–46.5	9.5	7.80	82.1
6H	03 April	2150	46.5–56.0	9.5	9.07	95.5
7H	04 April	0000	56.0–65.5	9.5	8.27	87.0
8H	04 April	0035	65.5–75.0	9.5	8.81	92.7
9H	04 April	0110	75.0–84.5	9.5	8.84	93.0
10H	04 April	0200	84.5–94.0	9.5	7.35	77.3
11H	04 April	0230	94.0–103.5	9.5	8.58	90.3
12H	04 April	0300	103.5–113.0	9.5	8.65	91.0
13H	04 April	0330	113.0–122.5	9.5	8.61	90.6
14H	04 April	0510	122.5–132.0	9.5	8.02	84.4
15X	04 April	0740	132.0–141.5	9.5	3.87	40.7
16X	04 April	0830	141.5–141.7	0.2	0.18	90.0
17X	04 April	0925	141.7–146.2	4.5	0.41	19.1
18X	04 April	1015	146.2–155.8	9.6	0.03	10.3
19X	04 April	1110	155.8–165.5	9.7	0.19	12.0
Coring totals				165.5	123.66	74.7
Hole 865C						
1H	04 April	1320	0.0–3.3	3.3	3.32	100.0
2H	04 April	1345	3.3–12.8	9.5	8.22	86.5
3H	04 April	1405	12.8–22.3	9.5	8.38	88.2
4H	04 April	1430	22.3–31.8	9.5	8.50	89.5
5H	04 April	1510	31.8–41.3	9.5	8.88	93.5
6H	04 April	1545	41.3–50.8	9.5	3.25	34.2
7H	04 April	1615	50.8–60.3	9.5	8.70	91.6
8H	04 April	1700	60.3–69.8	9.5	8.66	91.1
9H	04 April	1735	69.8–79.3	9.5	9.07	95.5
10H	04 April	1800	79.3–88.8	9.5	8.10	85.2
11H	04 April	1945	88.8–98.3	9.5	8.52	89.7
12H	04 April	2015	98.3–107.8	9.5	8.51	89.6
13H	04 April	2050	107.8–117.3	9.5	8.84	93.0
14H	04 April	2120	117.3–126.8	9.5	4.43	46.6
15H	04 April	2145	126.8–136.3	9.5	8.73	91.9
Coring totals				136.3	114.11	83.7

Site Survey, Roundabout Leg 10

For nearly five days in 1988, 1900 UTC, 4 December, to 1100 UTC, 9 December, Allison Guyot was extensively surveyed and dredged during Leg 10 of the Roundabout Expedition aboard the Scripps Institution of Oceanography research vessel *Thomas Washington.* Geophysical data collected were SeaBeam multibeam echo-sounder bathymetry, gravity, and magnetic measurements; 3.5-kHz echo-sounder profiles, and seismic-reflection profiles having an 80-in.3 water-gun source. The survey followed the perimeter reef rim with the SeaBeam swath bathymetry, criss-crossed the summit to obtain seismic records of the pelagic and limestone cap, and dredged on several sides of the summit to obtain both volcanic and reef rock (Fig. 2).

SeaBeam bathymetry shows that Allison has a broad, domal summit about 12 × 20 nmi (24 × 37 km) that rises to a depth of about 1500 m (unless specified otherwise, depths given in this section are

in uncorrected meters). The dome is the surface of the thick pile of pelagic sediments. At depths of 1800 to 2000 m, the summit gives way to guyot flank slopes, which have angles of about 20° to 40° and continue to depths slightly in excess of 3600 and 4650 m on the north and south sides, respectively. The depth difference is the result of a plateau-like construct, about 1 km in height, that underlies many Mid-Pacific Mountain seamounts (e.g., Nemoto and Kroenke, 1985).

The overall shape of the volcanic edifice beneath the limestone cap is similar to a four-legged asymmetric starfish, with large arms to the north and east, and stubby arms to the south and southwest. These "arms" are probably volcanic rift zones where constructional volcanism was greatest (Vogt and Smoot, 1984). The rift arm to the south is surmounted by a small satellite guyot having a summit 2 × 5 nmi (3.7 × 9.3 km) in area. Furthermore, the eastern rift is especially prominent and extends as a "panhandle" over 15 nmi (28 km) from the main edifice.

The guyot morphology displays several features that are cogent to the evolution of the reef cap. A series of elongate mounds or ridges at the edge of the guyot summit thought to be a perimeter reef, extends around much of the summit perimeter. These mounds are generally about 20 to 40 m high and about 0.5 km wide. A channel, more than 100 m deep, has developed just behind the perimeter mound on the north side. Its shape suggests that it was caused by both erosion and dissolution: it appears to be an erosional channel having sinkhole-type depressions and implies that the guyot was subjected to subaerial exposure and karstification (van Waasbergen and Winterer, in press). Seaward of the perimeter mound, and best developed also on the north side, is a terrace at a depth of about 1740 to 1800 m. This terrace suggests a sea-level lowstand and may represent either a wavecut bench or a lowstand fringing reef (van Waasbergen and Winterer, in press). The southeastern side has a scarp between 2100 and 2200 m, where there is no apparent perimeter mound and lagoonal seismic reflectors outcrop. This morphology indicates that a mass-wasting event removed a section of the perimeter reef, to expose the lagoonal facies limestones (van Waasbergen and Winterer, in press). Finally, numerous volcanic cones occur on the summit at about 179°15′W, where the panhandle connects to the main body of the guyot. The ages of these cones are uncertain, but they may represent a late stage or rejuvenation of volcanism on the guyot.

Seismic profiles over Allison Guyot show layered reflectors in the interior that fade into incoherent acoustic returns at the edges (Fig. 4). This has been interpreted as ponded, layered lagoonal facies limestones surrounded by reef facies limestones (Fig. 5). Atop the center of the edifice is a lens-shaped pelagic cap. Two seismic reflectors are prominent beneath the guyot summit seafloor. One is the interface between the pelagic cap and shallow-water limestone, and the other was thought to be volcanic basement (see "Seismic Stratigraphy" section, this chapter). Although this reflector appears to have been caused by basalt, the basalt is probably not true "basement."

The pelagic cap has a maximum thickness of just over 0.2 s of two-way traveltime (twtt) and is nearly transparent at low frequencies (Fig. 4). At 3.5 kHz, this cap exhibits stratification that correlates well with cored sediment layers of different ages (see "Seismic Stratigraphy" section, this chapter). Where it is free of pelagic covering, the reflector marking the top of shallow-water limestone occurs at about 2.24 s twtt. The basalt reflector occurs at about 2.71 s twtt in the deepest part of the lagoon, but arches upward in the center of the volcano by about 0.1 s twtt. This arch may represent a buried volcanic erosional remnant. Between the top of the limestone and basalt horizons are numerous minor seismic reflectors that are probably small unconformities or exposure surfaces caused by minor fluctuations in sea level during the growth of the carbonate cap (Schlanger, 1963; Grow et al., 1986; Lincoln and Schlanger, 1990; van Waasbergen and Winterer, in press). In addition, faint, coherent seismic returns suggest layers beneath the basalt reflection. The origin of these deeper reflectors is unclear, but they may be either interlayered volcanics and limestones or an earlier, buried lagoon sequence.

The magnetic anomaly of Allison Guyot is more complex than would be expected for a relatively homogeneously magnetized body (Sager, unpubl. data). Though the anomaly is mostly positive over the main body of the guyot, there are numerous relative highs and lows. The total peak-to-peak anomaly amplitude is about 600 nT, which is relatively low for a Cretaceous seamount (Sager, 1992; Sager et al., in press). We attempted inversion of the magnetic anomaly (Parker et al., 1987) to derive a mean magnetization direction and paleomagnetic pole, but the procedure gave an unrealistically large declination that implied the results were unreliable. Evidently, the magnetization of the guyot is too heterogeneous to yield tight constraints on the magnetization direction. Although the anomaly complexity might result from the occurrence of grossly heterogeneous rocks within the guyot, a more plausible explanation is that the seamount erupted during more than one geomagnetic polarity period.

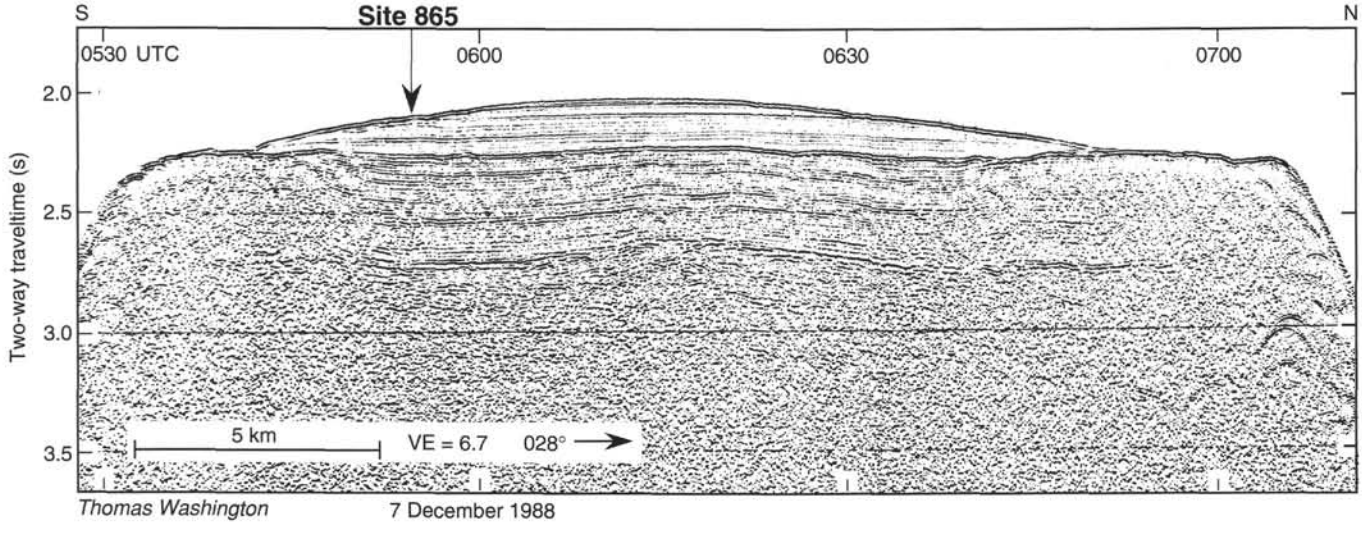

Figure 4. Single-channel seismic profile over the summit of Allison Guyot. This line was obtained from the Scripps Institution of Oceanography *Thomas Washington* during the Roundabout Leg 10 site-survey cruise. It was used to select Site All-A (later Site 865). The ship's speed while the line was recorded was 8.2 kt. An 80-in.^{3} water-gun seismic source was used. See Figure 3 for track location.

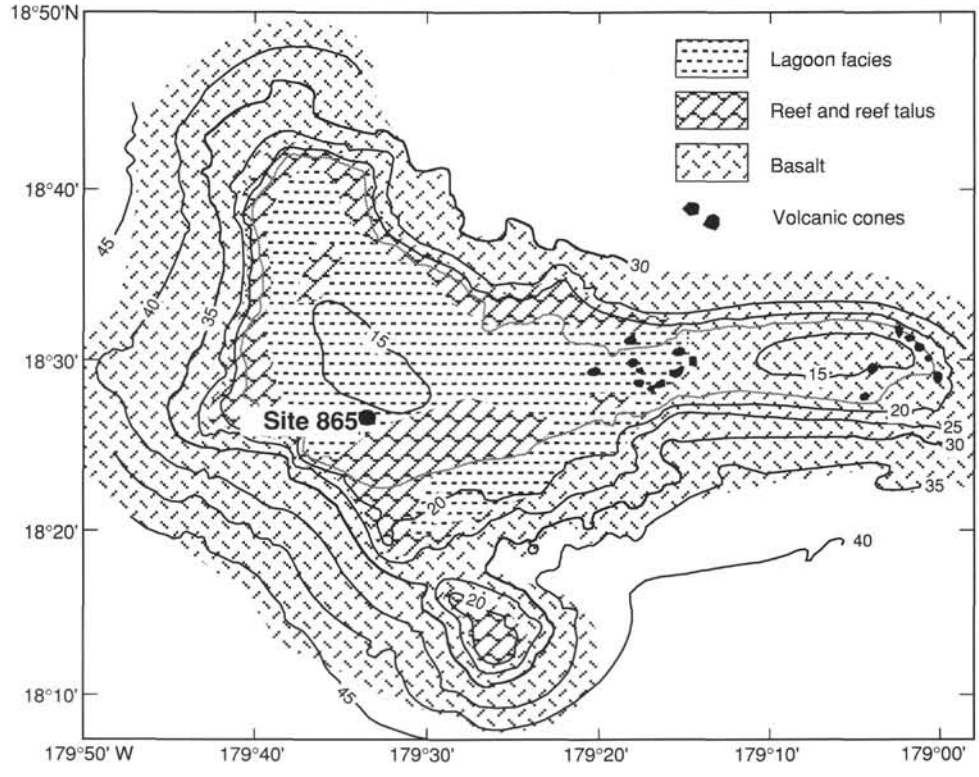

Figure 5. Sketch map of pre-drowning bedrock geology of Allison Guyot summit. Bathymetric contours are shown in hundreds of meters. Map was derived from seismic-reflection characteristics of the interface at the bottom of the pelagic cap. The database of seismic-reflection profiles was collected primarily during the Roundabout Leg 10 site-survey cruise.

Dates have been determined for rocks dredged from Allison Guyot: stratigraphic dates for carbonate fossils and 40Ar–^{39}Ar dates for basalt samples. Reef fossils were dated as Barremian to Aptian and late Albian and have been overlain by pelagic microfossils of Late Cretaceous age (van Waasbergen and Winterer, in press). Radiometric ages fell into two groups: two gave ages of 101.2 Ma and two others yielded 83.4 and 85.6 Ma (Winterer et al., in press).

Site Survey, Leg 143

The *JOIDES Resolution* approached Allison Guyot from the east, traversing the panhandle toward proposed Site All-A (Site 865). A magnetometer, seismic streamer, 80-in.^{3} water-gun, and 3.5-kHz echo-sounder were used to collect geophysical data. At a distance of 12 nmi (22 km) from the site, the ship was slowed to 6 kt to obtain higher quality seismic records. Soon after slowing, an expendable sonobuoy was dropped so that a seismic refraction line could be run en route to the site.

The ship continued to the proposed site and turned to the south (Figs. 2 and 6). Upon reaching the edge of the summit, the ship turned west and then north-northeast (course 028°) to follow the Roundabout Leg 10 line along which the site had been proposed. The 3.5-kHz echo-sounder was monitored until the depth, topography, and seismic character matched those of the site location on the site-survey line, when a beacon was dropped.

The seismic line recorded during the approach survey shows a character similar to that seen on the site-survey line (Fig. 7). Up to about 0.2 s twtt of relatively transparent pelagic cap appear at the top of the guyot. By contrast, this record differs from the site-survey line in that it shows a thicker section (0.8 s twtt) between the pelagic sediment/shallow-water limestone interface and the basalt reflector

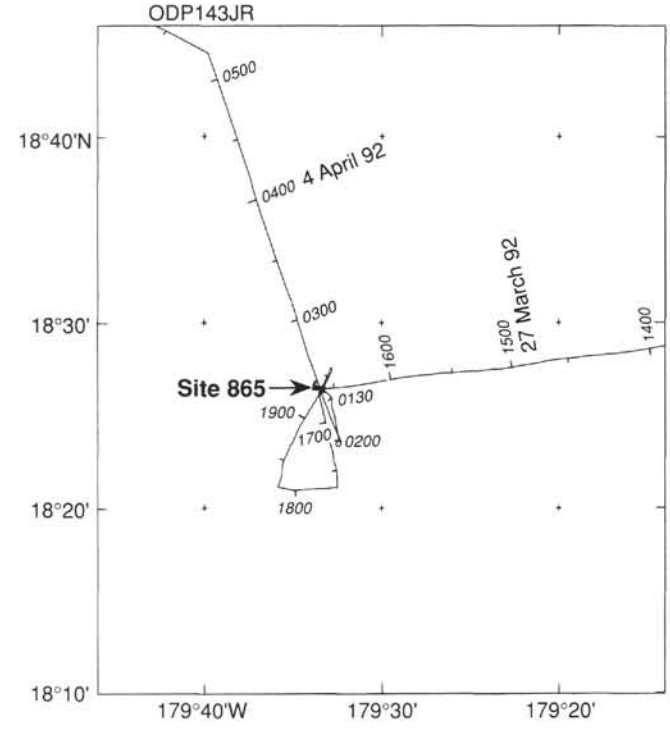

Figure 6. Annotated track of *JOIDES Resolution* approaching and leaving Site 865. Ticks are at 1/2-hr intervals.

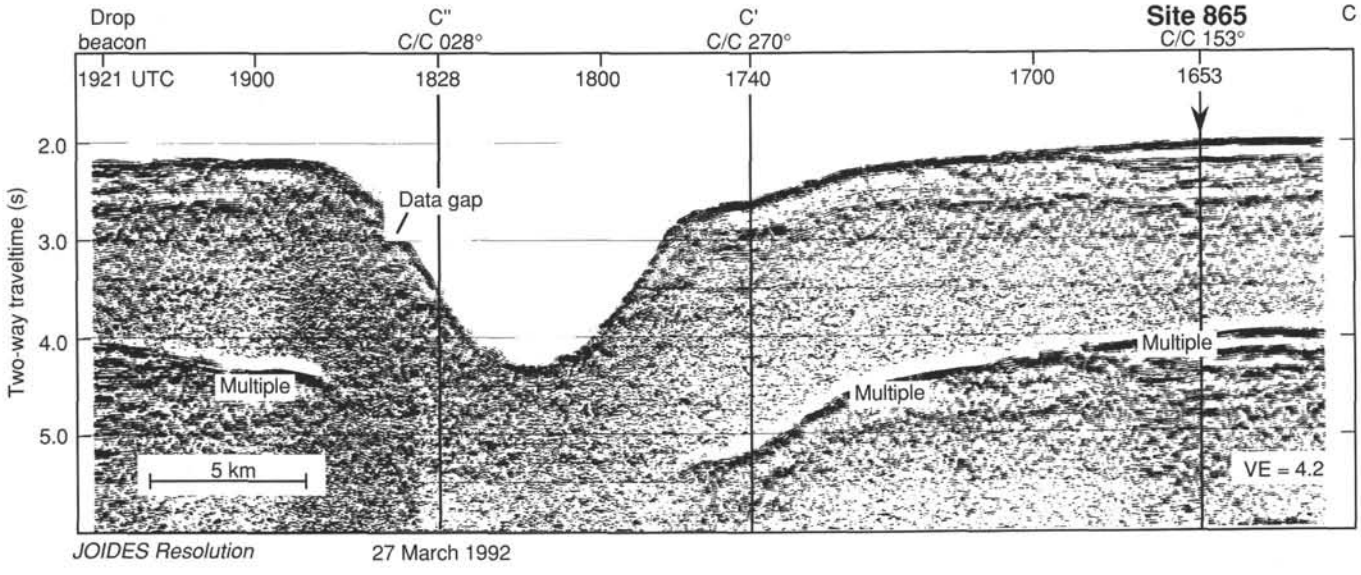

Figure 7. Seismic-reflection profile obtained aboard *JOIDES Resolution* upon approach and beacon drop at Site 865, 27 March 1992. The ship's speed was 6 kt, and the seismic source was an 80-in.^{3} water gun. See Figures 3 and 6 for ship's track locations.

on the eastern end of the guyot. In addition, the basalt reflector shallows by 0.5 s twtt between the eastern end of the line and the summit area, where Site 865 is located.

Upon leaving Site 865, the ship sailed about 2 nmi (3.7 km) to the south of the site while streaming geophysical gear. After deployment, the ship turned to sail north-northeast, shooting a seismic refraction line over the site using an expendable sonobuoy. A 200-in.^{3} water-gun seismic source was used to generate a stronger, lower-frequency signal for the seismic refraction experiment. The single-channel seismic record taken during this line shows a strong basalt reflector with approximately 0.1 s twtt of relief (See "Underway Geophysics" chapter, Line 2, 0130-0530 UTC, 4 April, this volume). It also shows what appears to be sub-basalt reflections approximately 0.12 s twtt below basalt in the vicinity of Site 865. The reflection from the top of the shallow-water limestone is also prominent and displays 0.12 s twtt of relief along the profile.

LITHOSTRATIGRAPHY

Lithologic units have been defined by characteristics such as color, carbonate and clay contents, fossil constituents, lithification, structures and diagnostic log signatures. Several of the lithologic boundaries coincide well with seismic discontinuities and features in the downhole logs, as do some lithological features of the sediments. The following major lithologies were encountered: (1) buff-colored foraminiferal nannofossil ooze; (2) phosphatized and manganese oxyhydroxide-encrusted pelagic limestone; (3) white shallow-water limestones; (4) clayey shallow-water limestone, locally pyritic and organic-rich (Fig. 8).

Lithologic Units

Unit I

Sections 143-865A-1R-1 to -16R-CC
Depth: 0–139.7 mbsf
Age: latest Pleistocene to late Paleocene

Sections 143-865B-1H-1 to -15X-CC
Depth: 0–141.5 mbsf
Age: latest Pleistocene to early Paleocene

Sections 143-865C-1H-1 to -15H-CC
Depth: 0–136.3 mbsf
Age: latest Pleistocene to late Paleocene

Unit I comprises buff-colored to pale yellow foraminiferal sand and foraminiferal-nannofossil ooze. The top one to three cores in the holes are conspicuously sandy in texture and essentially represent a structureless winnowed foraminiferal sand; black-brown specks within this sand probably represent iron-manganese oxyhydroxide micronodules. Mixed faunas and floras (Miocene-Pliocene to Pleistocene) occur in the top core of Holes 865B and 865C; Pleistocene forms dominate at the top of Hole 865A. From Core 143-865A-2R downward, centimeter-scale white mottles, more nannofossil-rich than the surrounding grainy matrix, are common; the less distorted examples clearly represent burrows and display a distinct ovoid geometry with dark linings that contain diffuse organic matter. Smaller millimeter-sized burrows similar to *Chondrites* occur in Core 143-865A-7R. Identical phenomena are observed in Holes 865B and 865C. Generally, the sediments become more nannofossil-rich downhole, although some intercalated grainy foraminiferal levels are seen.

Unit II, Subunit IIA

Cores 143-865A-17R to -24R
Depth: 139.7–207.3 mbsf
Age: late Campanian

Cores 143-865B-16X to -19X
Depth: 141.5–165.5 mbsf (part)
Age: early to mid-Turonian and late Coniacian to late Campanian

That part of Unit II (Subunit IIA) made up of mineralized pelagic limestone and cavity fills cannot be accurately assigned a thickness because it was recovered only as sparse pebbles in Cores 143-865A-17R through -20R of Hole 865A and Cores 143-865B-16X through -19X of Hole 865B; many of these undoubtedly represent cavings from above, as they are mixed together with shallow-water carbonates. The true interval represented by the pelagic mineralized facies should lie between the top of Core 143-865A-16R and the base of Core 143-865A-17R in Hole 865A. The shallow-water facies adjacent to the contact with the pelagic cover in Hole 865A are highly

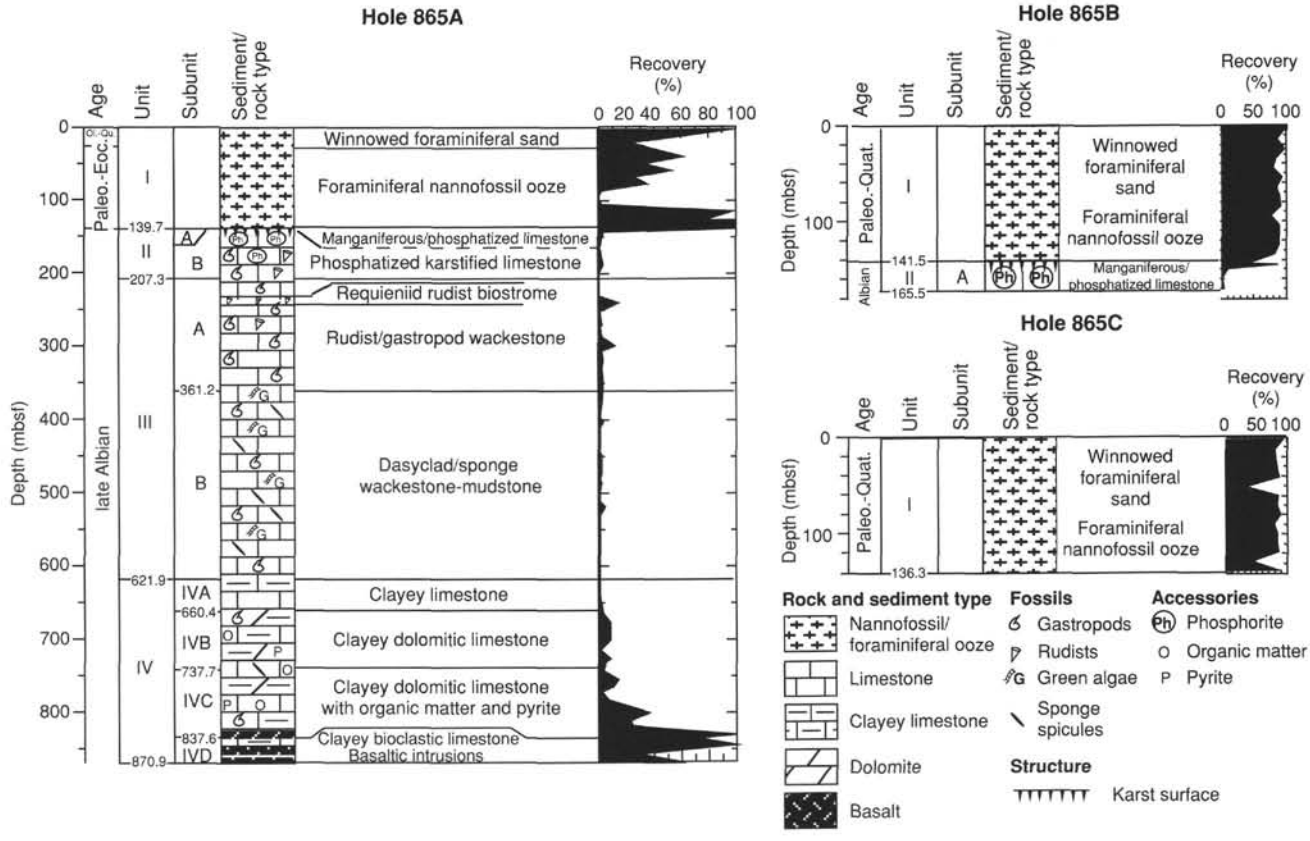

Figure 8. Interpretive stratigraphic columns of Holes 865A, 865B, and 865C.

variable and are locally silicified. The cherts contain sponge spicules and benthic foraminifers in a fine-grained matrix. The phosphatic rocks represent impregnated pelagic foraminiferal limestone, locally brecciated and invariably coated with manganese oxyhydroxides, either as substantial crusts, thin films, fissure fillings, or as clusters of dendrites. The microfauna associated with the mineralized layers suggests a late Campanian age. It is probable that a number of stratigraphically distinct crusts are present, one coating the locally silicified and phosphatized surface of the atoll carbonate itself and others developed within and above the phosphatized Cretaceous pelagic cover.

Within the limestone pebbles of Cores 143-865A-18R and 143-865A-19R, dark-brown geopetal mudstones fill dissolution cavities. In the pebbles from Hole 143-865B-16X and -17X, spectacular dissolution features, of at least centimeter scale, are present; these are partially filled with several generations of yellow-brown internal sediment, some of which is devoid of fossils, other parts of which contain distinct populations of planktonic foraminifers and nannofossils dated as late Coniacian to latest Campanian and early to mid-Turonian; void-filling, yellowish calcite and patinas of manganese oxyhydroxides are common in these cavities (Fig. 9).

Subunit IIB

Cores 143-865A-17R to -24R
Depth: 139.7–207.3 mbsf
Age: late Albian

Cores 143-865B-16X to -19X
Depth: 141.5–165.5 mbsf (part)
Age: late Albian

Recovered shallow-water carbonates comprise packstones and wackestones and, locally, contain requieniid rudists. The shallow-water facies give a positive test for phosphate using ammonium molybdate. The upper part of the shallow-water facies, which shows high gamma-ray values in the downhole logs (Fig. 10; see "Downhole Measurements" section, this chapter), is assumed to contain substantial amounts of phosphate: on this basis, it also has been assigned to Unit II (Subunit IIB) although, genetically, these facies pertain to Unit III. Within Subunit IIB, the resistivity logs show some evidence for sedimentary cycles.

Unit III

Cores 143-865A-24R to -67R
Depth: 207.3–621.9 mbsf
Age: late Albian

Unit III is 424.2 m thick and consists of poorly recovered white limestone of facies similar to those found associated with the mineralized shallow-water limestones of Unit II. Lithologic facies comprise peloidal mudstones, wackestones, packstones, and rare grainstones with molds of formerly aragonitic mollusks. High-spired gastropods, small bivalves, sponges, and large sponge spicules are common. Benthic foraminifers are common to abundant throughout the unit; ostracodes occur in small quantities. Dasycladacean algae are scattered and are generally very poorly preserved. Variable induration is manifested by the development of chalky to hard limestone. Secondary cementation occurs in some of the material as a fine equant spar lining bioclast molds.

A characteristic lithology, which consists of well-indurated wackestone with abundant requieniid bivalves (rudists), occurs in

Core 143-865A-28R (Fig. 11); sparse planktonic foraminifers also occur at this level. Such requieniid facies, although very poorly recovered, are also found in Cores 143-865A-26R, -32R, -35R and -18R (Unit II). Many of the rudists have articulated valves, with the body cavity unfilled by sediment, and the individuals lie about 2 cm apart (Fig. 11). A coral can be seen in Core 143-865A-26R. Only two levels of pelletal grainstones were found: in Cores 143-865A-34R and -39R, respectively. These grainstones contain abundant benthic foraminifers, fecal pellets, and gastropod debris, now present as molds, and appear to be the product of winnowing by waves or currents of the wackestone facies that represents the bulk of the recovered material. Bioturbation is common throughout Unit III. Recognizable burrows include millimeter-scale vertical tubes and centimeter-sized horizontal to vertical traces with ovoid cross sections.

Some possible indications of episodic subaerial exposure, albeit inconclusive, occur in the cored material: for example, brecciation of well-indurated wackestones, reddish staining and, in some places, erosional discontinuities within the sediment.

Two subunits can be distinguished within Unit III.

Subunit IIIA

Cores 143-865A-24R through -40R
Depth: 207.3–361.2 mbsf
Age: late Albian

This subunit is chiefly constituted by wackestone with minor packstone and grainstone. Rudists and scattered corals occur locally; and benthic foraminifers and high-spired gastropods are present throughout. Resistivity logs show saw-tooth patterns typical of sedimentary cycles.

Subunit IIIB

Cores 143-865A-41R through -67R
Depth: 361.2–621.9 mbsf
Age: late Albian

This subunit is richer in lime mud than that of Subunit IIIA and includes some mudstones as well as packstones; dasycladacean algae, ostracodes, sponge spicules, and sponges are characteristic. Some benthic foraminifers can be seen; gastropods are less abundant than in Subunit IIIA.

Unit IV

Cores 143-865A-68R to -94R
Depth: 621.9–870.9 mbsf
Age: late Albian

The upper boundary of this unit was placed at 621.9 mbsf, the top of Core 143-865A-68R, based on the first observed occurrence of clay. The unit extends to the base of the hole, at which level it has been intruded by several basaltic sills.

Four subunits are recognized with Unit IV and are described next.

Subunit IVA

Cores 143-865A-68R to Section 143-865A-71R-CC
Depth: 621.9–660.4 mbsf
Age: late Albian

This subunit was recovered only as pebbles, which are dominantly limestone (wackestone and packstone). The limestone is whitish with dark brown-black claystone laminae (2 mm thick). Bioclasts include benthic foraminifers, ostracodes, gastropods, bivalves, solitary corals (Section 143-865A-69R-CC), sponges, sponge spicules, and dasycladacean algae. Dark gray mudstone fragments occur as lithoclasts (black pebbles). The limestone is extensively bioturbated by *Thalassinoides*-type burrows. Moldic porosity is pervasive.

Subunit IVB

Cores 143-865A-72R to -79R
Depth: 660.4–737.7 mbsf
Age: late Albian

The facies of this second interval is basically the same as that in Subunit IVA. However, black pebbles are more abundant, and burrows are commonly dolomitized. Fine-grained pyrite occurs locally and is associated with these burrows. Possible desiccation cracks in Cores 143-865A-74R and 143-865A-75R may indicate subaerial exposure. Benthic foraminifers are abundant throughout; orbitolinids occur in Core 143-865A-76R. Planktonic foraminifers are present in Core 143-865A-79R. Traces of smectite are identifiable by X-ray diffractometry in the cores from this unit.

Subunit IVC

Sections 143-865A-80R-1 to -90R-5
Depth: 737.7–837.6 mbsf
Age: late Albian

This interval is characterized by the presence of finely dispersed carbonaceous fragments that become more abundant downhole and by interbeds of carbonaceous mudstone and strongly bioturbated and stylolitized clayey limestone similar to those described in the upper part of the unit. Dolomite is also present. Black pebbles are locally abundant (Fig. 12). Burrow fills are locally brecciated by compaction of the clayey matrix (Fig. 13). Pyrite is common and is associated with burrows and carbonaceous fragments. Planktonic foraminifers were observed in Cores 143-865A-80R, -81R and -85R; orbitolinid fragments were noted in Cores 143-865A-85R, -87R and -88R; glauconitized microfossils also occur in Core 143-865A-87R. Section 143-865A-89R-3 contains a root in growth position (Fig. 14) and coalified woody material (Section 143-865A-89R-5). Oyster fragments were observed in Core 143-865A-85R and several deeper cores. Dissolution by organic-rich interstitial waters has removed the shells of several large gastropods prior to lithification, leaving a characteristic brown-stained mold (Fig. 15). X-ray diffractometry has identified smectite, which becomes increasingly abundant with depth, in a number of insoluble residues from cores in this unit; associated clay minerals include kaolinite and/or chlorite. Furthermore, volcanic-derived materials, such as clinopyroxene, zeolites, feldspar, and palagonite, have been identified in Sections 143-865A-82R-2, and -88R-2.

Subunit IVD

Sections 143-865A-90R-5 to -94R-CC
Depth: 837.6–870.9 mbsf
Age: late Albian

Basaltic sills intrude the lower part of the unit. The topmost part of these sills occurs in Section 143-865A-90R-5. A clayey limestone bed can be seen in Core 143-865A-91R, a clayey limestone/carbonaceous mudstone section occurs in Core 143-865A-92R, and a carbonaceous mudstone section clearly displaying the intrusive relationship is evident in Section 143-865A-94R-4. The sediments adjacent to this igneous contact contain red algae, serpulids, and glauconite. Glauconite, together with echinoderm fragments, also occurs in Core 143-865A-90R. Overall, the facies of this subunit are similar to those of Subunit IVC, but are particularly rich in oyster and other bivalve shells. Wood fragments having well-preserved cellular structure, limestone nodules probably corresponding to burrow fills, and clus-

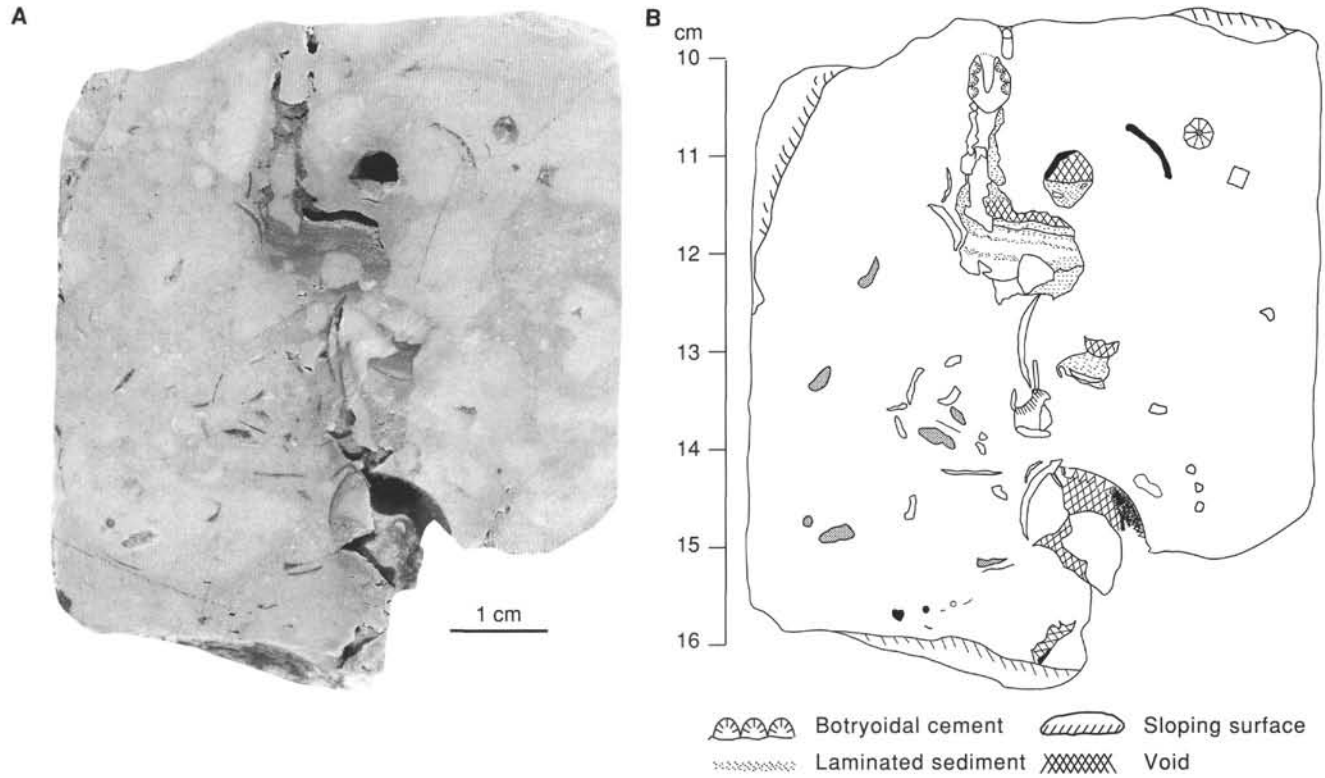

Figure 9. **A**. Photographic detail of dissolution features in atoll summit carbonates. **B.** Sketch of specimen illustrated in **A**. Some brown internal sediment is sterile of fauna and flora; other material contains nannofossils and planktonic foraminifers (Section 143-865B-17X-CC; age, late Albian).

ters of granular pyrite are clearly recognizable in the metamorphosed and metasomatized sediment adjacent to the sills.

An unambiguous base for this sedimentary unit was not reached in Hole 865A.

Interpretation

The vertical facies succession encountered in Hole 865A traces the evolution of a carbonate bank or atoll from early in its history to final drowning.

The lowermost part of the recovered sediments (Subunit IVD) contains abundant oysters and evidence of intense burrowing, probably by shrimps producing *Thalassinoides*-like burrows. The associated red algae, echinoderm fragments, serpulids, and glauconite suggest near-normal marine conditions, at least during some intervals, but at other times conditions may have been more restricted, judging by the overall paucity of fauna. Abundant lignitic organic matter and clays point to a near-by shoreline. The presence of pyrite associated with organic matter implies bacterial sulfate reduction in anoxic sediments, whereas the water was oxygenated enough to allow for shallow infaunal activity. Basaltic dikes intruded the sediment probably at very shallow depths (see "Igneous Petrology" section, this chapter). A lagoonal environment between a fringing reef or other form of barrier and a central volcanic island is envisaged.

A similar environment was maintained throughout the deposition of most of Subunit IVC. Soil-derived material, including smectite, was supplied from an extinct volcanic center. The climate was probably humid, favoring terrestrial run-off and a rich coastal vegetation. At times, the lagoon was replaced by a marsh, as suggested by the root trace in Core 143-865A-89R. Organic matter and pyrite-impregnated peloids, fossils, and lithoclasts to form black pebbles. The presence of dolomite is tentatively explained by seasonally evaporative conditions. Burrows were preferentially dolomitized owing to their higher permeability. Episodic periods of more normal marine conditions are suggested by the presence of glauconite and orbitolinid foraminifers; and fuller, albeit transient, connections with the open sea are indicated by the occurrences of planktonic species that were perhaps washed into the lagoon.

Land-derived organic matter gradually became less abundant and disappeared by the end of deposition of Subunit IVC. Dolomite was no longer formed after the deposition of Subunit IVB, and clay influx was terminated by the close of deposition of Subunit IVA. This evolution suggests that the shoreline gradually retreated, although water depth stayed approximately the same. Concentrations of clay seams appear every 20 to 50 cm in the recovered cores. This may be the result of autocyclic processes, such as shifting influx paths of terrigenous material, or to allocyclic fluctuations of sea level, rainfall intensity, carbonate production, or combinations of these. The final disappearance of clay conforms with an interpretation of an expanding lagoon and submergence of a central volcanic edifice, and is consistent with the Darwinian model of atoll formation (Darwin, 1842).

The clay-free facies of Unit III similarly suggest deposition in a quiet-water lagoon. The degree of faunal diversity is not high in any part of the unit, but the occurrence of rudists and corals higher in the section is suggestive of progressively evolving conditions from restricted (Subunit IIIB) to more normal marine (Subunit IIIA) through time. During the more normal marine phases, the lagoon was subject to the influence of occasional turbulent conditions, as indicated by the formation of winnowed carbonate sands. Red staining probably implies occasional periods of subaerial exposure. Evidence for prolonged emersion becomes more compelling toward the top of the shallow-water carbonates in Unit II (which genetically belong to Unit III), where abundant, partially filled, solutional cavities suggest one or multiple substantial periods of karstification. The internal sediment sterile of fauna and flora in these cavities thus may represent eolian-derived vadose silt. However, the absence of blocky meteoric-water cements in any of the cavities is puzzling if the subaerial inter-

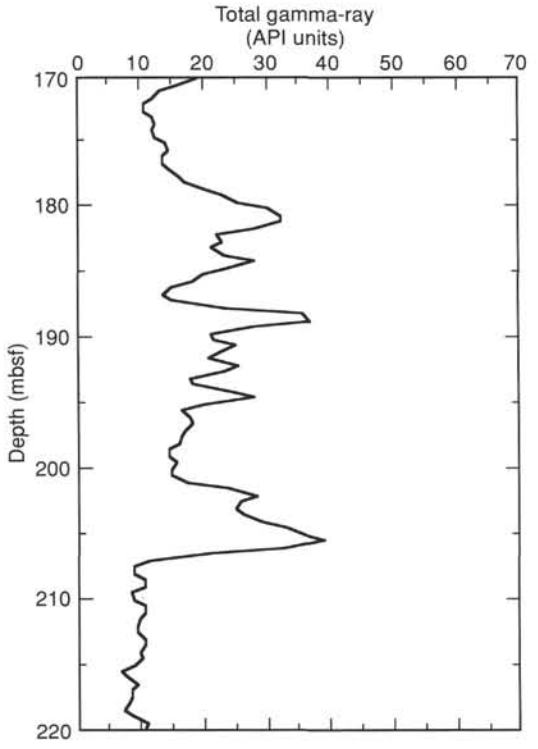

Figure 10. Gamma-ray log of Hole 865A, showing the signature used to divide Units II and III.

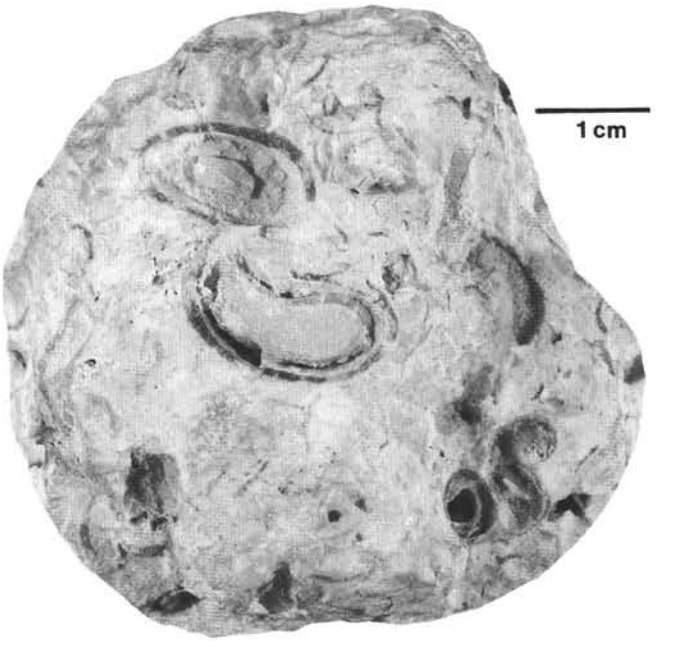

Figure 11. Detail of requieniid rudist bivalves (Interval 143-865A-28R-1, 47–49 cm; age, late Albian).

pretation is adopted. The causality of any relative fall in sea-level, whether related to regional tectonic uplift or a negative eustatic change, cannot be deciphered from the sedimentary record alone; neither can the causality of the subsequent submergence.

At a certain point during the Cretaceous, environmental conditions changed drastically. Regional studies of Allison Guyot (van Waasbergen and Winterer, in press) suggest that the shallow-water carbonate of the former bank or atoll is deeply karstified, an interpretation borne out by the much smaller-scale features observed in Hole 865B. The relative decrease in sea level that occasioned this phase of karstification is most attractively interpreted by regional uplift of part of the Pacific Plate during Albian time. Some time later, submergence of the edifice followed. Only a few tantalizing fragments of rock record this immediate post-drowning history. The heavily mineralized (phosphate and manganese oxyhydroxide) pelagic facies, dated as late Campanian by foraminifers and nannofossils, that represent this phase are clearly only a veneer coating the shallow-water edifice of the drowned carbonate structure. The thickness of this veneer may be as little as a few meters or so, and it encompasses a major, or a series of major, stratigraphic gaps, including much of post-Albian Cretaceous time. Clearly, the environment on the bank or atoll during its early sinking history remained essentially nondepositional for many millions of years. However, at least two generations of pelagic sediment trickled into the solutional cavities in the karstified top of the platform during early to mid-Turonian and late Coniacian to latest Campanian time to preserve a subtle record of this period. Although the subsiding Pacific Plate would have inexorably carried the exposed edifice downward to sea level, the well-documented Cenomanian-Turonian transgression (e.g., Suess, 1906; Hancock and Kauffman, 1979; Schlanger, 1986), whose global importance suggests a primary eustatic component, may well have been responsible for the ultimate submergence of the karstified atoll.

Associated either with the long period of nondeposition or perhaps with the prior period of emergence was a (hypothetical) process of deep penetrative phosphatization that extended through some 60 to 70 m of the highly permeable shallow-water carbonate body.

Sedimentation recommenced with the deposition of upper Paleocene foraminiferal-nannofossil oozes, probably when the site approached the high-productivity zone around the equator. Several distinct stratigraphic gaps within the Tertiary section indicate that accelerated bottom-current activity was important during a number of intervals; winnowing is also implied by the more grainy foraminiferal levels. The Miocene-Pleistocene part of the succession is, again, particularly rich in planktonic foraminifers relative to nannofossils and must represent an erosional lag, as also has been demonstrated by the faunal and floral mixing. The uppermost core in Hole 865A is dominated by Pleistocene biotic elements, with rare Miocene-Pliocene forms; in the top of Holes 865B and 865C, the situation is the reverse. It is probable that a submarine dune field of foraminiferal sands exists on the summit of Allison Guyot, as is the case with many current-scoured seamounts at the present time.

BIOSTRATIGRAPHY

Calcareous Nannofossils

Hole 865A

Calcareous nannofossil biostratigraphy of the pelagic cap section of Hole 865A indicates a thin cover of Quaternary age overlying a thick sequence of early Miocene to late Paleocene age. One sample every alternate section was examined in Hole 865A, in addition to core catcher samples. The cores are not only extremely disturbed, but also have a very high water content and are possibly contaminated by caving in places. These factors are reflected in the nannofossil assemblages, which contain a fair amount of mixing of species of different ages. In the following, we describe broad generalities of assemblages, not the biostratigraphic problems brought about by rotary coring.

Assemblages in Core 143-865A-1R contain *Emiliania huxleyi,* indicating that they belong to Zone NN21 of Martini (1971). Intermixed in several samples are large numbers of *Pseudoemiliania lacunosa,* which reflect reworking of material that is middle Pleistocene or older. Core 143-865A-2R contains a transition from lower

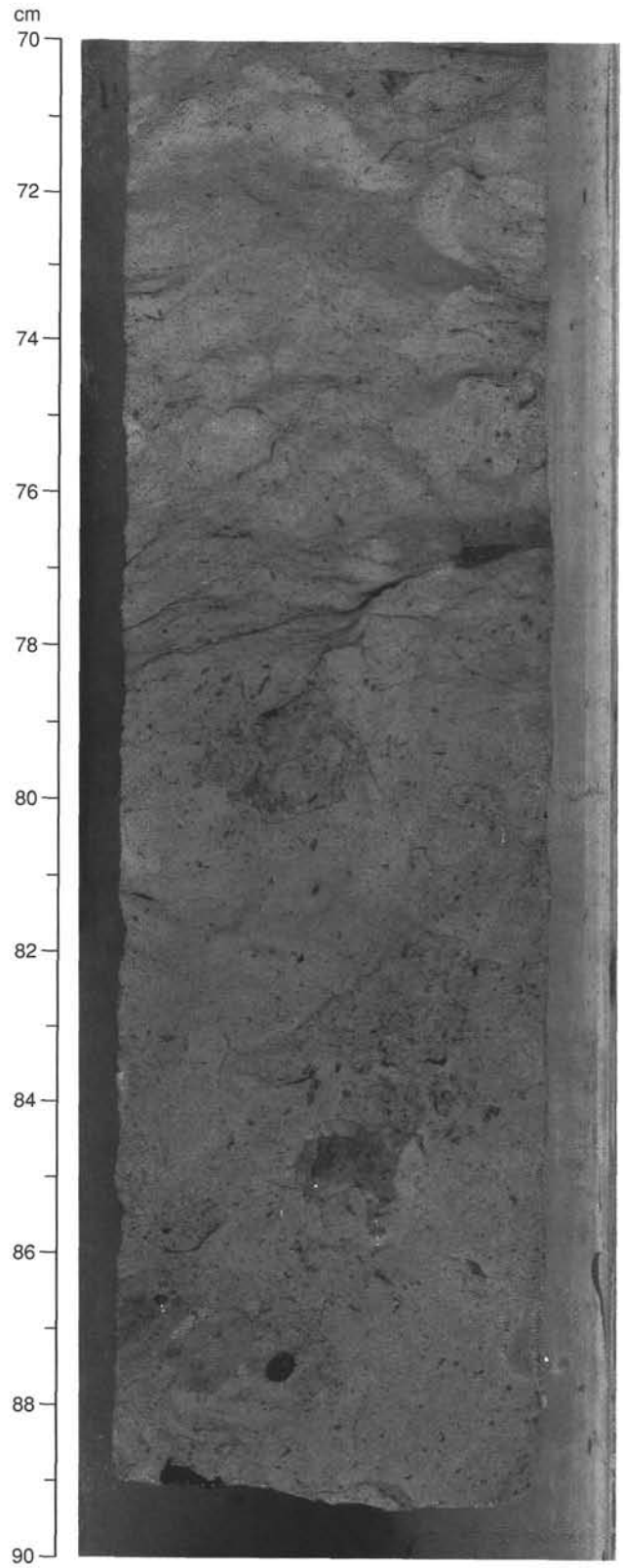

Figure 12. Black pebbles, here seen as dark flecks, in bioturbated limestone containing woody carbonaceous fragments (Interval 143-865A-90R-1, 70–90 cm; age, late Albian).

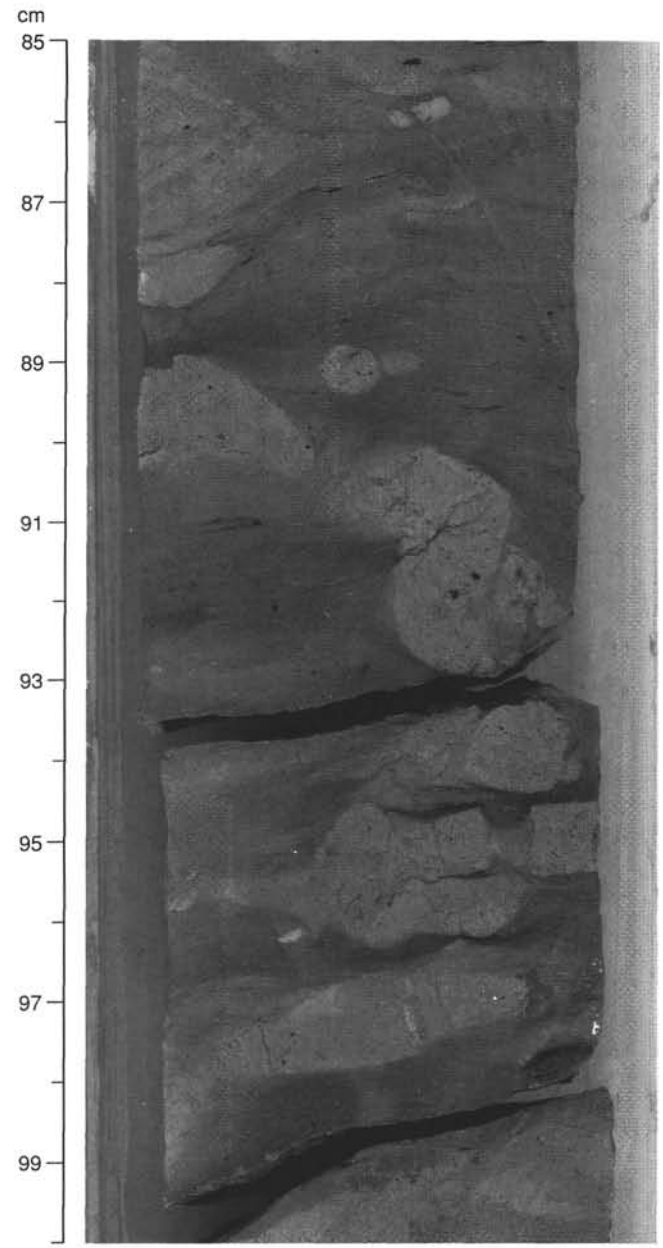

Figure 13. Nodular fabric produced by compaction of clay seams around carbonate-filled burrows (Interval 143-865A-90R-2, 85–100 cm; age, late Albian).

Miocene to upper Oligocene. Sample 143-865A-2R-1, 62-65 cm, contains *Sphenolithus belemnos, Sphenolithus dissimilis,* and *Sphenolithus conicus,* which suggest Zone NN2. Sample 143-865A-2R-2, 60-61 cm, contains *S. dissimilis* and *Discoaster calculosus,* but no *S. belemnos* or *Sphenolithus ciperoensis,* indicating Zone NN1. Various samples in Section 143-865A-2R-3 are from lower Oligocene Zone NP22, based on the occurrence of *Sphenolithus predistentus, Dictyococcites bisectus, Reticulofenestra umbilica* (in most samples), and the absence of *Discoaster barbadiensis* and *Ericsonia formosa.* It is not possible to conclude that Zones NP23 through NP25 are absent in Hole 865A because specimens of *S. ciperoensis* and *Sphenolithus distentus* have yet to be observed. Core 143-865A-3R belongs to upper Eocene Zones NP17 through NP20, based on the occurrences of *S. predistentus, D. barbadiensis,* and *E. formosa* and the absence of *Chiasmolithus solitus.* Samples from Cores 143-865A-

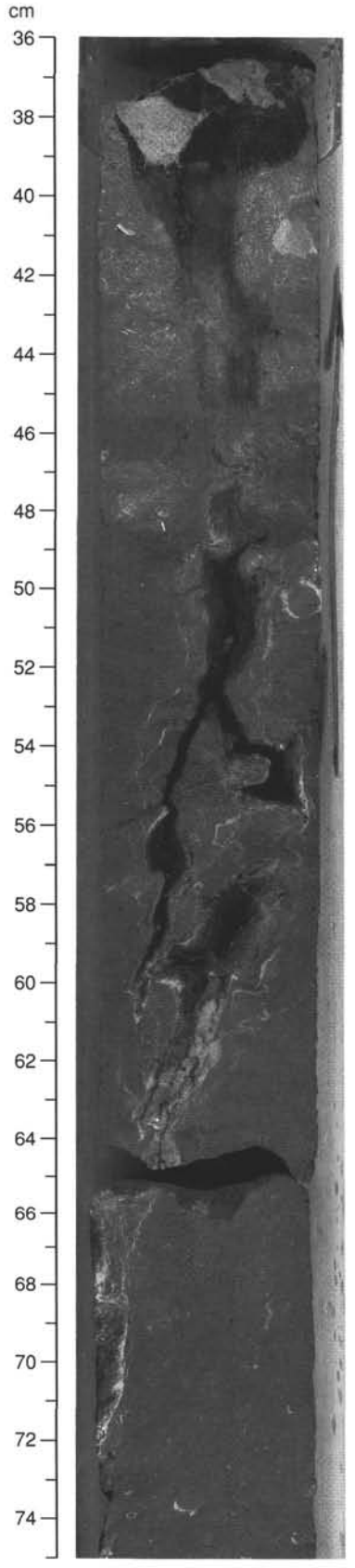

Figure 14. Tree or plant root in growth position; note bifurcation of root system (Interval 143-865A-89R-3, 36–75 cm; age, late Albian).

4R and -5R contain *Sphenolithus furcatolithoides, Chiasmolithus grandis, Chiasmolithus solitus,* and *Chiasmolithus nitidus.* These occurrences and the absence of *Chiasmolithus gigas* and *Nannotetrina fulgens* indicate that this interval lies in middle Eocene Zone NP16. Samples 143-865A-6R-CC and -7R-CC and Section 143-865A-8R-2 correlate to Zone NP15, based on the occurrence of *N. fulgens, S. furcatolithoides,* isolated specimens of *C. gigas* and the absence of *R. umbilica.*

It is extremely difficult to date the lower and lower middle Eocene of Hole 865A as almost all of the traditional marker species are absent, extremely rare, or much overgrown, including *Tribrachiatus* (all species), *Discoaster lodoensis* and *Discoaster sublodoensis.* Sections 143-865A-8R-CC through 10R-CC have been tentatively assigned to Zones NP12 to NP14, based on the occurrence of rare, very overgrown *D. lodoensis.* Section 143-865A-11R-CC is apparently of latest Paleocene or earliest Eocene age (Zones NP9-NP10), based on the occurrence of rare *Discoaster multiradiatus, E. formosa* and *Fasciculithus tympaniformis* and common *Toweius callosus* and *Toweius occultatus* and the absence of *Zygrhablithus bijugatus* and *Sphenolithus radians.* Upper Paleocene Zone NP9 correlates to Sections 143-865A-12R-CC to -14R-2, based on the combined occurrence of *D. multiradiatus* and *F. tympaniformis.* Sections 143-865A-14R-4 to -16R-CC lie in upper Paleocene Zone NP5 as indicated by the presence of *F. tympaniformis* and numerous specimens of *Fasciculithus pileatus* and *Fasciculithus billii* and absence of *Heliolithus kleinpellii.*

Only one sample from the Cretaceous shallow-water limestones was found to be nannofossiliferous. Chalk that filled in a cavity in a manganese-encrusted Albian shallow-water carbonate sample from Section 143-865A-20R-CC contains a poorly preserved assemblage that includes the markers *Eiffellithus eximius* and *Arkhangelskiella cymbiformis.* These markers have a very narrow overlap in the upper Campanian sediments of several sequences (e.g., Perch-Nielsen, 1985; Bralower and Siesser, 1992). More than 100 smear slides were made of the shallow-water carbonates recovered in Hole 865A, but none was nannofossiliferous.

Hole 865B

A similar Cenozoic sequence was recovered in Hole 865B, but because the APC was used in drilling, recovery was much better and sediments are much less disturbed than those in cores from Hole 865A. Nonetheless, the high water content of sediments in Hole 865B poses potential biostratigraphic problems, such as downward mixing of specimens, and these have been monitored throughout these preliminary studies. We have examined one sample every other section throughout this hole and one sample every section in Cores 143-865B-11H and 143-865A-12H, close to the Paleocene/ Eocene boundary. Preliminary nannofossil biostratigraphy of Hole 865B is illustrated in Figure 16.

Assemblages in the upper part of Section 143-865B-1H-1 contain *Emiliania huxleyi* and *Pseudoemiliania lacunosa,* indicating that they belong to Zone NN21 of Martini (1971), with some reworking of Pleistocene material. The lower part of this section down through Sample 143-865B-2H-1, 100 cm, contains a lower Miocene assemblage that includes *Sphenolithus heteromorphus, Discoaster variabilis* and *Discoaster exilis,* which indicates either Zones NN4 or NN5. Samples 143-865B-2H-3, 100 cm, and -2H-4, 100 cm, contain *Sphenolithus belemnos, Sphenolithus delphix* and *Sphenolithus conicus,* but no *D. variabilis,* which suggests lower Miocene Zone NN2. As in Hole 865A, the upper Oligocene sequence appears to be missing in Hole 865B, with the lowermost Oligocene Zone NP21 represented by the interval between Samples 143-865B-2H-5, 115 cm, and -3H-1, 32 cm, based on the occurrence of *E. formosa, Ericsonia subdisticha, Dictyococcites bisectus, R. umbilica,* but no *Discoaster barbadiensis.*

A thick Eocene section was recovered in Hole 865B, however, it is exceptionally difficult to date this material precisely, not because of the preservation, which is adequate, but because traditional zonal markers of Martini (1971) and Bukry (1973) are largely absent. As in

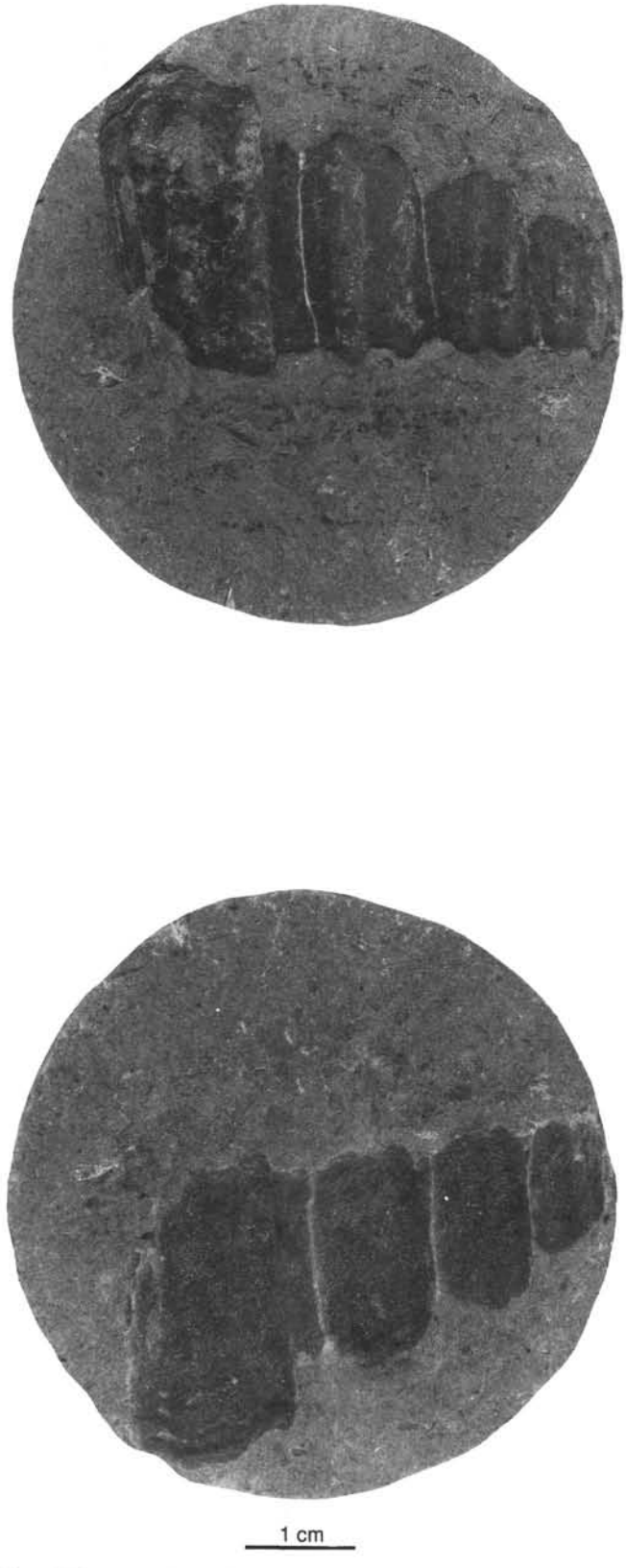

Figure 15. Brown-stained mold of gastropod (Interval 143-865A-92R-1, 25–31 cm; age, late Albian).

Hole 865A, it is difficult to separate upper Eocene Zones NP18 through NP20 in Hole 865B because of the absence of the critical markers, *Chiasmolithus oamaruensis* and *Isthmolithus recurvus.* The last occurrence of *Chiasmolithus grandis* is widely taken to lie in Zone NP17, and this event correlates to Sample 143-865B-4H-1, 16 cm. Similarly, Zone NP16 correlates to the interval between Sample 143-865B-4H-3, 91 cm, which is the last occurrence of the primary marker, *Chiasmolithus solitus,* and 143-865B-6H-1, 80 cm, which is the last occurrence of the secondary marker, *Chiasmolithus gigas* (e.g., Perch-Nielsen, 1985). The latter marker is used to approximate the extent of Zone NP15, the lowest occurrence of which lies in Sample 143-865B-8H-1, 80 cm.

Markers for Zones NP10 to NP14 were not observed in Hole 865B. The interval from Sample 143-865B-8H-3, 80 cm, to -10H-3, 32 cm, has been tentatively assigned to Zones NP12 through NP14, based on the range of (very overgrown specimens of) *Discoaster lodoensis.* The last occurrence of *Discoaster multiradiatus,* assumed by most authors to lie in Zone NP10, lies in Sample 143-865B-11H-1, 129 cm. Therefore, the interval between this and Sample 143-865B-10H-5, 60 cm, is inferred to correlate to Zones NP10 and NP11.

The Paleocene/Eocene boundary interval (Zones NP9 and NP10) is one of rapid turnover of calcareous nannofossils, including numerous events that could be well determined in Hole 865B. These include the last occurrences of *Cruciplacolithus tenuis, F. tympaniformis* and other species of *Fasciculithus* (e.g., *F. schubii, F. alanii*) *Toweius eminens, Toweius pertusus, D. multiradiatus* and the first occurrences of *Toweius occultatus, Toweius callosus, Campylosphaera dela, Zygrhablithus bijugatus, E. formosa, D. barbadiensis,* and *S. radians.* Determination of the exact order of these events will be the subject of detailed shore-based investigations. Actual definition of the Paleocene/Eocene boundary and the completeness of the boundary interval in the absence of the traditional marker, *Tribrachiatus bramlettei,* is uncertain, although numerous authors use the extinction of the fasciculiths. This group shows a dramatic change in abundance between Cores 143-865B-11H and -12H, and the last occurrences of subsidiary species, *Fasciculithus schaubii* and *Fasciculithus alanii,* lie in this interval. The last occurrence of *F. tympaniformis* lies in Sample 143-865B-11H-4, 150 cm, although this species is comparatively rare in the uppermost few meters of its range.

The upper Paleocene section in Hole 865B can be easily subdivided using the zonation of Martini (1971) as all of the traditional marker species are present. The base of Zone NP9 corresponds to the first occurrence of *Discoaster multiradiatus* in Sample 143-865B-14H-1, 100 cm. The remainder of the upper Paleocene zones appear on first sight to be present, albeit of reduced thickness, in Hole 865B. The bases of the zones and their definitions are as follows: base Zone NP8, first occurrence of *Heliolithus riedelii,* Sample 143-865B-14H-3, 93 cm; base Zone NP7, first occurrence of *Discoaster mohleri,* Sample 143-865B-14H-4, 109 cm; base Zone NP6, first occurrence of *Heliolithus kleinpellii,* Sample 143-865B-14H-5, 95 cm; base Zone NP5, first occurrence of *F. tympaniformis,* Sample 143-865B-14H-CC. Core 143-865B-15X lies in lower Paleocene Zone NP4, based on the absence of *F. tympaniformis,* and on the occurrence of *Ellipsolithus macellus* and the subsidiary markers, *F. pileatus, Sphenolithus moriformis* (*S. primus*), and *T. pertusus.*

As in Hole 865A, nannofossiliferous Cretaceous pelagic sediments fill in cavities in shallow-water carbonate Sample 143-865B-17X-CC. Brown claystone recovered from one cavity (Cavity A) in this sample yielded a poorly preserved Cretaceous assemblage that contains *Eiffellithus eximius* and *Micula decussata,* which indicate a late Coniacian to latest Campanian age (e.g., Thierstein, 1976). A second claystone sample from within a different cavity (Cavity B) in this sample contains a sparse, but well preserved and diverse (28 different species identified) Upper Cretaceous assemblage. This assemblage is of two different preservational states, and the significance of these has been interpreted using age information obtained from planktonic foraminifers in these cavities (see below). Well-preserved

Core	Section	Nannofossil zone	Hole 865B	Hole 865C	Nannofossil zone	Section	Core
		NN21	Quaternary				
1H	1H-1 to 2H-1	NN4/NN5	lower Miocene	Quaternary	NN 21 to NN19	1H-1 to 1H-CC	1H
2H	2H-1 to 2H-4	NN1		lower Miocene	NN1-NN3	2H-2	2H
	2H-5 to 3H-1	NP21	lower Oligocene	upper Oligocene to lower Miocene	NP25-NN1	2H-6	
					NP24 - 25	2H-CC	
3H	3H-1 to 3H-CC	NP18-NP20	upper Eocene	lower Oligocene	NP21	3H-1 to 3H-3	3H
	4H-1	NP17		upper Eocene	NP20	3H-CC	
4H	4H-1 to 6H-1	NP16	middle Eocene	middle Eocene	NP16 - 17	4H-CC	4H
5H					NP16 - 17	5H-CC	5H
6H	6H-1 to 8H-1	NP15			NP16 - 17	6H-CC	6H
7H					NP15	7H-CC	7H
8H	8H-1 to 10H-3	NP12-NP14	lower Eocene		NP14	8H-CC	8H
9H					NP12 - 13	9H-CC	9H
10H	10H-3 to 11H-4	NP10/NP11		lower Eocene	NP12 - 13	10H-CC	10H
11H					NP12 - 10?	11H-1 to 11H-3	11H
12H	11H-4 to 14H-1	NP9	upper Paleocene	upper Paleocene	NP 9	11H-5 to 12H-CC	12H
13H							13H
14H	14H-1 to 14H-3	NP8			NP 8	13H-CC	14H
	14H-4	NP7					
	14H-5	NP6					
	14H-CC	NP5					
15X	15X-1 to 15X-CC	NP4	lower Paleocene		NP 7	14H-CC to15H-3	15H
					NP 5 - 6	15H-5	
					NP 4	15H-CC	

Figure 16. Cenozoic nannofossil biostratigraphy of Holes 865B and 865C. Intervals of Martini's (1971) zones are illustrated for each hole, as well as corresponding series. Unconformities are shown with bold lines.

specimens dominate the nannoflora and possess a moderate amount of etching and almost no overgrowth typical of the claystone from which they were derived. This assemblage includes species such as *Broinsonia signata, Broinsonia enormis, Eiffellithus eximius, Prediscosphaera cretacea, P. spinosa, Vagalapilla octoradiata, Microrhabdulus decoratus,* and *Cribrosphaerella ehrenbergii.* The second, very minor component contains very overgrown and minimally etched specimens typical of chalk preservation, including taxa such as *Parhabdolithus embergeri, Watznaueria barnesae,* and *Micula decusata.* These two different preservational states indicate influx of pelagic material into Cavity B in two stages. The first stage occurred between the mid-Turonian and the late Coniacian, based on the well-preserved assemblage that lacks *M. decussata* (first occurrence in late Coniacian), and correlates with Zones CC11-13 of Sissingh (1977) and Zone NC1 of Roth (1978). This age is consistent with that obtained from planktonic foraminifers. The second stage occurred between the late Coniacian and the late Maastrichtian, based on the range of overgrown specimens, which include *M. decussata* (LO at Cretaceous/Tertiary boundary). This latter age is consistent with that obtained from the assemblage within Cavity A. Almost no Cenozoic nannofossils were found in either cavity. The ages obtained from microfossil assemblages in these cavity fills are complex and can be interpreted in a number of ways. However, it is clear from our data that the shallow-water limestone was open to infiltration by pelagic marine sediments on more than one occasion during the Late Cretaceous.

Hole 865C

Calcareous nannofossils in Hole 865C are very similar to those in Holes 865A and 865B in abundance, preservation, and biostratigraphy. In addition to the core-catcher samples, material was examined from critical intervals, including Sections 143-865C-1H to -3H and Sections 143-865C-11H to -12H (Fig. 16).

Sample 143-865C-1H-CC is of Quaternary age (Zone NN21-NN19), as indicated by the co-occurrence of *Pseudoemiliania lacunosa* and *Gephyrocapsa oceanica.* Reworked nannofossils of early Miocene age include *Cyclicargolithus floridanus* and *Discoaster variabilis;* Miocene floras outnumber the autochthonous younger elements by far. A major break is indicated by the assemblage of Sample 143-865C-2H-2, 80 cm, which consists exclusively of lower Miocene floras (NN3-NN1). These include *C. floridanus, Discoaster deflandrei,* and *Helicosphaera euphratis.* The subsequent assemblage of Sample 143-865C-2H-6, 40 cm, has been assigned an earliest Miocene to latest Oligocene age (NN1-NP25), based on the occurrence of *Sphenolithus delphix, C. floridanus, Dictyococcites bisectus,* and *Discoaster deflandrei.* The presence of *Cyclicargolithus abisectus, C. floridanus,* and *D. bisectus* suggest a late Oligocene age (NP25-NP24) for Sample 143-865C-2H-CC. Yet another break is indicated by the floras of Sample 143-865C-3H-1, 80 cm. *D. bisectus, Ericsonia subdisticha,* and *Reticulofenestra hillae* suggest that this sample is of earliest Oligocene age (NP21).

Sample 143-865C-3H-CC is of latest Eocene age (Zone NP20) as it contains *Sphenolithus pseudoradians, S. predistentus, R. umbilica,* and *E. formosa.* Samples 143-865C-4H-CC to -6H-CC yield *Chiasmolithus grandis, E. formosa, Sphenolithus radians, D. bisectus,* and *Zygrhablithus bijugatus* and thus have a middle Eocene age (NP16-NP17). The assemblage of Sample 143-865C-7H-CC has been dated as middle Eocene (NP15) because it possesses *C. grandis, C. gigas, E. formosa, S. predistentus,* and *Rhabdosphaera inflata.* The subsequent Sample 143-865C-8H-CC is slightly older (Zone NP14) because *S. predistentus* and *C. gigas* are absent. Samples 143-865C-9H-CC through 11H-3, 80 cm, are of early Eocene age (Zone NP13-NP12), based on the co-occurrence of *Toweius callosus, Ellipsolithus macellus,* and *Helicosphaera seminulum.*

As in Holes 865A and 865B the upper Paleocene sequence (Zone NP9) is of considerable thickness: the interval from Sample 143-865C-11H-5, 80 cm, to -12H-CC contains *D. multiradiatus, Chiasmolithus bidens, T. eminens,* and *F. tympaniformis.* It is not clear from our preliminary observations whether the lowermost Eocene (Zones NP10-NP11) is missing. Based on the absence of *D. multiradiatus,* Sample 143-865C-13H-CC has been assigned a late Paleocene age (NP8). The upper Paleocene nannofossil Zone NP7 is represented by *Discoaster mohleri, F. tympaniformis, E. macellus, Chiasmolithus consuetus,* and *T. eminens* in Samples 143-865C-14H-CC to -15H-3, 80 cm. Samples 143-865C-15H-5, 80 cm, to 143-865C-15H-CC, are of mid-Paleocene age (Zones NP6-NP4), indicated by *E. macellus, F. tympaniformis,* and *Sphenolithus primus.*

It is not possible to determine from this preliminary analysis of Holes 865A, 865B, and 865C whether differences in stratigraphy exist between these closely located sections.

Foraminifers

Hole 865A

Cenozoic planktonic foraminifers in Hole 865A are mostly abundant and at least moderately well preserved well into sediments of Eocene age. The following zonal assignments for the Cenozoic sequence are based on the examination of core-catcher samples (see Fig. 17 for correlation with nannofossil biostratigraphy). Sample 143-865A-1R-CC is attributed to Zone N22, based on the occurrence of *Truncorotalia truncatulinoides, Sphaeroidinella dehiscens, Globorotalia tumida,* and *Pulleniatina obliquiloculata,* among others. The assemblage is mixed with Pliocene elements represented by stained specimens of *Globigerinoides fistulosus, Globorotalia flexuosa,* and *Dentoglobigerina altispira,* among others.

A major change occurs between Cores 143-865A-1R and -2R with the presence of a mixed assemblage in Sample 143-865A-2R-CC. This assemblage is difficult to date owing to the abundance of Eocene and Oligocene elements. Nonetheless, the presence of *"Globigerina" ciperoensis, Paragloborotalia kugleri, Dentoglobigerina globosa,* and *Globigerinoides obliquus,* indicates placement in the early Miocene (Zone N4-N5) near the Oligocene/Miocene boundary.

Cores 143-865A-3R through -10R have been assigned to the Eocene and progress downhole from Zones P17 to P9. The assemblage in Sample 143-865A-3R-CC includes *Turborotalia cerroazulensis, T. cocoaensis, T. cunialensis,* and *Hantkenina alabamensis* and identifies a lower Eocene interval ranging from the upper part of Zone P16 to Zone P17. A thick middle Eocene sequence follows, that includes Cores 143-865A-4R through -7R. The presence of *Acarinina topilensis, Morozovella lehneri, Hantkenina alabamensis,* and *Globorotaloides suteri* in Sample 143-865A-4R-CC suggests assignment to Zones P13 through P14. The same assemblage, plus the addition of *Acaranina primitiva,* has been used to indicate Zone P14 or older in Sample 143-865A-5R-CC. The occurrence of *Morozovella aragonensis* in Sample 143-865A-6R-CC indicates Zone P11, followed by Sample 143-865A-7R-CC, with a similar assemblage plus *Globigerinatheka micra* that suggests an older age assignment, or Zone P10. The co-occurrence of *G. micra* and *Morozovella quetra* in Sample 143-865A-8R-CC suggests placement in Zone P9 or possibly P10. Lower Eocene Zone P9 can be identified in Samples 143-865A-9R-CC and -10R-CC. The latter assemblage includes *Morozovella caucasica, Acarinina topilensis,* and *Muricoglobigerina soldadoensis,* among others.

Cores 143-865A-11R to -16R are late Paleocene in age and extend from Zone P5 to Zone P3a. Although the planktonic foraminifers are common to abundant the preservation decreases down the section, and specimens are increasingly fragmented and dissolved. Samples 143-865A-11R-CC and -12R-CC were placed in Zone P5, based on the appearance of *Morozovella velascoensis* and *Acarinina mckannai.* Zone P4 is indicated for Samples 143-865A-13R-CC and -14R-CC by the occurrence of *Planorotalites pseudomenardii* and *Moro-*

Figure 17. Nannofossil and planktonic foraminiferal biostratigraphy of Hole 865B. Foraminifer zone shows correlative series in brackets. Series at right is based on nannofossil biostratigraphy.

zovella angulata, followed by Zone P3b in Sample 143-865A-15-CC that has been based on the presence of *M. angulata, Igorina pusilla* and *Planorotalites compressus.* Finally, Sample 143-865A-16R-CC has been placed in Zone P3a based on the presence of *Morozovella praecursoria, M. uncinata, M. conicotruncata,* and *M. angulata.*

Age determinations for the Cretaceous sequence at Hole 865A has been based on thin-section examination for planktonic and benthic foraminifers from the indurated carbonates. The majority of samples contain rare-to-common, poorly preserved benthic foraminifers that provide good potential for age control. However, several samples contain very rare, whole, or fragmented specimens of planktonic foraminifers. An isolated manganese-encrusted pebble from the bottom of Core 143-865A-16R contains a rare, poorly preserved assemblage that includes *Globotruncanita stuartiformis, Globotruncana linneiana, Pseudotextularia elegans,* smaller heterohelicids and hedbergellids, and questionable *Globotruncanita stuarti,* and *Rugoglobigerina* sp. that suggest a late Campanian or Maastrichtian age. Elements of this assemblage were found in a manganese-encrusted pebble from Sample 143-865A-20R-CC and, in addition, include *Globotruncanella havanensis* and *Globotruncana ventricosa.* Again, the assemblage yields a late Campanian to possible early Maastrichtian age, possibly because of caving or because of a deeply karstified surface of the intervening reefal rocks that are Albian in age, based on planktonic and benthic foraminifers (see below).

Sample 143-865A-28R-CC consists of micrite that surrounds large rudistid fragments. The extremely rare foraminifer assemblage includes two transverse (cut perpendicular to the axis of coiling) sections of planktonic foraminifers that are referred to *Praeglobotruncana stephani* of late Albian to Turonian age. Fragments in Sample 143-865A-79R-1, 39–40 cm, were tentatively assigned to *Rotalipora subticinensis* of late Albian age. This species may also be present in Sample 143-865A-80R-1, 31–32 cm, with the addition of several fragments attributed to *Rotalipora appenninica* of late Albian to Cenomanian age. Several additional occurrences include questionable *Rotalipora subticinensis* in Sample 143-865A-81R-2, 62–64 cm, and questionable *Praeglobotruncana stephani* in Sample 143-865A-85R-2, 44–45 cm.

Benthic foraminifers from the shallow-water carbonates consist of two general assemblages: (1) micritic sediments dominated by miliolids and textulariids with lesser amounts of *Nezzazata* and cuneolinids and (2) coarser packstone with a diverse agglutinated assemblage that includes more abundant cuneolinids together with calcareous species of *Nezzazata* and rare specimens of larger foraminifers. Both assemblages are found throughout the Mesozoic sequence, but the coarser samples increase in abundance at the base of the sedimentary section. The presence of *Nezzazata* sp. cf. *N. simplex* and *Cuneolina* sp. cf. *C. pavonia* throughout the section, and *Sabaudia* sp. cf. *S. minuta* in Samples 143-865A-19R-CC and -23R-CC, noted visually in Section 143-865A-88R-1 suggest that the limestone sequence is Albian in age. Rare, small fragments of orbitolinids can be found in Samples 143-865A-85R-2, 44–45 cm, -87R-2, 81-82 cm, and -88R-2, 93–94 cm.

The benthic foraminifers are indicative of shallow-water environments: more restricted in the case of the micritic, miliolid-rich sediments and less restricted, more normal marine in the coarser, more diverse assemblages. The progression of biogenic material throughout the Cretaceous sequence indicates greater marine influence in the coarser bioclastics from Core 143-865A-79R down the section, followed by the development of an increasingly restricted, lagoonal environment up the section that was periodically inundated by coarser, higher-energy, bioclastic debris, perhaps during storms. The same mechanism no doubt transported the planktonic foraminifers into the lagoonal environment. Anoxic conditions in the subsurface lagoonal mud is indicated by the pyritic infilling and coating of benthic foraminifers and other bioclastic debris.

Scraps of manganese-encrusted late Campanian to early Maastrichtian age sediments provide the only evidence of Cretaceous pelagic sedimentation at Hole 865A. No evidence of intervening sediments was recovered.

Hole 865B

Cenozoic planktonic foraminifers at Hole 865B are very similar to those of Hole 865A in biostratigraphic zonation, abundance, and preservation. Sample 143-865B-1H-CC is early Miocene (Zone N4) in age, as indicated by the co-occurrence of *Paragloboratalia kugleri* and *Globorotalia peripheroronda.* Other species present include *Globoquadrina dehiscens, Globigerinoides primordius, Dentoglobigerina altispira, Dentoglobigerina globosa, Catapsydrax dissimilis,* and *Catapsydrax stainforthi.* The sample contains reworked Eocene forms as well as abundant, caved, younger material.

Sample 143-865B-2H-CC repeats the major break observed at Hole 865A with the presence of a late Eocene age (Zone P17) assemblage mixed with middle Eocene (Zone P14) species. The Zone P17 assemblage contains *Turborotalia cunialensis, "T." ampliapertura, Hantkenina alabamensis,* and *Pseudohastigerina micra,* in the absence of *Cribrohantkenina inflata.* The Eocene sequence continues down the section to the base of Core 143-865B-10H. Sample 143-865B-3H-CC is attributed to the upper Eocene (lower P16 or upper P15) by the occurrence of *Globigerinatheka semiinvoluta, Turborotalia cocoaensis, T. ceroazulensis,* and *Hantkenina alabamensis.* The presence of a few specimens of *Acarinina rohri* are considered part of the reworked Zone P14 assemblage.

A thick, middle Eocene sequence extends from Core 143-865B-4H down the section through Core 143-865B-8H. The transition from upper to middle Eocene that occurs between Samples 143-865B-3H-CC and -4H-CC is close to the transition from soupy, homogeneous sediments to less soupy sediments (with distinct sedimentary structures) that were found in Section 143-865B-3H-4. Reworking of the middle Eocene planktonic foraminifers throughout the upper cores resulted from resedimentation processes that extended down to, at least, the lower part of Core 143-865B-3H. Sample 143-865B-4H-CC includes *Acarinina rohri, Acarinina topilensis, Morozovella lehneri, Morozovella spinulosa, Turborotalia pomeroli, Globogerinatheka luterbacheri,* and *Acarinina bullbrooki* and has been placed in Zone P14. Sample 143-865B-5H-CC contains the same assemblage and was assigned to Zone P14 or possibly P13 in the absence of *Orbulinoides beckmanni.* The presence of *Globigerinatheka kugleri, Morozovella aragonensis, "Turborotalia" griffinae, Subbotina frontosa,* and *Subbotina higginsi* in Sample 143-865B-6H-CC indicates Zone P11. A similar assemblage plus *Hantkenina nuttalli* and *Hantkenina mexicana* in Sample 143-865B-7H-CC has been placed in Zone P11. The appearance of *Subbotina boweri* and *Globigerinatheka micra* in Sample 143-865B-8H-CC, together with *Subbotina frontosa* and *Morozovella aragonensis* was used to identify Zone P10.

The lower Eocene (Zone P9) was noted in Sample 143-865B-9H-CC by the presence of *Muricoglobigerina soldadoensis, Acarinina topilensis,* and *Morozovella quetra,* among others. This was followed by the appearance of *Morozovella formosa* in Sample 143-865B-10H-CC that identified Zone P7.

The Paleocene samples begin in Core 143-865B-11H and extend down the section through Core 143-865B-15X. Again, as at Hole 865A, specimen preservation noticeably decreases owing to dissolution and fragmentation. Sample 143-865B-11H-CC has been placed at or near the boundary between Zones P4/P5 by the occurrence of *Morozovella velascoensis, Muricoglobigerina soldadoensis, Igorina pusilla,* and *Planorotalites pseudomenardii.* The presence of *Morozovella velascoensis, Morozovella acuta,* and *Igorina pusilla* without *Muricoglobigerina soldadoensis* identifies Zone P4 in Sample 143-865B-12H-CC. A similar assemblage plus *Morozovella angulata* and *M. conicotruncata* was used to assign Sample 143-865B-13H-CC to Zone P4. Sample 143-865B-14H-CC with *Morozovella angulata, Igorina pusilla,* and *Planorotalites compressus* has been placed in the upper Paleocene Zone P3b, followed by lower Paleocene

Zone P2 in Sample 143-865B-15X-CC, identified by the presence of *Morozovella uncinata, M. trinidadensis,* and *M. pseudobulloides* in the absence of *M. angulata* and *Igorina pusilla.*

Cretaceous foraminifers were found in Cores 143-865B-16X and -17X. Small limestone fragments from Sample 143-865-16X-CC (examined in thin section) contain two foraminiferal assemblages: (1) an assemblage of rare, very poorly preserved planktonic foraminifers confined to a thin, millimeter thick, tan layer beneath a manganese crust and overlying cream-colored limestone that consists of ghosts of *Hedbergella, Heterohelix, Globigerinelloides,* and a small, keeled, trochospiral form. This assemblage is late Santonian or younger in age and most likely represents the age equivalent of the late Campanian assemblage from Hole 865A, and (2) an assemblage from the underlying limestone that consists of cuneolinids, miliolids, textulariids, and *Nezzazata* sp. cf. *N. simplex* that is regarded as Albian in age. A second group of planktonic foraminifers was recovered from a small, 1-cm- cavity in Sample 143-865B-17X-CC. This assemblage of whole specimens washed from brown micrite contains *Helvetoglobotruncana helvetica, Marginotruncana sigali, M. pseudolinneiana, Praeglobotruncana gibba,* and several species of whiteinellids, among others. The age of this assemblage is early to middle Turonian (Zone KS-21), which represents the oldest pelagic facies yet recovered from the surface of the drowned Albian atoll at Allison Guyot.

Palynomorphs

Core-catcher samples from Cores 143-865A-1R through -16R (pelagic ooze) were processed for palynomorphs. All samples are barren. The shallow-water carbonates recovered, beginning from Core 143-865A-17R, were not processed unless visual examination of the cores gave reason for expecting organic matter to be preserved. Samples 143-865A-71R-CC, -78R-CC, and -79R-CC contained stringers of organic-rich material. Samples 143-865A-88R-CC, -89R-3, 25-27 cm, and -89R-5, 52-55 cm, consisted of dark brown, clayey limestones that were adjacent to thick layers of woody/coaly tissue in the cores. These six samples were processed with HCl, and part of the residue was sieved to remove the clay-size fraction. Samples 143-865A-71R-CC, -78R-CC, and -79R-CC contain small amounts of woody tissue, amorphous organic matter, and rare trilete spores. Samples 143-865A-88R-CC, -89R-3, 25-27 cm, and -89R-5, 52–55 cm, either contain very little organic matter or the organics are hidden in the large amount of silt-sized residue. Further processing of these samples with HF in shore based studies will concentrate the organic matter for microscopic examination.

No samples from either Hole 865B or Hole 865C were processed for palynology.

Rudists

The rudist encountered in abundance in Core 143-865A-28R, with fragments in Cores 143-865A-18R and -35R, is a small requieniid. Both valves have circular-oval outlines and lack keels. In this regard, it is probably a primitive *Apricardia* or *Requienia.* During preliminary investigations no trace of the internal (originally) aragonitic layer was found which would have aided descrimination between these two genera. The larger of the two valves (AV or RV) is 1 to 2 cm long and is spirogyrate having two or more entire whorls; the small valve (FV or LV) is not merely operculiform, but has some depth (up to 7 mm). These two characteristics resemble the *Requienia* sp. aff. *R. migliorini* of Johnson et al. (1986) from the El Abra Formation in northeastern Mexico. The lagoonal facies in which it occurs is given an Aptian-Albian range. *Requienia migliorini* Tavani was described from the Albian of Somalia and is known from the Barremian of the south of France and Albian in Italy, Mexico, Algeria, Greece and Oman (J.P. Masse, pers. comm, 1992). This rudist is also very similar to the species named by Palmer (1928) as *Apricardia asymmetrica* from southern Mexico in beds assigned then to the Cenomanian. The range of this form in the Caribbean Province is now considered to be lower Albian with possible extension as high as the lower Cenomanian (Kauffman, Johnson and Sohl, unpublished range chart). The absence of this form during the Barremian, Aptian, or later Cenomanian may result merely from the absence of suitable facies at those times; no obvious ecological replacement for this form exists.

PALEOMAGNETISM

Measurements for Site 865 differed with lithology and with coring method. Archive halves of cores were measured with the pass-through cryogenic magnetometer where pieces within the core were long enough to exceed the approximately 20-cm long sensing window, thus, reliable measurements were possible. If cores were highly fractured or disturbed, discrete samples were taken from the working half of the core.

For the pelagic-cap sediments of rotary-core Hole 865A, pass-through measurements were performed on the first few cores to determine their degree of disturbance. These measurements were done on the archive halves, at a spacing of 10 cm. After measuring the natural remanent magnetization (NRM), the cores were subjected to alternating field (AF) demagnetization at steps of 5, 10, and 15 mT. Discrete samples of 6 cm^3 volume were taken from the working half at a frequency of one sample per section. These discrete samples were cleaned at AF steps of 5, 10, 15, and 30 mT. The 30-mT step was applied using the Schonstedt GSD-1 AF demagnetizer, whereas the others were applied with the in-line demagnetization coils in the pass-through system.

No cores or discrete samples from the shallow-water limestones of Hole 865A were measured because of poor recovery and the lack of sensitivity of the ship's cryogenic magnetometer for small discrete samples. Measurement of these samples has been deferred to shore-based laboratories.

A few basalt and sediment pieces from the deeper portion of Hole 865A were measured. Pass-through measurements were performed on suitably complete sections of the archive halves of Cores 143-865A-89R through -94R. Shipboard discrete samples were taken from the working half of the core to characterize the basalt magnetizations further.

Pass-through measurements were performed on pelagic-cap sediments obtained by the APC from Holes 865B and 865C, and in both holes, sediments from the archive half were measured at intervals of 5 cm and cleaned at steps of 5, 10, and 15 mT. No discrete samples were taken from cores from Holes 865B and 865C because paleomagnetic sampling of the working half was deferred to shore-based laboratories.

Magnetic susceptibility measurements were performed on pelagic sediment cores and on limestone, claystone, and basalt cores from Hole 865A, where recovery was adequate, using the Bartington MS-2 susceptibility meter with the 80-mm sensor loop. Recovery of the shallow-water limestone was too sparse for reliable pass-through susceptibility measurements. Susceptibility measurements were attempted on discrete samples using the small-sample sensor with the Bartington unit, but the meter drift was too large to measure the weakly magnetic limestone reliably. Whole-core magnetic susceptibility measurements were performed on the APC sediments in Holes 865B and 865C using the MST.

Pelagic-cap Sediments

NRM intensities varied on the order of 0.1 to 1000 mA/m in samples from the nannofossil ooze in Holes 865A, 865B, and 865C. In all three holes, the intensity peaks tended to occur within the top 40 to 50% of each core, in the sections with the most water (Fig. 18). Cores 143-865B-2H, -6H, -865C-1H, -9H, -10H are the only cores out of the 28 cores measured that did not exhibit this behavior (Fig. 19). Typically, the upper-core intensity peak varies in magnitude from 10 to 1000 times the intensity values in the lower sections. Those

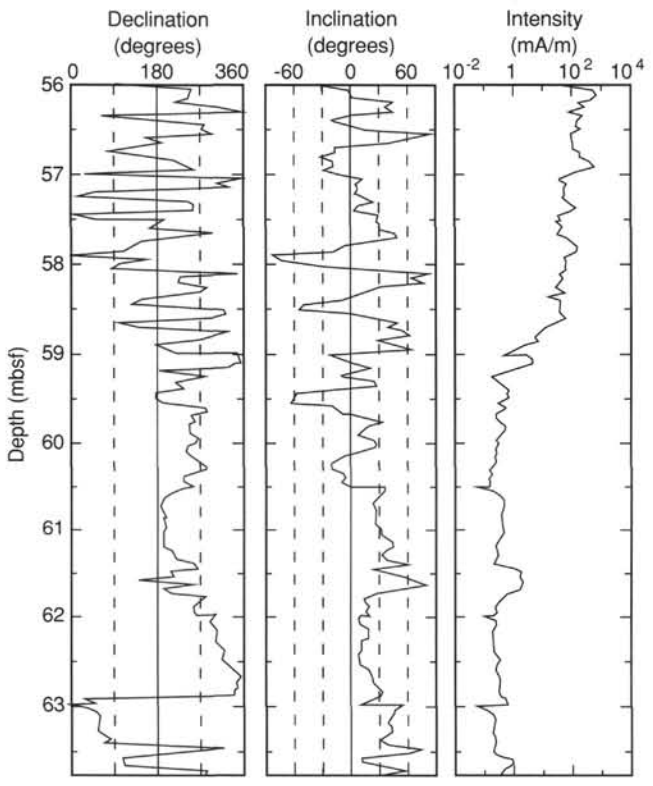

Figure 18. Declination, inclination, and intensity measurements performed with the pass-through cryogenic magnetometer on the archive half of Core 143-865B-7H, after magnetic cleaning at 15 mT. This core shows anomalously high intensities in the upper 40% to 50% of the core.

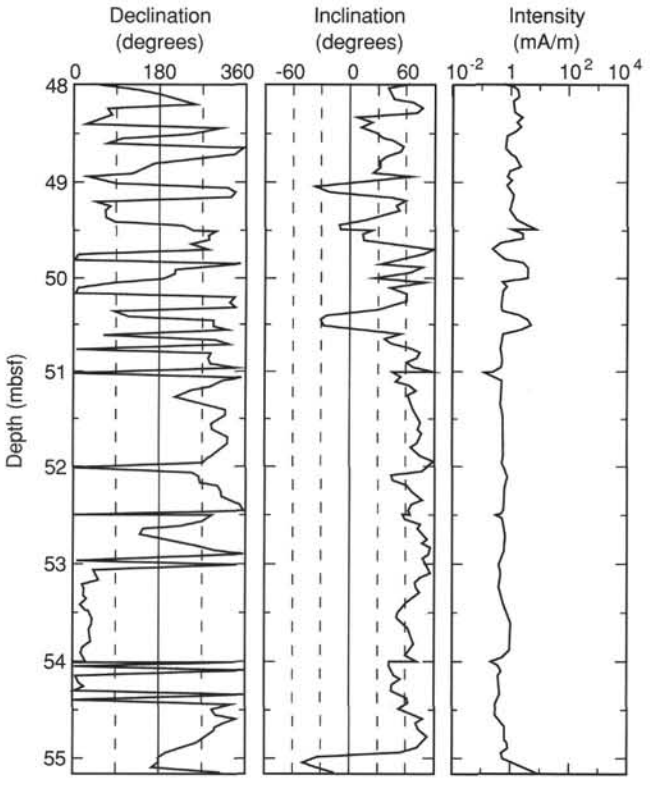

Figure 19. Declination, inclination, and intensity measurements performed with the pass-through cryogenic magnetometer on the archive half of Core 143-865B-6H, after magnetic cleaning at 15 mT. This is one of the few cores that does not show anomalously high intensities at the top.

sections that are very wet exhibit erratic variations in intensity, inclination, and declination, even where the sediments appear undisturbed within the core (Fig. 18).

Rust contamination, a common feature noted in previous ODP studies (e.g., Sager, 1986; 1988; Tarduno et al., 1991), might be the cause of the abnormally high intensities observed in the wet, upper portions of these cores. Whatever the cause of this contamination, it occurred during both rotary and piston coring. The discrete samples from pelagic sediments from Hole 865A exhibit strong overprints, and the samples give erratic directions during demagnetization (Fig. 20). The mean destructive force (MDF) of each of these discrete samples appears to be greater than 30 mT (Fig. 20). The magnetic carrier in these sediments is uncertain, partly because isothermal remanent magnetization data could not be obtained because the impulse magnetizer was returned to shore for repair.

Magnetic Polarity Stratigraphy

Cores of pelagic ooze from Hole 865A were greatly disturbed by rotary coring and are not suitable for magnetic stratigraphy. Large portions of the cores from Holes 865B and 865C are also unsuitable. Magnetic directions are extremely erratic, and therefore unreliable, in the sections that exhibit the high magnetization intensity. It may be possible to resolve reversals in the lower sections of a few cores, but discrete samples from the working half must first be taken on shore, magnetically cleaned, and compared to the shipboard measurements of the archive half.

Magnetic Susceptibility

In the pelagic-cap sediments, the range of magnetic susceptibility readings is on the order of 0 to 100 μcgs, with the highest susceptibilities at the top of each core (Fig. 21). These peaks correspond to peaks in magnetic intensity mentioned earlier. The actual variation in the lower, undisturbed part of the core is fairly small. In Holes 865B and 865C, susceptibility varies from 0.1 to 1 μcgs, with values approaching zero down the core (Fig. 21).

Basalts

Measurement of select archive sections from Cores 143-865A-91R to 143-865A-94R with the pass-through cryogenic magnetometer indicates that the recovered basalts record a relatively strong magnetization having an NRM inclination of approximately -30°. To determine whether the basalt NRM values were dominated by a primary magnetization, discrete samples were drilled from core pieces that appeared least altered. After removal of a minor, possibly viscous magnetization, stepwise AF demagnetization defined a stable magnetization, which is apparently a single component in nature (Fig. 22). Limited stepwise thermal demagnetizations showed similar behavior. The component content is in apparent conflict with the altered state of the rocks (see "Igneous Petrology" section, this chapter). One way to resolve this apparent conflict is to evoke alteration coincident with cooling; thus, the whole rock and magnetic minerals may reflect "alteration," but a primary magnetization is still faithfully recorded. The lowermost basalts have directions similar to those in the uppermost basalts, consistent with the hypothesis that all basalts cored represent the same shallow intrusive episode (see "Igneous Petrology" section, this chapter).

To obtain a rigorous estimate of the primary inclination of each sample, more detailed demagnetizations should be applied. In addition, least-squares fits to the demagnetization data should be used to isolate the characteristic magnetizations. To obtain a shipboard esti-

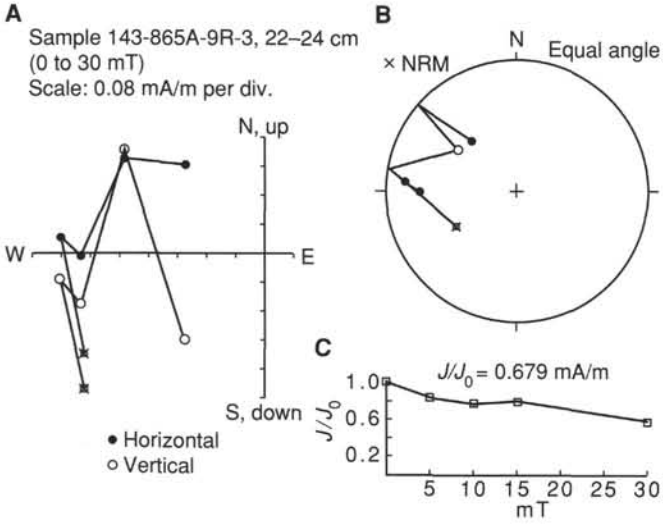

Figure 20. Discrete Sample 143-865A-9R-3, 22–24 cm, exhibits typical erratic behavior of discrete pelagic-sediment samples from Hole 865A, interpreted here as the demagnetization of a relatively strong overprinting that obscures any primary direction. **A.** Orthogonal vector plot of vector endpoints during AF demagnetization. **B.** Equal angle stereonet plot of magnetization vector endpoints at 0 (NRM), 5, 10, and 15 mT AF demagnetization steps. **C.** Plot showing normalized intensity remaining at various AF demagnetization steps.

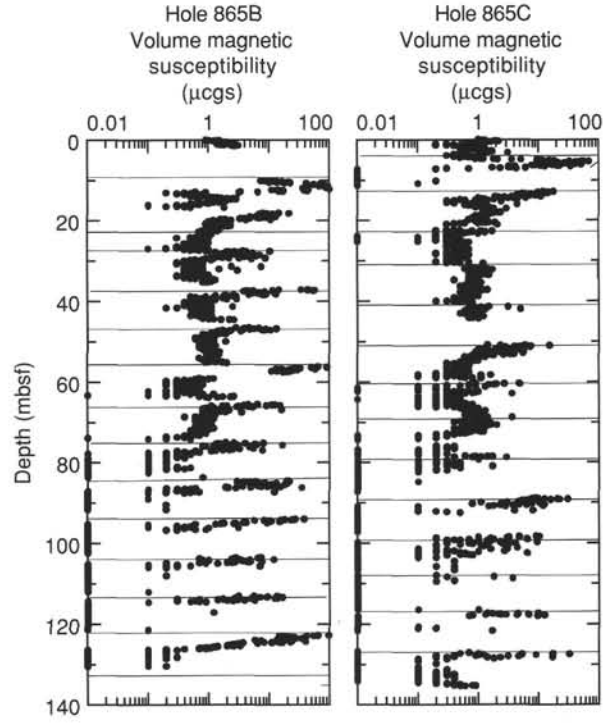

Figure 21. Volume magnetic susceptibility for Holes 865B and 865C (in μcgs). Horizontal lines mark core tops. Susceptibility peaks tend to occur at the top of each core.

mate of the overall inclination recorded by the basalts, we considered the vector endpoints after moderate AF (15 mT) and thermal (150°C) treatment. The inclination range represented by these demagnetization levels is –20° to –38°. To average these values, we must account for the bias toward shallow values implicit in any numerical average of inclination-only data. We applied the method of McFadden and Reid (1982) to compensate for this averaging error and derived a maximum-likelihood inclination estimate of -31.2° (n = 14, k = 85, α_{95} = 4.4°). The simplest interpretation of this average is that it represents a normal polarity field direction recorded while the site was in the Southern Hemisphere. The average inclination implies a nominal paleolatitude of 17°S, but one must keep in mind that this value is likely derived from instantaneous recording of Earth's magnetic field. To obtain a meaningful paleolatitude, this "spot" reading must be combined with other values from Albian-age rocks on the Pacific Plate to average secular variation. The shipboard data indicate that the Hole 865A basalts can contribute such a "virtual" inclination value to the Pacific apparent polar wander path through further shore-based study.

Core Orientation

Cores 143-865B-3H through -5H, -14H, and -865C-5H through -14H were oriented using the multishot tool. Orientation data for these cores are given in Table 3. The orientation record is incomplete for Hole 865B because of insufficient film in the multishot camera in Core 143-865B-6H and as a result of camera failure in Cores 143-865B-7H through -9H. The camera was not used for Cores 143-865B-10H through -13H. In Hole 865C, the multishot tool was not deployed until Core 143-865C-5H because the previous cores were judged to contain too much water to be considered reliable.

SEDIMENTATION RATES

Figure 23 shows a plot of depth vs. age and sedimentation rates for the Cenozoic section recovered in Hole 865B. This hole was selected for sedimentation rate analysis because it was subjected to more detailed biostratigraphic analyses than the other holes. The ages used in calculations are based on nannofossil zonal boundaries taken from the Berggren et al. (1985) time scale. In Figure 23A, the plot of depth vs. age shows that a major depositional episode took place during the Paleogene, with minor intervals in the upper part of Hole 865B from the Miocene and Quaternary sections. This plot shows the position of the three postulated unconfomities in the Neogene and upper Oligocene parts of the section. There is no definitive evidence at this time to propose any hiatuses in the Eocene and upper Paleocene parts of the section.

Figure 23B shows a plot of age vs. sedimentation rate for Hole 865B. This figure illustrates highly variable rates of deposition in the Paleogene part of the section, between 0.5 and 18 m/m.y. Some of this variation may be derived from our assumptions that certain zones (e.g., NP17) are complete in this hole, where they may be only partly represented. However, it is clear from the data that sedimentation rates increased markedly during the late Paleocene (Zone NP9), fell somewhat in the early and middle Eocene and then tailed off considerably in the early Oligocene.

No sedimentation rates have been calculated for the Albian part of the section in Hole 865A because no definitive zonal boundaries can be delimited at this time.

INORGANIC GEOCHEMISTRY

Interstitial Waters

Interstitial waters were taken from 40 core samples in Holes 865A, 865B, and 865C and analyzed according to the methods outlined in the "Explanatory Notes" chapter (this volume). Thirty-five of these samples came from pelagic sediments in the upper 141.5 m. Below this depth, most of the recovered material was too lithified for pore-water extraction using normal squeezing techniques. Nonetheless, five samples from 679.7 to 816.6 mbsf yielded some water (Table 4).

Two interstitial-water samples were taken with the water sampling temperature probe (WSTP) at 65.5 and 141.5 mbsf, within the pelagic sediment of Hole 865B. The WSTP is an in-situ sampling device that

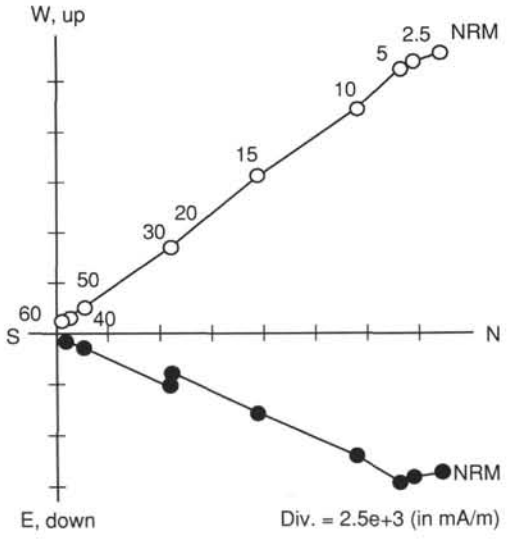

Figure 22. Orthogonal vector plot of progressive AF demagnetization of a basalt sample from Hole 865A. Open circles = inclination; closed circles = declination (unoriented). Vector end points labeled in mT.

Table 3. APC core orientation data, Site 865.

Core no.	Inclination Direction (deg)	Inclination Drift (deg)	Declination (deg)
143-			
865B-3H	5	0.0	77
865B-4H	15	0.5	160
865B-5H	11	0.0	224
865B-14H	3	0.0	248
865C-5H	41	2.0	15
865C-6H	21	1.0	263
865C-7H	37	1.3	314
865C-8H	15	2.0	15
865C-9H	44	2.0	357
865C-10H	36	2.0	340
865C-11H	12	2.0	177
865C-12H	31	2.5	26
865C-13H	10	2.0	170
865C-14H	20	2.5	100

Note: Magnetic declination at Site 865 is 10°. Inclination direction = tilt direction of core. Inclination drift = off-vertical (tilt) angle of core. Declination = direction of double line on core liner relative to magnetic north, positive clockwise.

consists of a probe that is inserted into the sediments 1 m ahead of the drill stem. A stainless-steel filter is housed within the last 21 cm of this probe through which pore waters are filtered when a vacuum is applied through a stainless-steel tubing. The vacuum is generated when the tool is inserted into the sediments and a valve in the tubing that connects a pressure cylinder (deployed at one atmosphere pressure) to the filter is automatically opened for 15 min. Pore waters are drawn from the sediment through the tubing and into the cylinder by the pressure differential. On deployment, the tubing is filled with nanno-pure water. When the pore waters pass through the tubing, they flush the nanno-pure water out of the tubing through a check valve. A relatively pure 11-mL sample remains in a coil of titanium tubing (WT, Table 4). The several liters of water that have flushed into the cylinder (WT, Table 4) also reflect in-situ conditions, but are diluted by ~20 mL of nanno-pure water. Several thousand pounds of additional sand-line wire tension were recorded when the WSTP tool was extracted from the sediments, indicating that the WSTP tool penetrated into firm sediment during both deployments.

Salinity and Chlorinity

Pore-water salinities in the upper 141.5 m range from 35 to 36.0‰ and generally reflect seawater (Fig. 24). By contrast, the samples from 679.9 mbsf and below range from 35.5 to 38.0‰ ($\bar{x}$ = 36.6 ± 1). Chlorinities also are within the range of normal seawater composition (540-568 mM Cl^-) and suggest a trend to increasing values (Fig. 25). A maximum chlorinity value of 579 mM was measured in the deepest sample (816.6 mbsf).

Alkalinity, pH, Calcium, Magnesium, Sodium, Potassium, Strontium, Rubidium, and Lithium

Calcium, magnesium, sodium, potassium, rubidium, and lithium concentrations remain constant with depth in the pelagic cap and are similar to seawater (Fig. 24). The pH and alkalinity values that were measured in the pelagic sediments have mean values of 7.64 ± 0.08 and 2.6 ± 0.2, respectively, and exhibit no depth trend.

Silica

Silica concentrations range between 101 and 168 µM throughout all of the samples (Table 4). The silica content of the pore water reflects the local seawater composition and the low biogenic silica and quartz concentrations in these relatively pure carbonate sediments.

Ammonium and Sulfate

The ammonium contents vary between 0 and 236 µM, but all of the samples in the upper 141.5 m contained little (<35 µM) or no ammonium (Fig. 25). The absence of an ammonium buildup indicates that reactions associated with organic-matter decomposition are not significantly altering these fluids. Moreover, the sulfate values do not decrease significantly within the pelagic cap, which suggests that sulfate reduction is not occurring fast enough to deplete the sulfate concentrations. On the other hand, the increase in ammonium (up to 236 µM) and the decrease in sulfate (down to 25.6 mM) in the deeper samples (679-816 mbsf, Fig. 25) indicate some sulfate reduction has occurred at depth within the platform.

Nitrite

Nitrite concentrations were measured in all the samples from the upper 141.5 m. The only samples that contained detectible amounts (1–2 µM) of nitrite were in Sections 143-865A-1R-3 and -865B-1H-6. Both samples came from near the top of these holes and were collected in a bucket because a sediment and water slurry flowed out through the bottom of the core liner. Because nitrite occurs in the oceanic water above the seafloor, but is not stable in an anoxic environment, we interpret these data to suggest that these interstitial-water samples were not heavily contaminated with seawater.

Comparison among Sampling Techniques

The ionic concentrations for the interstitial-water samples from the three replicate holes through the pelagic cap (≤141.5 m) and from the WSTP tools are indistinguishable, which further confirms that these seawater-like samples represent in-situ pore-water compositions.

ORGANIC GEOCHEMISTRY

At Site 865, in addition to safety monitoring for hydrocarbon gases, 174 samples were used to determine carbonate content. Of these, 69 samples were also analyzed for total organic carbon (TOC) contents. The procedures used for these determinations are outlined in the "Organic Geochemistry" section, "Explanatory Notes" chapter (this volume).

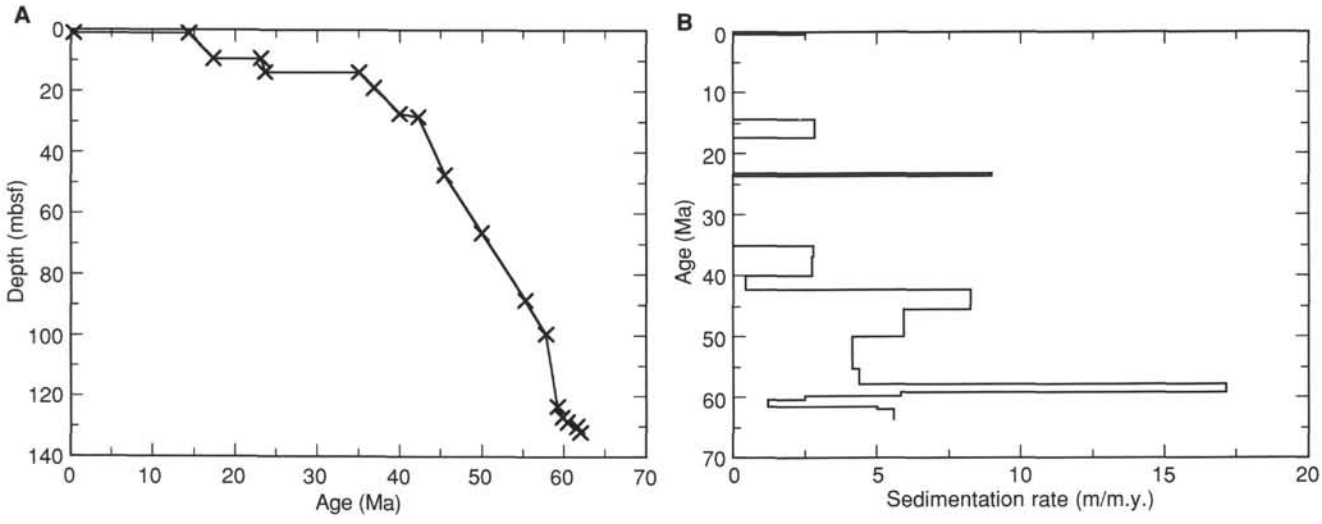

Figure 23. **A.** Plot of age vs. depth for Hole 865B. **B.** Plot of sedimentation rate vs. age for Hole 865B.

Volatile Hydrocarbons

As part of the shipboard safety and pollution monitoring program, hydrocarbon gases were measured in the sediments at Hole 865A, using the headspace technique and Carle gas chromatograph to determine the C_1–C_3 concentrations. The results of 39 headspace analyses are reported in Table 5. Very low levels of volatile hydrocarbon were detected. Methane concentrations in 5-mL headspace volume range from 3 to 5 ppm, whereas traces of ethane were noted, but are below the concentration threshold of the integrator. Compared with a laboratory background of 2 ppm, the concentrations in the sediment are minor. The low overall content of methane in the sediments suggests that either the biogenic methane usually produced during microbial degradation of organic matter migrated out of the sedimentary column, or that conditions were not favorable for sustaining methanogenesis. In the Tertiary pelagic sediments, the content of originally deposited organic matter may have been too low to maintain bacterial metabolism. In Cores 143-865A-80R to -94R, where coal intervals are common, the biogenic gases probably escaped rapidly from the sediment and have a marsh gas aspect. Furthermore, burial depth is too low to produce thermogenic gas.

Inorganic Carbon

Inorganic carbon (IC) was measured with the Coulometrics carbon dioxide Coulometer. In Hole 865A, 112 samples (part of the samples used for physical property, paleontological, and interstitial-water analyses) were analyzed for IC (Table 6). The physical-property samples taken in soft sediments show lower carbonate contents than squeeze cake or paleontological samples. After 12 hrs of freeze-drying, the physical property samples presented higher carbonate contents (Fig. 26). We suspect that, after oven drying, the sediments in the physical-property beaker absorbed water from the atmosphere, making them heavier and thus biasing their $CaCO_3$ content lower. At Holes 865B and 865C, separate samples were taken specifically for analyses of carbonate contents.

According to the carbonate record from squeeze cake and paleontological samples (Fig. 27), the sediment sequence in Hole 865A can be divided into three parts that correspond to lithologic Units I, III, and IV (Fig. 27; see "Lithostratigraphy" section, this chapter). The upper 139.7 mbsf (Cores 143-865A-1R to -16R) are characterized by high carbonate contents that range from 92% to 98% $CaCO_3$. The middle part (Cores 143-865A-23R to -66R), corresponding to shallow-water carbonate facies, shows consistent values of about 99% $CaCO_3$. The lower part, from 660.4 to 849.2 mbsf (Cores 143-865A-71R to -92R), is characterized by high-amplitude variations that range from 26.4% in dark claystones to 99.4% in some packstone intervals.

In Hole 865B and 865C, the amounts of carbonate show slight variations of between 92% and 98% (Table 7 and Fig. 28), as in Unit I of Hole 865A.

Organic Carbon Contents

The contents of total carbon (TC), nitrogen, and sulfur were determined using the NA1500 NCS analyzer. Total organic carbon (TOC) values were calculated by difference between TC and IC. The results of 69 analyses from Holes 865A and 865B are reported in Tables 6 and 7.

TOC amounts fluctuate from 0.06% to 0.57% in the upper 142 m of Hole 865A. The middle part (Cores 143-865A-23R to 143-865A-66R), corresponding to Unit III, also shows very low total organic contents. The organic content increases in Core 143-865A-71R and has a 1.94% value. The lower part (Unit IV) presents significant variations of the organic content. TOC amounts vary from 0.23% in carbonate facies to 35.4% in one coaly interval. In organic-rich samples, the sulfur content is relatively high (between 2.8% and 11.8%) and may be correlated with the abundance of pyrite. On the basis of the TOC/nitrogen ratios, the nature of organic matter preserved in these sediments is mainly marine within Unit II, seems mixed in Unit III and is more typically terrigenous in Unit III (Fig. 29). Nevertheless, three samples show lower TOC/nitrogen ratios, which may indicate a mixed origin of the organic material in these intervals. No data are available for the maturity and quality of the organic-rich layers because of technical problems in shipboard Geofina hydrocarbon meter and Rock-Eval analyzers. More detailed shore-based studies (elemental analysis and gas-chromatography investigations on extracted kerogens) will permit better characterization of the organic matter encountered in sediments at Hole 865A.

At Hole 865B, the organic contents are relatively low, but slightly higher than in Unit I of Hole 865A. TOC concentrations fluctuate from 0.04 to 0.74, with an average of 0.24% (Fig. 30). The concentrations of total sulfur are low, and concentrations of total nitrogen were often below the detection limit of the NCS analyzer.

IGNEOUS PETROLOGY

One of the main objectives of Leg 143 for drilling 340 m deeper than originally planned at Site 865 (see "Background and Scientific Objectives" section, this chapter) was to sample and to investigate the

Table 4. Interstitial-water data from Holes 865A, 865B, and 865C.

Core no.	Depth (mbsf)	Water (mL)	pH	Salin.	Alkal.	K^{+}(mM)	Na^{+}(mM)	Mg^{+2}(mM)	Ca^{+2}(mM)	Sr^{+2}(μM)	Rb^{+}(μM)	Li^{+}(μM)	Si^{+4}(μM)	$Cl^{(-)}$(mM)	NH_4(μM)	$SO_4^{(-)}$(mM)
143-865A-																
1R-3	4.45	40.0	7.74	36.0	3.02	10.3	479.	53.3	11.2	99.	1.65		114.	547.	0.0	
2R-3	10.15	46.0	7.64	35.0	2.64	10.1	476.	54.2	11.1	104.	1.53	23.	149.	549.	26.4	27.9
3R-1	16.15	50.0	7.65	35.5	2.56	10.3	482.	53.2	11.2	99.	1.54	24.	149.	541.	16.2	27.5
4R-2	24.95	42.0	7.60	36.0	3.35	10.4	488.	53.9	11.3	99.	1.58	22.	151.	540.	0.0	28.5
5R-3	36.80	42.0	7.69	36.0	2.56	10.4	489.	53.8	11.2	104.	1.65	24.	151.	542.	0.0	29.2
6R-1	44.72	50.0	7.69	36.0	2.56	10.5	489.	54.5	11.2	101.	1.51	23.	168.	549.	4.2	28.8
7R-3	55.79	50.0	7.71	36.0	2.51	10.4	491.	53.7	11.2	99.	1.51	23.	168.	548.	0.0	28.8
8R-1	63.82	38.0	7.69	36.0	2.56	10.5	487.	53.7	11.2	110.	1.54	25.	166.	556.	0.0	28.8
9R-1	73.25	40.0	7.70	35.5	2.61	10.3	489.	53.2	11.5	99.	1.46	26.	164.	552.	0.0	28.7
13R-4	116.75	28.0	7.40	35.5	2.58	10.2	477.	54.0	11.4	99.	1.44	26.	160.	557.	10.7	28.6
14R-3	124.95	52.0	7.70	35.5	2.59	10.5	487.	54.2	11.4	110.	1.45	23.	155.	564.	33.5	28.2
15R-4	136.05	46.0	7.67	36.0	2.56	10.4	492.	53.5	11.4	101.	1.47	22.	166.	556.	10.9	29.1
15R-6	139.07	19.0	7.64	35.5	2.75	9.8	461.	53.8	11.3	101.	1.52	26.	176.	558.	0.0	28.2
15R-7	139.59	22.0	7.67	35.5	2.38	10.5	484.	53.1	11.3	119.		31.	166.	557.	11.0	28.5
16R-4	141.00	36.0	7.64	35.5	2.50	10.4	492.	54.4	11.3	101	1.52	26.	176.	558.	0.0	28.2
16R-5	142.15	35.0	7.64	35.5	2.59	10.4	492.	53.4	11.1	99.	1.52	26.		550.	10.0	28.5
74R-1	679.70	3.5		35.5		4.4	474.			105.				571.	129.0	27.8
76R-1	699.80	1.0		38.0										573.	145.0	
78R-1	719.00	1.0		36.5		10.1	470.			110.				575.	137.0	26.9
87R-3	808.94	5.5		35.5		8.6	469.			170.				568.	236.0	25.7
88R-1	816.50	1.5		37.5									101.	579.	119.0	
143-865B-																
1H-6	8.30	100.0	7.68	35.5	1.94	10.8	542.	52.8	11.2	99.	1.43	28.	145.	549.	4.2	28.2
2H-5	15.95	42.0	7.58	35.5	2.66	11.1	489.	52.9	11.2	105.	1.49	20.	145.	552.	13.3	28.3
3H-6	26.95	29.0	7.70	35.5	2.59	10.5	511.	52.9	11.3	105.			147.	549.	6.8	28.9
4H-5	34.95	66.0	7.64	35.5	2.68	9.4	428.	53.1	11.2	101.	1.50	27.	135.	549.	0.3	28.8
5H-4	42.95	62.0	7.69	36.0	2.55	10.9	474.	53.3	11.4	101.	1.53	21.	126.	552.	1.5	29.4
6H-5	53.95	48.0	7.60	36.0	2.70	10.8	471.	52.7	11.5	104.	1.51	20.	143.	552.	1.5	29.4
7H-1-WO	58.95	555.0	7.80	36.0	2.74	10.4	484.	53.3	11.4	103.	1.43	21.	126.	538.	8.2	29.0
7H-1-WT	58.95	11.0						53.3	11.3	95.				553.	6.9	28.9
7H-2	58.95	49.0	7.67	36.0	2.65	10.8	479.	53.8	11.4	101.	1.51	21.	145.	554.	0.0	29.0
8H-5	72.95	25.0		36.0				53.4		95.			141.	556.		
9H-5	82.95	54.0	7.68	36.0	2.74	10.4	479.	53.8	11.5	106.	1.47	22.	137.	562.	0.0	28.5
10H-4	90.45	65.0	7.64		2.52	10.0	557.	53.7	11.4	105.	1.46	20.	145.	557.	0.0	28.6
12H-5	110.95	30.0	7.62	36.0	2.71	10.6	522.	53.7	11.4	99.	1.48	20.	141.	563.	0.0	28.9
13H-5	120.45	42.0	7.72	36.5	2.67	10.9	470.	53.4	11.6	104.	1.48	17.	141.	564.	0.0	28.4
14H-3	126.95	16.0	7.55	36.0	2.72			53.2	11.6	96.			137.	568.		
14H-5	129.95	46.0	7.47	36.0	2.71	11.1	483.	53.3	11.6	102.	1.47	19.	139.	567.	2.9	28.7
15X-1-WO	133.45	550.0	7.54	36.0	2.77	11.1	478.	52.4	11.3	103.	1.51	20.	116.	547.	70.6	29.0
15X-1-WT	133.45	9.0						53.0	11.6	97.			104.	562.	2.9	
15X-1	133.45							52.9	11.2				139.	558.	8.2	28.7
15X-2	134.95	40.0	7.66	35.5	2.59	10.9	480.	52.9	11.3	104.	1.51	20.	137.	561.	0.0	28.6
143-865C-																
1H-2	2.40	28.0	7.58	35.0	2.91	10.1	467.	53.6	11.2	102.	1.57	22.	145.	550.	1.5	27.4
3H-4	15.75	22.0	7.65	35.0	2.69	10.1	463.	53.1	11.6	102.		21.	137.	547.	13.5	28.2
4H-5	22.25	26.0	7.54	35.0	2.71	9.7	463.	53.0	11.6	106.	1.50	22.	137.	554.	0.2	28.2

Note: Core: designations include the core, drill type (R, rotary; H, hydraulic piston cores; and X, extended-core barrel) and section number; depth = meters below seafloor; water = water yield in the analyzed samples; WO = samples of overflow waters from the WSTP tool; and WT = samples from the flushed tubing in the WSTP tool.

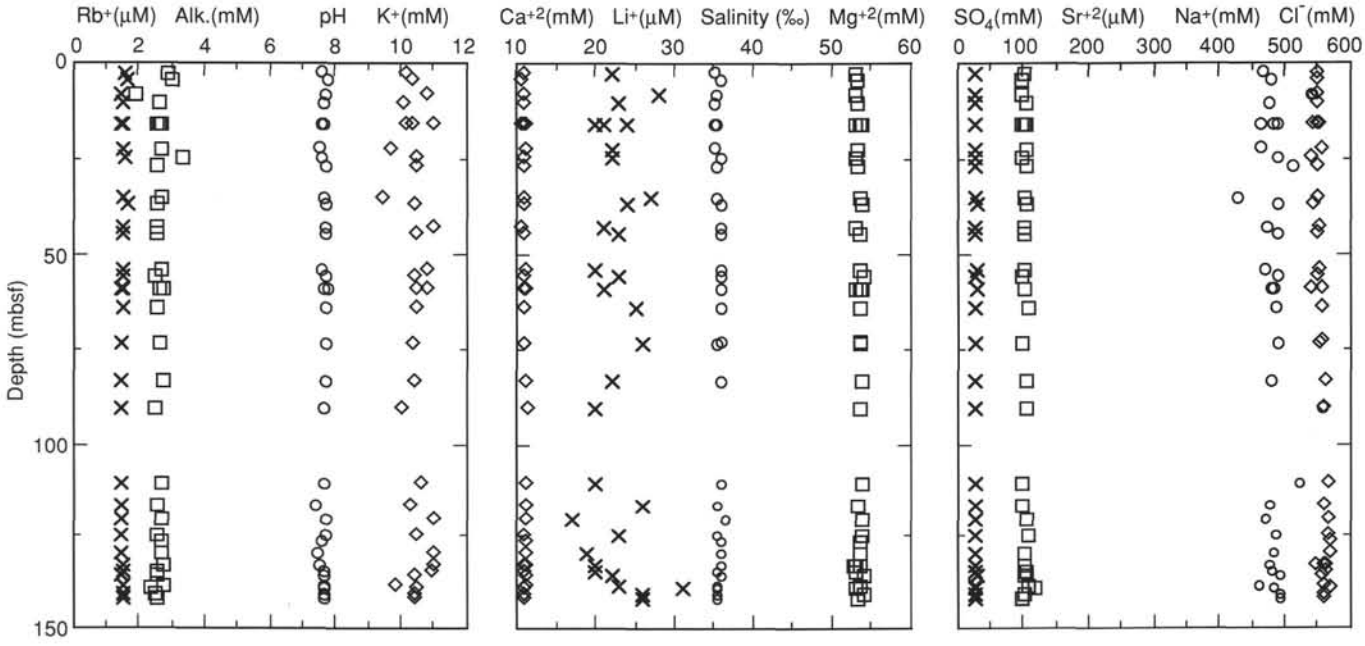

Figure 24. Concentration of determined pore-water parameters as a function of depth in the pelagic caps of Holes 865A, 865B, and 865C. The concentration values remain constant at near-seawater values throughout the 141.5-m pelagic cap.

volcanic basement of Allison Guyot. In Hole 865A, fine-grained igneous rocks were recovered at ~840 mbsf, beneath Albian clayey dolomitic limestone rich in organic matter and locally pyritic (i.e., beneath lithologic Subunit IVC; see "Lithostratigraphy" section, this chapter). However, several lines of evidence indicate that these basaltic rocks may not represent true basement, for they are not lava flows, but sills that intruded soft sedimentary rocks. First, the basalt units recovered from Hole 865A are separated by clayey bioclastic limestone subunits (Fig. 31), which, like the other clayey limestone subunits of lithologic Unit IV, belong to a shallow marine limestone facies (see "Lithostratigraphy" section, this chapter). Contact relations between the basalt units and these interbedded limestones are inconsistent with a lava-flow origin of these basalts. For example, a ~2-m-thick decarbonated, metasomatized, lignite-bearing sedimentary layer that contains fragments of very highly to completely altered basalts separates basalt Unit 1 from the overlying clayey dolomitic limestone. This layer has a soft and muddy upper portion and a well-indurated lower part, near basalt Unit 1 (Fig. 32), most probably owing to the higher temperature adjacent to the intrusion. These textural features of the highly disturbed layer could not have been produced by normal shallow-marine deposition on top of a lava flow. Second, morphologic features usually associated with subaerially or submarine-erupted oceanic lavas, such as pillowed or sheeted lava flows having sharp glassy selvages, are not present in the basalt units. Instead, the top and bottom contacts between the basalt units and the interbedded clayey bioclastic limestone are very irregular and generally gradational. In addition, usually a reaction halo is seen in the basalt unit, where it comes in contact with the limestone, that is unlikely to have developed were the contact depositional. Third, neither the subaerial oxidation surfaces nor submarine alteration zones, typically associated with oceanic island and seafloor lava flows (e.g., Honnorez et al., 1983), respectively, were observed on the upper parts of the basalt units, despite the fact that actual top contacts of Units 1 and 4 were recovered. In fact, the contact between Unit 4 and the overlying limestone is subvertical, rather than horizontal (Fig. 33). Finally, isolated pieces of the clayey bioclastic limestone are enclosed within the basalt unit, indicating that the latter is younger. Pieces near the margin of the basalt are still calcareous and fossiliferous (Fig. 34); these are reddish-yellow (5YR 6/8) and produce alteration halos in the host rock. Farther into the interior of the basalt unit, the inclusions are completely decarbonated and are devoid of any sedimentary textures. These are deep red to dark reddish-brown (2.5YR 2.5/4) and generally lack alteration halos (Fig. 35), which is consistent with the notion that any enclosed sedimentary rock fragments would be completely thermally metamorphosed in the hotter, interior portion of the intrusive unit.

Although the basalt units are intrusive, they were probably emplaced penecontemporaneously with, or shortly after, the deposition of the clayey bioclastic limestone. This hypothesis is based on the high degree of alteration near the margins of the basalt units and on the disturbed and metasomatized nature of the sedimentary rock in contact with the units, suggesting that the clayey bioclastic limestone was still wet and soft when the intrusion occurred. In addition, the different basalt units are geochemically very similar, except for slight differences in texture and degree of alteration within and among the units (see below). These similarities suggest that all the units are connected to a single intrusive body.

Lithology

Although four units are indicated in Figure 31, essentially only three basalt units can be seen in the lowermost part of Hole 865A. Unit 2 consists of only three rounded cobbles at the top of Core 143-865A-92R, which could be fragments of Unit 1 that fell to the bottom of the hole before Core 143-865A-92R was drilled. Most importantly, Unit 2 is lithologically very similar to Unit 1 and lacks the gradational basalt-sediment contacts that are present at the top and bottom of the other basalt units.

Unit 1 occurs from 837.6 (143-865A-90R-5, 76 cm) to 844.5 (143-865A-91R-3, 60 cm) mbsf, but its actual recovered thickness is only 4.9 m. This unit is a single cooling unit because no contact or change in composition or texture was observed within the unit. A highly disturbed sedimentary layer separates Unit 1 from the overlying clayey dolomitic limestone. The highly to completely altered basalt fragments

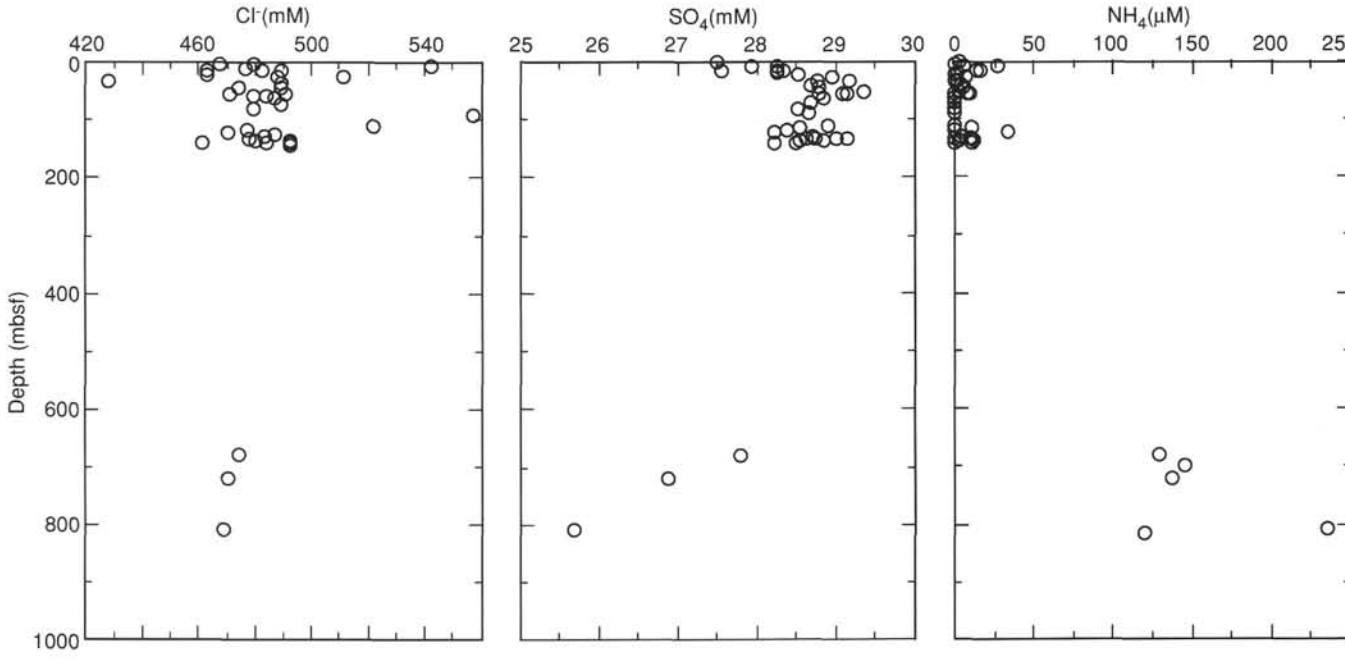

Figure 25. Concentrations of chloride, sulfate, and ammonium at Site 865.

within this layer (Fig. 32) are most probably apophyses of Unit 1, to which these fragments are petrologically identical. At the contact with the disturbed layer, Unit 1 is quenched and has very irregular tongues that extend into the limestone. The texture is aphanitic to hypohyaline (now completely altered to clay) and contains <1% subhedral microphenocrysts (~1 mm, average size) of olivine and pyroxene that are completely pseudomorphed by clay. Immediately below and including the quenched margin is an 8 to 15 cm alteration halo. This is gray (2.5G 6/2) and is sparsely (~2%) microphyric (~1.5 mm, average size) olivine-pyroxene basalt with a highly altered (40%-80%) groundmass of clay interspersed between fine-grained (<<1 mm) plagioclase. Below the halo is the typical interior portion of Unit 1, which is a moderately to highly altered (10%-80%), amygdaloidal (~3%-5%), sparsely microphyric olivine-pyroxene basalt (Fig. 35) having an intergranular matrix. This basalt is dark gray (2.5G 4/0) and contains subrounded, light greenish-gray (2.5G 6/2; clay-filled) or, in a few places, white (2.5G 8/0; calcite-filled) amygdules. The microphenocrysts and amygdules are randomly distributed.

The orange, calcareous fragment enclosed in Unit 1 (Fig. 34) occurs at ~15 cm above the contact of Unit 1 with the underlying clayey bioclastic limestone. The fragment was probably plucked by the sill from the limestone during intrusion and was partially thermally metamorphosed. It has a narrow (~5-10 cm) alteration halo around it and, although badly deformed, still contains skeletal fragments and limestone nodules. However, in the interior of Unit 1, dark reddish-brown clay and irregular streaks of Fe-oxyhydroxides cemented with quartz (e.g., Fig. 35) are present in some places and invariably have alteration halos around them. These inclusions are mainly smectite and were interpreted as original clayey bioclastic limestone now completely thermally metamorphosed.

Unit 3 starts from ~850 mbsf (143-865A-92R-3, 68 cm) and ends at ~866 mbsf (143-865A-94R-2, 112 cm), with a total of 8.8 m recovered. Its actual contact with the overlying clayey bioclastic limestone was not sampled, but the top of the unit is a highly altered basalt that grades from dark grayish-green (2.5G 4/2) at the top to very dark gray (2.5 G 3/0) toward the bottom of the section. The unit then becomes very highly to almost completely altered basalt in the remainder of Core 143-865A-92R. This altered portion of Unit 3 is dark reddish-brown (5YR 3/2) that grades to dark reddish-gray (5YR 4/2) near the numerous (5%), thin (<3 mm), crosscutting fractures filled with Fe-oxyhydroxides (+ pyrite) and scattered green clays. This portion is soft and clayey, although it retains relict igneous texture with clay and Fe-oxyhydroxide (+ pyrite) pseudomorphs after amygdules and microphenocrysts set in a clayey groundmass.

Unit 3 is only moderately (10% to 40%) altered from ~853 to ~866 mbsf (entire Core 143-865A-93R and upper portion of Core 143-865A-94R). In fact, the majority of the vesicles in Unit 3 are coated only on their walls with green clay minerals and calcite, instead of being completely filled in as those in Unit 1 (compare Fig. 35 to Fig. 36). Also, instead of being dark gray as Unit 1, Unit 3 is dark bluish-gray (5B 4/1). Despite these differences, Unit 3 is still a variably microphyric olivine-pyroxene basalt having a microcrystalline, intergranular groundmass. Again, Unit 3 is underlain by a clayey bioclastic limestone, and its bottom contact shows alteration halos similar to those observed along the contacts of Unit 1.

The subvertical boundary of Unit 4 with the overlying clayey bioclastic limestone at ~867 mbsf (Interval 143-865A-94R-4, 0–55 cm) is irregular but sharp (Fig. 33) because of the quenching effect of the cold limestone on the presumably hot igneous intrusive. Neither the metasomatized sedimentary layer above Unit 1 nor the highly altered top portion of Unit 3 is present in Unit 4, and the alteration halo is also less pronounced in Unit 4 compared with those in Units 1 and 3. Similar to Unit 3, the vesicles in Unit 4 are only partially filled in with calcite and clay minerals, indicating that Unit 4 is less altered than Unit 1 and the top portion of Unit 3. Unit 4 is a moderately to highly microphyric olivine-pyroxene basalt having a microcrystalline, intergranular groundmass. Its bottom contact was not penetrated.

Petrography

At its freshest, the basalt is dark bluish-gray (5B 4/1) and is a variably microphyric rock in which two types of phenocrysts can be discerned in the hand specimen. A reddish-yellow (5YR 6/8) mineral is probably an alteration product of olivine, and a greenish (7.5G 5/4) mineral has been interpreted as a pseudomorph after clinopyroxene.

Table 5. Hydrocarbon gas data for Hole 865A.

Core, section, interval (cm)	Depth (mbsf)	Sample type	C_1 (ppm)
Hole 865A			
2R-3, 142–145	10.12	HS	4
3R-2, 0–3	16.20	HS	4
4R-3, 0–3	27.20	HS	4
5R-4, 0–3	36.85	HS	4
6R-2, 0–3	44.70	HS	4
7R-4, 0–3	55.79	HS	4
8R-2, 0–3	63.80	HS	4
9R-2, 0–3	73.30	HS	3
10R-CC, 10–13	81.90	HS	4
12R-CC, 10–13	101.30	HS	4
13R-5, 0–3	116.80	HS	4
14R-4, 0–3	125.00	HS	4
15R-5, 0–3	136.10	HS	3
16R-5, 0–3	141.10	HS	5
21R-CC, 0–3	168.81	HS	5
22R-CC, 0–3	178.40	HS	3
23R-CC, 0–3	188.00	HS	4
24R-CC, 0–3	197.70	HS	3
28R-1, 109–112	237.39	HS	4
29R-CC, 0–3	245.90	HS	3
51R-CC, 9–10	457.69	HS	3
52R-CC, 8–9	467.38	HS	3
53R-CC, 3–4	477.03	HS	3
54R-CC, 4–5	486.64	HS	4
55R-CC, 5–6	496.35	HS	3
56R-CC, 29–30	506.19	HS	4
58R-CC, 16–17	525.36	HS	3
59R-CC, 7–8	534.87	HS	4
64R-CC, 9–10	583.19	HS	4
66R-CC, 34–35	602.84	HS	4
68R-CC, 31–32	622.21	HS	3
70R-CC, 1–3	641.01	HS	3
72R-CC, 24–25	660.64	HS	4
73R-1, 20–21	670.30	HS	3
74R-1, 82–83	679.75	HS	3
75R-1, 80–82	690.20	HS	3
76R-1, 69–70	699.79	HS	3
78R-1, 70–72	719.01	HS	5
81R-1, 31–32	747.71	HS	4

HS = headspace vial.

Progressive alteration is most apparent toward fractures and some of the limestone inclusions. Intense alteration starts about 3 cm from the contacts and is marked by the onset of a paler color in the hand specimen and by gradual textural changes. Plagioclase becomes less clearly defined, and a network or mesh texture develops close to the contact: the olivine and pyroxene phenocryst pseudomorphs survive into the alteration zone.

Thin-section examination confirms that the ferromagnesian minerals have been almost completely pseudomorphed by clay minerals, talc(?), Fe-oxyhydroxides, and calcite. In one of the better preserved rocks from Unit 3 (Sample 143-865A-93R-3, 85–86 cm), no fresh olivine phenocrysts are seen and only about one-half of the clinopyroxene phenocrysts are preserved. Pseudomorphs after olivine make up about 5% of the total volume and range in size from 0.3 to 1.0 mm. Subhedral pseudomorphs after clinopyroxene phenocrysts (8%) are somewhat larger (0.5–3.0 mm). In contrast, plagioclase microphenocrysts (10%) are remarkably well preserved and are zoned within the range An_{70} to An_{60}. Although these plagioclase laths are small (0.3–1.0 mm), they have been treated as microphenocrysts because they are distinctly larger than the groundmass generation. In addition to plagioclase laths (35%), the matrix contains some fresh intergranular clinopyroxene (18%), opaque oxides including brown spinels in olivine pseudomorphs (7%), and traces of apatite. Clay minerals, probably mainly smectites, zeolites, and chlorite, as well as talc, pyrite, iron oxides, and calcite make up about 30% of this rock. Glass may have been present in the original rock, but is now completely converted to clay. Vesicles in this sample have been filled in with smectite and oolitic chlorite(?).

A very highly altered specimen (Sample 143-865A-91R-3, 51–52 cm, Piece 9), from an alteration halo in Unit 4 has had all its phenocrystic olivine and clinopyroxene completely pseudomorphed by clays, chlorite, calcite, and Fe-oxyhydroxides. Even some of the larger (>0.5 mm) plagioclase microphenocrysts have been severely saussuritized. The groundmass, which presumably contained glass originally, has been almost completely altered to clays, except for the tiny plagioclase laths that are also cloudy because of clay alteration. In contrast to the fresher sample described above, which has subhedral grains and feathery needles of opaque oxide minerals, the opaque minerals in this sample are rusty red and finely disseminated throughout. Some of these fine opaques are concentrated along the outlines of the phenocrystic pseudomorphs.

A well-preserved contact between Unit 4 and the clayey bioclastic limestone (Sample 143-865A-94R-4, 5–6 cm, Piece 1) shows that the basalt has a ~3-cm quenched zone, that together with the whole rock itself, has been very highly altered (see also, Fig. 33). Mineralogically, this basalt is very similar to the other two samples. The main differences, in addition to the quenched texture of the groundmass, are (1) that it is hyalomicrophyric and (2) that calcite predominates over clays as the main alteration/amygdaloidal mineral. Except for a thin (0.1-0.25 mm) sparry calcite rim, the effect of the basalt intrusion on the limestone appears to be minimal.

Geochemistry

Major and trace elements determined by X-ray fluorescence (XRF) spectrometry (see "Explanatory Notes" chapter, this volume) in five basalt samples (representing basalt Units 1, 3, and 4 from Hole 865A) are listed in Table 8. The basalts show large variations in their content of CaO (3.8–10.8 wt%), K_2O (1.1–2.6 wt%), Rb (10–42 ppm), Sr (490–860 ppm), and Zn (11–88 ppm) with the two samples from the highly altered Unit 1 (Samples 143-865A-90R-6, 105–107 cm, and -91R-1, 131–133 cm) generally showing the larger variations. These two samples also have higher loss on ignition (LOI) values (6.6 and 9.2 wt% vs 3.1–5.9 wt% for the other three samples); high LOI values are generally considered to have been caused by seawater alteration (e.g., Floyd and Castillo, 1992). Thus, the chemical variation of the basalts is most probably from alteration. Indeed, some of the known alteration-resistant elements generally exhibit small variability (e.g., TiO_2 = 3.4–4.0 wt%; Nb = 70–86 ppm; Y = 27–30 ppm; Zr = 350–380), suggesting that the three units are compositionally similar. Another characteristic geochemical feature of these basalts is that they are fairly primitive having high magnesium numbers (Mg# = 63–76) and Ni content (120–200 ppm). This suggests that some of the basalts must have experienced fairly limited magmatic differentiation on their way to the crust from their source in the mantle.

All samples plot above the line that separates Hawaiian alkalic and tholeiitic basalts (Fig. 37) and therefore are alkali basalts, which is consistent with their observed mineralogy. They overlap with some of the Hawaiian alkali basalts and with those from St. Helena, which are classified as moderately alkalic (Baker, 1969). Hole 865A basalts also overlap with the highly variably altered alkali basalts previously dredged from the surface of Allison Guyot (Natland et al., in press). The alkaline signature of the new samples is also supported by their trace-element data (Fig. 38). Similar to typical alkali basalts, their trace-element contents progressively increase with the degree of incompatibility relative to tholeiitic normal-mid-ocean ridge basalts (N-MORB); for example, the Jurassic MORB from the Pigafetta Basin to the northwest of Allison Guyot. Their overall trace-element pattern is very similar to that of the Allison surface samples (Natland et al., in press) despite the facts that Hole 865A basalts have more variable Rb and K_2O contents from alteration and the surface samples simply do not have some of these trace-element data (i.e., Zr, Ce, and

Table 6. Concentrations of total, inorganic, and organic carbon and total nitrogen and sulfur for Hole 865A.

Core, section, interval (cm)	Depth (mbsf)	Sample type[a]	Inorg. carbon (%)	Total carbon (%)	TOC (%)	$CaCO_3$ (%)	Nit. (%)	Sulf. (%)	TOC/N	TOC/S
143-865A-										
1R-1, 78–80	0.78	PP	9.08			75.6				
1R-2, 78–80	2.28	PP	8.84			73.6				
1R-3, 74–76	3.74	PP	9.56			79.6				
1R-3, 145–150	4.45	IWSC	11.65	11.13	0.52	92.7	0.43	0.00	1.2	
1R-4, 59–61	5.09	PP	8.60			71.6				
2R-1, 76–78	6.46	PP	8.20			68.3				
2R-2, 76–78	7.96	PP	9.02			75.1				
2R-3, 76–78	9.46	PP	10.44			87.0				
2R-3, 145–150	10.15	IWSC	11.80	11.69	0.11	97.4	0.04	0.00	2.7	
2R-4, 48–50	10.68	PP	10.67			88.9				
3R-1, 75–77	15.45	PP	10.69			89.0				
3R-1, 145–150	16.15	IWSC	11.85	11.75	0.10	97.9	0.05	0.00	2.0	
3R-2, 22–24	16.42	PP	10.36			86.3				
3R-CC, 4–6	16.68	PP	11.01			91.7				
4R-1, 75–77	24.95	IWSC	11.13			92.7				
4R-1, 75–77	24.95	PP	10.80			90.0				
4R-2, 75–77	26.45	PP	10.70			89.1				
4R-2, 145–150	27.15	IWSC	11.59			97.6				
4R-3, 55–57	27.75	PP	10.27			85.5				
5R-1, 50–52	34.20	PP	10.73			89.4				
5R-2, 30–32	35.00	PP	10.32			86.0				
5R-3, 82–83	36.10	PP	10.60			88.3				
5R-3, 152–157	36.80	IWSC	11.83	11.69	0.14	97.4	0.09	0.01	1.5	14.0
5R-4, 48–50	37.33	PP	10.86			90.5				
5R-5, 30–32	38.15	PP	10.72			89.3				
6R-1, 40–42	43.60	PP	11.35			94.5				
6R-1, 152–157	44.72	IWSC	11.91	11.69	0.22	97.4	0.06	0.00	3.6	
6R-2, 74–76	45.44	PP	10.30			85.8				
7R-1, 60–62	53.30	PP	10.54			87.8				
7R-1, 60–62	53.30	IWSC	11.38			94.8				
7R-2, 50–52	54.20	PP	10.90			90.8				
7R-3, 74–76	55.01	PP	10.34			86.1				
7R-3, 152–157	55.79	IWSC	11.76			98.0				
7R-4, 54–56	56.33	PP	10.54			87.8				
7R-5, 36–38	57.25	PP	10.74			89.5				
8R-1, 75–77	63.05	PP	10.89			90.7				
8R-1, 152–157	63.82	IWSC	11.80	11.74	0.06	97.8	0.05	0.00	1.0	
8R-2, 50–52	64.30	PP	10.76			89.6				
9R-1, 69–71	72.49	PP	10.66			88.8				
9R-1, 145–150	73.25	IWSC	11.91	11.69	0.22	97.4	0.08	0.00	2.7	
9R-2, 83–85	74.13	PP	10.24			85.3				
9R-3, 18–20	74.98	PP	10.36			86.3				
10R-CC, 7–9	81.87	PP	10.57			88.0				
12R-CC, 7–9	101.27	PP	10.46			87.1				
13R-1, 43–45	111.23	PP	9.87			82.2				
13R-2, 80–82	113.10	PP	10.78			89.8				
13R-3, 75–77	114.55	PP	10.66			88.8				
13R-4, 75–77	116.05	PP	9.92			82.6				
13R-4, 145–150	116.75	IWSC	11.97	11.75	0.22	97.9	0.08	0.00	2.7	
13R-5, 75–77	117.55	PP	10.25			85.4				
13R-6, 75–77	119.05	PP	10.70			89.1				
13R-CC, 4–5	120.38	PP	10.71			89.2				
14R-1, 75–77	121.25	PP	11.00			91.6				
14R-2, 78–80	122.78	PP	10.43			86.9				
14R-3, 78–80	124.28	PP	10.87			90.5				
14R-3, 145–150	124.95	IWSC	12.03	11.70	0.33	97.5	0.11	0.00	3.0	
14R-4, 78–80	125.78	PP	10.64			88.6				
14R-5, 77–79	127.27	PP	10.41			86.7				
15R-1, 122–124	131.32	PP	10.66			88.8				
15R-2, 124–126	132.84	PP	10.60			88.3				
15R-3, 118–120	134.28	PP	10.94			91.1				
15R-4, 120–122	135.80	PP	10.43			86.9				
16R-1, 75–77	135.85	PP	10.79			89.9				
15R-4, 145–150	136.05	IWSC	11.90	11.71	0.19	97.5	0.06	0.00	3.1	
15R-5, 80–82	136.90	PP	10.05			83.7				
16R-2, 40–42	137.00	PP	11.16			93.0				
15R-6, 81–83	138.41	PP	10.21			85.0				
16R-3, 75–77	138.85	PP	10.07			83.9				
15R-6, 147–150	139.07	IWSC	11.82	11.72	0.10	97.6	0.05	0.00	2.0	
15R-7, 49–52	139.59	IWSC	11.82	11.58	0.24	96.5	0.09	0.00	2.6	
16R-4, 75–77	140.35	PP	11.01			91.7				
16R-4, 140–150	141.00	IWSC	12.09	11.52	0.57	96.0	0.07	0.02	8.1	28.0
16R-5, 54–56	141.64	PP	10.01			83.4				
16R-5, 105–110	142.15	IWSC	11.85	11.58	0.27	96.5	0.02	0.00	13.0	

Table 6 (continued).

Core, section, interval (cm)	Depth (mbsf)	Sample type[a]	Inorg. carbon (%)	Total carbon (%)	TOC (%)	$CaCO_3$ (%)	Nit. (%)	Sulf. (%)	TOC/N	TOC/S
143-865A-										
23R-CC, 1–5	188.01	PP	11.86			98.8				
24R-CC, 3–6	197.73	IWSC	12.06	11.89	0.17	99.0	0.02	0.00	8.5	
28R-1, 89–93	237.19	PP	12.16	11.93	0.23	99.4	0.00	0.00		
28R-1, 112–115	237.42	IWSC	11.90			99.1				
30R-CC, 0–2	255.60	IWSC	12.18	11.93	0.25	99.4	0.02	0.00	12.0	
31R-CC, 0–2	265.20	PAL	11.89			99.0				
31R-CC, 12–15	265.32	IWSC	12.11	11.87	0.24	98.9	0.02	0.00	12.0	
34R-1, 30–35	294.50	PP	11.96			99.6				
34R-1, 94–98	295.14	IWSC	12.18	11.92	0.26	99.3	0.00	0.00		
36R-CC, 27–31	313.37	PP	11.86			98.8				
37R-CC, 0–2	322.80	IWSC	12.08	11.60	0.48	96.6	0.00	0.00		
38R-CC, 4–7	332.44	PP	11.90			99.1				
39R-CC, 10–13	342.00	IWSC	12.24	11.94	0.30	99.5	0.03	0.00	10.0	
40R-CC, 2–5	351.62	PP	11.88			99.0				
44R-CC, 1–5	390.11	PP	11.89			99.0				
45R-CC, 10–13	400.00	IWSC	12.31	11.94	0.37	99.5	0.01	0.00	37.0	
52R-CC, 1–5	467.31	PP	11.99			99.9				
58R-CC, 1–5	525.21	PP	11.79			98.2				
60R-CC, 6–8	544.56	PP	11.61			96.7				
66R-CC, 1–6	602.51	PP	11.92			99.3				
66R-CC, 10–12	602.60	PP	11.94			99.5				
71R-CC, 0–2	650.80	PAL	7.79	5.85	1.94	48.7	0.06	5.29	32.3	0.4
72R-CC, 28–29	660.68	PP	11.37			94.7				
73R-1, 56–66	670.66	PP	11.80			98.3				
74R-1, 0–5	679.70	IWSC	12.07	11.78	0.29	98.1	0.02	0.00	14.0	
74R-1, 5–6	679.75	PAL	10.60	8.52	2.08	71.0	0.05	2.85	41.6	0.7
74R-1, 33–36	680.03	PP	11.77			98.0				
76R-1, 70–75	699.80	IWSC	12.19	11.41	0.78	95.0	0.05	0.06	15.0	13.0
78R-1, 69–70	718.99	PAL	10.16			84.6				
78R-1, 70–75	719.00	IWSC	12.09	11.86	0.23	98.8	0.00	0.00		
79R-1, 35–40	728.45	IWSC	12.14	11.95	0.19	99.5	0.01	0.01	19.0	19.0
82R-1, 33–38	757.43	IWSC	12.23	11.85	0.38	98.7	0.01	0.00	38.0	
84R-1, 68–69	777.18	IWSC	12.29	11.93	0.36	99.4	0.01	0.06	36.0	6.0
86R-3, 8–10	798.84	PAL	9.19	6.70	2.49	55.8	0.05	11.8	49.8	0.2
87R-2, 51–54	807.31	PP	11.97	11.32	0.65	94.3	0.02	0.60	32.0	1.0
88R-1, 140–145	816.50	IWSC	11.69	10.17	1.52	84.7	0.01	2.20	152.0	0.7
89R-6, 11–13	831.48	BAU	6.53	3.17	3.36	26.4	0.05	11.6	7.2	0.3
92R-2, 58–60	849.21	BAU	35.60	0.21	35.39	1.7	0.29	4.8	122.0	7.4

[a] Samples: PP = physical property, IWSC = interstitial-water squeeze cake, PAL = paleontology, BAU = personal samples.

Nb). The Hole 865A basalt trace-element pattern also overlaps with the moderately alkalic St. Helena basalts (only those with >5 wt% MgO), except for the most incompatible elements, where the St. Helena samples are relatively less enriched.

Conclusions

Basalt was emplaced as a multiple sill and was intruded into wet, unconsolidated clayey, bioclastic limestone, implying that only a short time elapsed between the deposition of the sediment and the igneous intrusion. The soft consistency of the host rock is suggested by bulbous and irregular projections of sediment into basalt and vice-versa.

Both rock types show contact phenomena. The basalt has formed a chilled margin (~2 mm) against the sediment (e.g., Interval 143-865A-94R-4, 3–16 cm). However, more commonly, the basalt has been intensely hydrothermally altered, presumably during devolatilization of the wet sediment. Much of this alteration is concentrated along fractures that acted as pathways for the fluids driven from the sediment. The effect on the basalt is visible for a few cm on either side of these fractures. Intense alteration is also associated with inclusions of the sediment stopped by the basalt during intrusion.

The inferred prevalence of olivine and clinopyroxene phenocrysts in the rocks suggests that these are alkali basalts. This inference is supported by (1) the high contents of alkali elements in the samples and (2) the increase in concentration with increasing incompatibility of their trace-element contents relative to tholeiitic N-MORB. Excluding alteration effects, Hole 865A alkali basalts have a fairly uniform composition, and some of them are undifferentiated; they are similar to the basalts dredged from the surface of Allison Guyot.

No other igneous rocks were encountered in Hole 865A and only slight traces of volcanogenic minerals could be seen in one or two of the sedimentary horizons (see "Lithostratigraphy" section, this chapter). Although clearly a terrigenous component exists in the mudstones of lithologic Unit IV, no evidence can be found to suggest the proximity of an active volcano. The sills may represent a late pulse of igneous activity following the cessation of the major phase of volcanism at Allison, similar to the post-erosional volcanic stage of Hawaiian volcanism (Macdonald, 1968). This would indicate that the volcanic basement of Allison Guyot is just a few meters or tens of meters below the sills. Alternatively, the sills were formed in an appreciably later magmatic episode, perhaps unrelated to the construction of Allison seamount. The presumed volcanic basement of Allison Guyot therefore might lie at significantly greater depth than that attained in Hole 865A.

PHYSICAL PROPERTIES

Introduction

The objectives of the physical property measurement program at Site 865 were (1) to measure standard shipboard physical properties as index properties, to analyze *P*-wave velocities in lithified sedi-

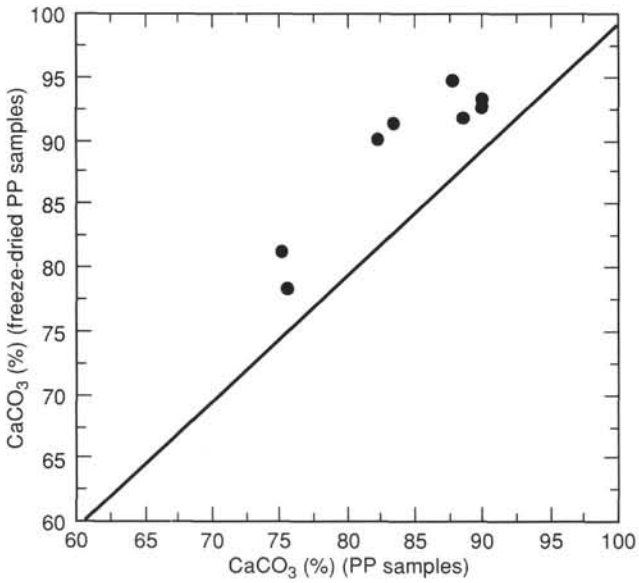

Figure 26. Carbonate content in PP samples vs. carbonate content in the same samples that were freeze-dried for 12 hr.

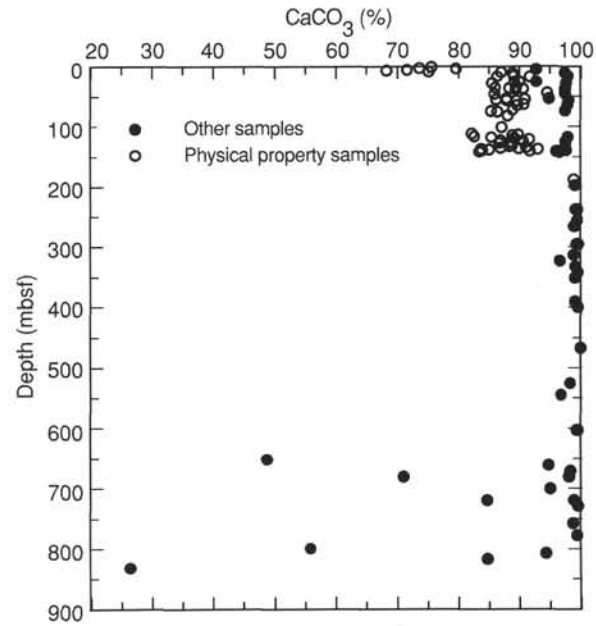

Figure 27. Vertical distribution of $CaCO_3$ concentrations at Hole 865A (open circles represent PP samples from soft sediment).

ments (carbonate platform succession), basalts, and unlithified sediments, to measure thermal conductivity, and to collect GRAPE density, *P*-wave velocity, and magnetic susceptibility readings from the multisensor track (MST); (2) to identify physical property units for correlation among holes and downhole logs at Leg 143 sites. The last objective includes the detailed comparison of the downhole logs (sonic velocity, gamma ray, and density) with measurements of *P*-wave velocity and bulk density of discrete samples to estimate to what extent the recovered sediments represent the sedimentary record present in the boreholes.

Sediments recovered at Site 865 comprise unlithified pelagic ooze (0–139.7 mbsf), lithified shallow-water carbonate platform sediments (139.7–837.6 mbsf), and mixed carbonates and basalt (837.6–870.9 mbsf). The platform limestones vary from lime mudstone to wackestone with local bioclasts (gastropods and rudists), silt to fine sand-sized peloidal packstone and coarse sand-sized skeletal to peloidal grainstone. Below 621.9 mbsf, the limestones show a downhole increase in clay content and organic material.

The pelagic sediments recovered at Holes 865A, 865B and 865C showed indication of coring disturbance (liquefaction and fluidization). This disturbance inhibited reliable measurements of *P*-wave velocity on the MST and the *P*-wave logger (PWL), and thermal conductivity meter. Readings from the MST for *P*-wave velocity as well as discrete measurements made by employing the P-wave logger showed velocities close to that of normal sea water, and consequently were regarded as unreliable. Discrete measurements of index properties, bulk density, porosity, water content (expressed as a percentage of the dry sample weight), and grain density (see "Explanatory Notes" chapter, this volume), in Hole 865A, however, seemed to be in good agreement with the GRAPE density logs. In the lithified platform sediments, cored with the rotary core barrel (RCB), *P*-wave velocity was measured in both longitudinal and transverse directions where recovery allowed. In addition, index properties and carbonate content were analyzed.

Laboratory measurements of *P*-wave velocity and index properties could be correlated only on a gross scale because the data set collected from the entire platform section was sparse. Good correlation requires a large number of laboratory measurements on all lithologies making up the sedimentary section. Logging results, on the other hand, are of good quality and continuous from approximately 100 mbsf downwards and allow tentative conclusions about the representiveness of the recovered sediment and the correlation between seismics, well logs and rock.

Physical Property Units

Good core recovery in the pelagic cap (0 to 139.7 mbsf), especially in Holes 865B and 865C, allowed close-spaced sampling (one per section) for index properties and carbonate content. Hole 865C was especially dedicated to shore-based paleontologic analyses and therefore not analyzed for physical properties other than the GRAPE density. The number and quality of the samples (and data set as a whole) decreased significantly below 139.7 mbsf because of poor recovery (on average less than 5%) in the shallow-water carbonates.

Acoustic compressional velocity was measured with the digital sound velocimeter (DSV) and Hamilton frame systems (see "Explanatory Notes" chapter, this volume). Measurements made using the *P*-wave logger and the MST in the pelagic sediments were rendered unreliable by coring disturbance. *P*-wave measurements were nevertheless obtained with the DSV (Table 9). *P*-wave velocities on the lithified sediments below 139.7 mbsf were made using the Hamilton frame. Overall, data from acoustic velocity and index properties are sparse.

Four major physical property (PP) units were defined for Site 865 based on significant downhole trends in index properties and *P*-wave values (Tables 10 and 11, Figs. 39 through 42). The upper boundaries of most of these PP units are associated with lithologic features (see Fig. 43), depositional age (Fig. 44, pelagic sediments), and/or units derived from the well logs (Fig. 45). These features did not serve as definition criteria for PP units. Note that owing to low recovery, most boundaries for PP units have been arbitrarily placed midway between isolated samples, in some places tens of meters apart.

Physical Property Unit 1 (0–139.7 mbsf)

Mass-index properties in the upper 139.7 mbsf (lithologic Unit I) show small but subtle variations in bulk density, porosity and water content (Figs. 39 and 41). Porosity in Hole 865A varies from 46 to 78.3%, bulk density ranges from 1.43 to 1.82 g/cm^3, and water content ranges from 127.6 to 38.7% dry weight. Porosity in Hole 865B ranges from 52 to 79.6%, bulk density ranges from 1.41 to 1.88 g/cm^3, and

Table 7. Concentrations of total, inorganic, and organic carbon and total nitrogen and sulfur for Holes 865B and 865C.

Core, section, interval (cm)	Depth (mbsf)	Sample type[a]	Total carbon (%)	Inorg. carbon (%)	TOC (%)	$CaCO_3$ (%)	Nit. (%)	Sulf. (%)	TOC/N	TOC/S
143-865B-										
1H-2, 73–74	2.23	CARB		11.30		94.1				
1H-4, 73–74	5.23	CARB	11.57	11.19	0.38	93.2	0.01	0.12	38.0	3.1
1H-6, 30–31	7.80	CARB		11.51		95.9				
1H-6, 80–85	8.30	IWSC	12.07	11.71	0.36	97.5	0.00	0.01		36.0
2H-2, 71–72	10.71	CARB		11.34		94.5				
2H-4, 72–73	13.72	CARB	11.74	11.38	0.36	94.8	0.01	0.06	36.0	6.0
2H-5, 145–150	15.95	IWSC	12.03	11.76	0.27	98.0	0.01	0.01	27.0	27.0
2H-6, 31–32	16.31	CARB		11.63		96.9				
3H-1, 75–76	18.75	CARB		11.45		95.4				
3H-3, 67–68	21.67	CARB	11.69	11.48	0.21	95.6	0.01	0.14	21.0	1.5
3H-5, 74–75	24.74	CARB		11.56		96.3				
3H-6, 145–150	26.95	IWSC	12.03	11.82	0.21	98.5	0.01	0.00	21.0	
3H-7, 20–22	27.20	CARB	11.65	11.63	0.02	96.9	0.01	0.00	2.0	
4H-1, 86–87	28.36	CARB		11.56		96.3				
4H-3, 75–76	31.25	CARB	11.63	11.53	0.10	96.0	0.00	0.03		3.3
4H-5, 86–87	34.36	CARB		11.52		96.0				
4H-5, 145–150	34.95	IWSC	12.01	11.68	0.33	97.3	0.01	0.00	33.0	
5H-2, 118–119	39.68	CARB		11.57		96.4				
5H-4, 76–77	42.26	CARB	11.62	11.58	0.04	96.5	0.00	0.00		
5H-4, 145–150	42.95	IWSC	11.86	11.72	0.14	97.6	0.00	0.00		
5H-6, 29–30	44.29	CARB		11.49		95.7				
6H-2, 70–71	48.70	CARB		11.61		96.7				
6H-3, 75–76	50.25	CARB	11.50	11.47	0.03	95.5	0.00	0.07		0.4
6H-4, 51–52	51.51	CARB		11.62		96.8				
6H-5, 128–129	53.78	CARB	11.80	11.58	0.22	96.5	0.00	0.00		
6H-5, 145–150	53.95	IWSC	12.01	11.70	0.31	97.5	0.00	0.05		6.2
7H-2, 110–112	58.60	CARB	12.31	11.66	0.65	97.1	0.00	0.00		
7H-2, 145–145	58.95	IWSC	12.07	11.66	0.41	97.1	0.00	0.00		
7H-4, 55–56	61.05	CARB	11.74	11.64	0.10	97.0	0.00	0.02		5.0
8H-1, 114–115	66.64	CARB		11.71		97.5				
8H-3, 110–111	69.60	CARB		11.61		96.7				
8H-5, 89–90	72.39	CARB	11.71	11.53	0.18	96.0	0.00	0.00		
8H-5, 145–150	72.95	IWSC	11.82	11.73	0.09	97.7	0.00	0.00		
9H-1, 75–76	75.75	CARB		11.62		96.8				
9H-3, 77–78	78.77	CARB	11.76	11.50	0.26	95.8	0.00	0.00		
9H-5, 78–79	81.78	CARB		11.57		96.4				
9H-5, 145–150	82.45	IWSC	11.94	11.77	0.17	98.0	0.00	0.01		17.0
10H-2, 76–77	86.76	CARB		11.21		93.4				
10H-4, 30–31	89.30	CARB	11.65	11.62	0.03	96.8	0.00	0.00		
10H-4, 145–150	90.45	IWSC	11.87	11.76	0.11	98.0	0.00	0.02		5.5
11H-1, 76–77	94.76	CARB		11.51		95.9				
11H-3, 76–77	97.76	CARB	11.85	11.11	0.74	92.5	0.01	0.00	74.0	
11H-5, 75–76	100.75	CARB		11.32		94.3				
12H-1, 61–62	104.11	CARB		11.50		95.8				
12H-3, 79–80	107.29	CARB	11.72	11.59	0.13	96.5	0.00	0.00		
12H-5, 57–58	110.07	CARB		11.54		96.1				
12H-5, 145–150	110.95	IWSC	11.85	11.39	0.46	94.9	0.00	0.00		
13H-1, 52–53	113.52	CARB		11.48		95.6				
13H-3, 76–77	116.76	CARB	11.98	11.69	0.29	97.4	0.00	0.00		
13H-5, 60–61	119.60	CARB		11.60		96.6				
13H-5, 145–150	120.45	IWSC	11.80	11.46	0.34	95.5	0.00	0.00		
14H-2, 74–75	124.74	CARB		11.46		95.5				
14H-3, 145–150	126.95	IWSC	11.98	11.97	0.01	99.7	0.00	0.00		
14H-4, 70–71	127.70	CARB	11.85	11.43	0.42	95.2	0.00	0.00		
14H-5, 145–150	129.95	IWSC	11.75	11.37	0.38	94.7	0.00	0.00		
14H-6, 20–21	130.20	CARB		11.52		96.0				
15X-1, 145–150	133.45	IWSC	11.99	11.99	0.00	99.9	0.00	0.00		
15X-2, 72–73	134.22	CARB	11.78	11.50	0.28	95.8	0.00	0.01		28.0
15X-2, 145–150	134.95	IWSC	11.63	11.53	0.10	96.0	0.00	0.00		
143-865C-										
1H-1, 90–95	2.40	IWSC		11.57		96.4				
3H-2, 145–150	15.75	IWSC		11.72		97.6				
4H-2, 145–150	25.25	IWSC		11.83		98.5				

[a] Samples: CARB = carbonate: IWSC = interstitial-water squeeze cake.

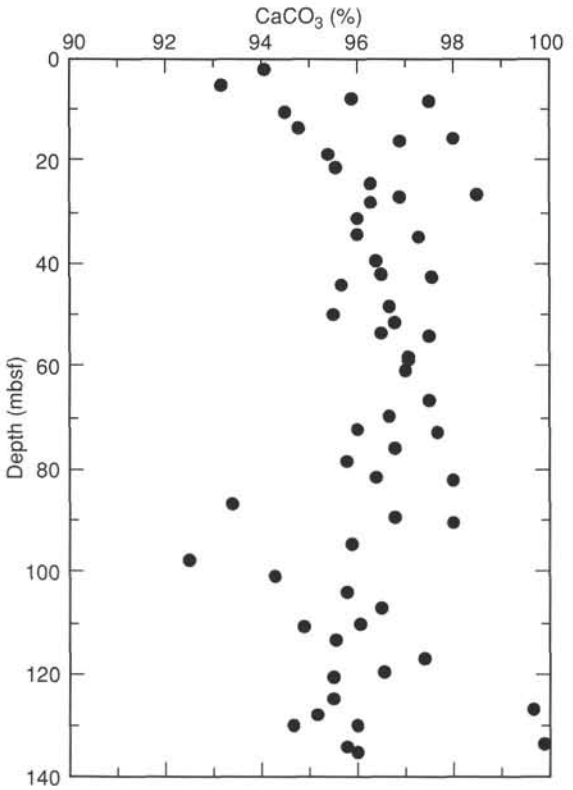

Figure 28. Vertical distribution of $CaCO_3$ concentrations at Hole 865B.

water content varies from 39.5 to 132.4% dry weight. Pelagic sediments are nearly one-hundred percent $CaCO_3$; carbonate content ranges from 92.5 to 98.5% in Hole 865B. The values of 68.3 to 94.5% for Hole 865A are erroneous owing to problems with the analytical procedures (see "Organic Geochemistry" section, this chapter). Although recovery rates in Hole 865A were lower than those in Hole 865B, the S-shaped curve in bulk density, porosity and water content is apparent and reflected in the GRAPE-density curves (Fig. 42). Holes 865A, 865B and 865C are only tens of meters apart, so their GRAPE-density curves are nearly identical. Physical property Subunit 1a (0 to about 10–15 mbsf) shows a substantial shift in bulk density, porosity and water content with respect to the underlying, denser, pelagic sediments, PP Subunit 1b. From about 10 to 15 mbsf down to approximately 70 mbsf, bulk density shows a gradual increase. From about 70 to 75 mbsf, bulk density decreases and resumes its downward gradual increase from about 90 to 95 mbsf.

Physical Property Unit 2 (139–650 mbsf)

The top of this unit shows a dramatic downward change in both index properties and acoustic velocity that corresponds to the change from lithologic Unit I to lithologic Unit II (see Fig. 45). No differentiation in physical properties could be made between the karstic limestones of lithologic Subunit IIA and the facies in Unit III. The lower boundary of PP Unit 2 has been arbitrarily chosen at 650 mbsf, between two sample points almost 60 m apart, and shows a significant change in velocity that may reflect the downward increase in clay content. This boundary correlates with the lithologic transition from Units III to IV. Overall, data coverage is poor owing to low recovery rates, generally less than 2%. Based on the range in sonic velocity and index properties, two PP subunits were recognized.

Physical Property Subunit 2a (139–490 mbsf)

P-wave velocities in this predominantly mollusk-rich (rudists and gastropods) lime wackestone to mudstone range from 4.11 to 5.62 km/s. Bulk density ranges from 2.33 to 2.68 g/cm^3, porosity from 2.81 to 23.14% and water content from 1.06 to 11.05% (dry weight). Carbonate content for these carbonate platform limestones varies between 98.79 to 99.87%, indicating nearly pure carbonate. Most velocity measurements were from unoriented samples (see Fig. 46). Owing to the sparse data it was difficult to achieve better correlation with the lithology.

Subunit 2b (490–650 mbsf)

P-wave velocities in PP Subunit 2b show a wider range than those in Subunit 2a; from 2.05 to 5.17 km/s. This latter high velocity was measured in a dense, 2.60 g/cm^3, lime mudstone, rich in sponge spicules and possibly indicative of a sponge mound facies. Bulk densities range from 2.25 to 2.60 g/cm^3, porosity from 5.97 to 25.77%, and water content from 2.35 to 12.91%. Carbonate contents vary between 96.71 and 99.71%. Velocity analyses were mostly unoriented owing to low recovery. The change in physical properties from Subunit 2a to Subunit 2b, a decrease in *P*-wave velocity, may be correlated to an increase in micro-porosity. Either the dolomitization or formation of micro-molds by leaching may be a cause for this change.

Physical Property Unit 3 (650–837.9 mbsf)

Physical property Unit 3 correlates well with lithologic Subunits IVA through IVC, which are all characterized by increased clay content and the presence of dolomite. Longitudinal-wave velocity ranges from 2.26 to 3.14 km/s. Bulk densities vary from 2.29 to 2.51 g/cm^3, porosity ranges from 10.42 to 22.64%, and water content ranges from 4.29 to 12.10% (dry weight). Overall, range and mean values of velocity and bulk density are significantly lower than those for Unit 2.

Physical Property Unit 4 (837.6–870.9 mbsf)

The top of PP Unit 4 is clearly defined and reflects the change from lithologic Subunits IVA through IVC, clayey dolomitic lime wackestone to packstone, into lithologic Subunit IVD, mixed clayey bioclastic wackestone to packstone and basaltic intrusions. Limestones have *P*-wave velocities of about 3.3 to 3.4 km/s, basalts have velocities ranging from about 2.8 to 4.9 km/s. The latter show considerable differences between velocities measured in transverse and longitudinal directions. In addition, differences show between *P*-wave velocities measured in fresh and altered basalt lithologies. Values for anisotropy in the basalts range from 5.61% to 11.57%, *P*-wave velocity in fresh basalt ranges from 4.49 to 4.85 km/s and in altered basalt ranges from 2.80 to 3.41 km/s.

Thermal Conductivity

Thermal conductivity was measured in samples from Holes 865A and 865B, using the needle-probe method in the full-space mode for the unlithified to semi-lithified pelagic sediments (0–139.7 mbsf). Measurements were restricted to core sections that showed little mechanical disturbance. Thermal conductivity in Holes 865A and 865B ranges from 0.97 to 1.329 W/(m · K), which is in agreement with values expected for unlithified pelagic ooze. No significant trends are visible in the data set. All thermal conductivity values obtained are listed in Table 12.

Discussion

The distribution of physical properties with depth is a key to understanding the correlation between seismics, well-log data, and the recovered lithologic record or depositional history of the sediments at the Site.

Recovery in the pelagic sediments in Hole 865A was relatively poor, but improved significantly by Holes 865B and 865C. Bulk

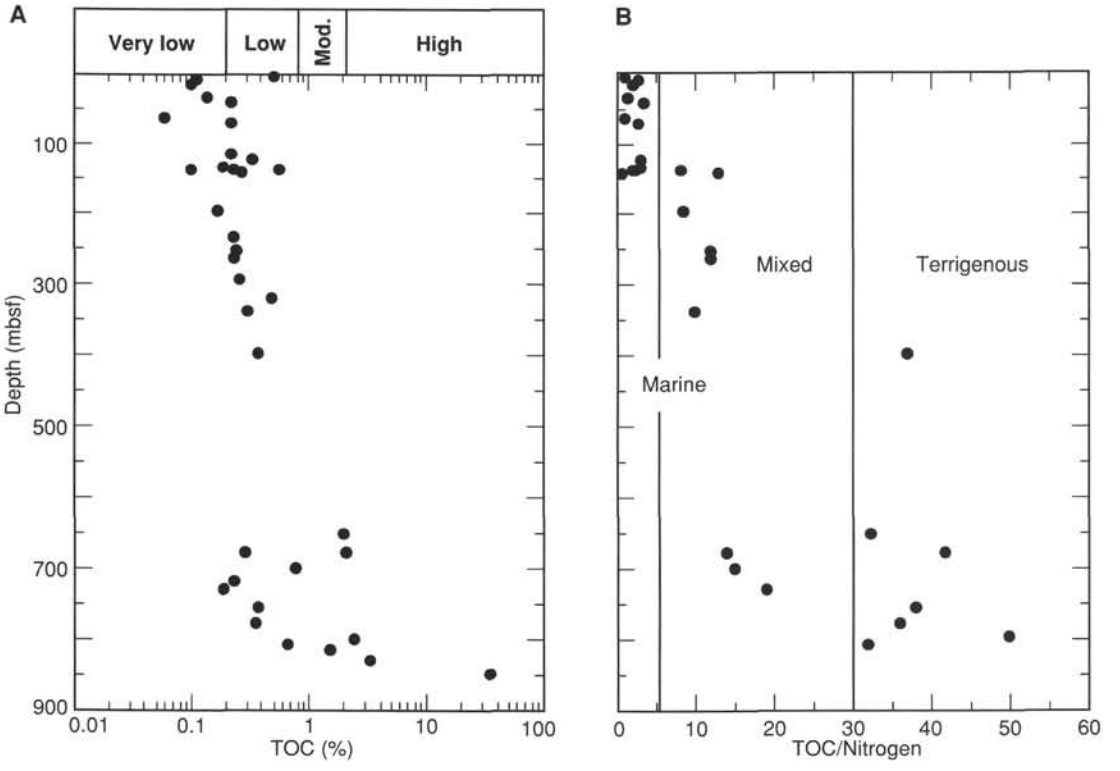

Figure 29. Distribution with depth of concentrations of total organic carbon (**A**) and nitrogen (**B**) at Hole 865A.

density measured on discrete samples and GRAPE-density measured by the MST in Holes 865A, 865B and 865C show comparable ranges in value and have a similar S-shaped curve (see Figs. 39 through 41). Values of discrete bulk density measurements generally are up to about 5% to 10% lower than those measured by the MST, which may be related to an incipient loss of water during and immediately after sampling. Figure 44 compares GRAPE-density from Holes 865A, 865B and 865C with depositional age. If the biostratigraphic dates are correct, differences in bulk density could be related to rates of deposition.

Unfortunately, recovery in the shallow-water limestone and mixed basalt limestone in Hole 865A was poor (see Fig. 45), casting doubt on the assumption that the recovered sediments are representative of the entire rock sequence. The comparison between sonic velocity of the recovered samples, the recovery plot and the sonic well log, strongly suggests that only the high-velocity and dense lithologies were recovered. Especially in the zone between 139.7 and 361.2 mbsf, it is estimated that less than 3% of the lithologic succession was recovered. Therefore, the prominent change in acoustic velocity and density visible on the sonic well-log (at 360 mbsf) could not be identified (and analyzed) in the recovered rock samples. For the same reasons it was not possible to identify, in terms of physical-property measurements, the more subtle, and higher-frequency, rhythms present in the sonic log between 310 and 830 mbsf, which display a distinct increase upward in acoustic velocity. The shift in sonic velocity and index properties at 360 mbsf, however, correlates with a change in lithology and the boundary between lithologic Subunits IIIA and IIIB (see Fig. 45).

Between about 650 and 837.6 mbsf, sonic velocity shows a narrower range, most likely related to elevated clay content and/or increased micro-porosity caused by leaching of the silt- to sand-sized skeletal fraction or recrystallization by dolomitization. The cross plot in Figure 46 clearly demonstrates that, although Lithologic Subunits IIA and IIB have comparable bulk densities, there is a significant difference in sonic velocity.

With the first occurrence of basalts, below 837.6 mbsf, the variation in density and sonic velocity increases again. As suggested by Busch et al. (in press), fresh basalts have higher sonic velocities, up to 5 km/s, than altered basalts, up to about 3.5 km/s.

The correlation between compressional-wave velocity and bulk density measured in discrete samples shown in Figure 46 (samples grouped into PP units) shows the overlap between PP Subunit 2b and Units 3 and 4, and the isolated position in the data set of PP Subunit 2a. The sediment fabric of PP Unit 2 samples is generally tight and dense wackestone or packstone, with low porosities, averaging 12.6%. Sediment fabrics of PP Units 3 and 4 have slightly higher porosities (16.3%) or in addition, increased clay content (up to 5%–8% insoluble residue). Whether porosity, clay content, or leaching/dolomitization controls the observed differences in sonic velocity remains uncertain. We suggest that the transition between PP Subunits 2a and 2b should produce an impedance change that must have a correlatable reflector in the seismic record (see "Seismic Stratigraphy" section, this chapter). In addition, the transition between PP Units 3 and 4, between carbonates and mixed carbonates-basalt (lithologic Subunits IVC and IVD) at the base of Hole 865A, is suggested to have a correlatable reflector on the seismic record. However, this is not necessarily the transition from sediment into true volcanic basement.

DOWNHOLE MEASUREMENTS

Introduction

Wireline measurements were conducted at this site to measure the in situ properties of sediments within the lagoonal/backreef sediments. Hole 865A, which penetrated 870.9 meters of calcareous oozes, wackestones and packstones, and basalts at Allison Guyot, was the only hole logged at Site 865. We positioned the bottom of the drill pipe at 102.5 mbsf and good logs were obtained within the open borehole between 102.5 and 867 mbsf. Five tool strings were run during the logging program at Hole 865A, including the sonic-porosity-density-

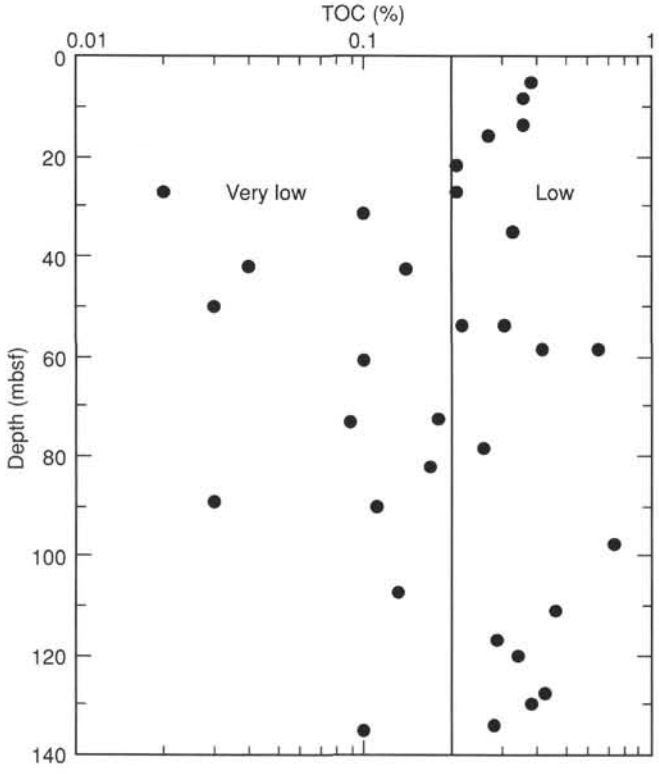

Figure 30. Distribution with depth of concentrations of total organic carbon at Hole 865B.

gamma-ray, the resistivity-gamma-ray, the geochemical tool string, the Japanese downhole magnetometer, and the FMS tool string (see "Operations" section, this chapter, Table 1).

Reliability of Logs

The log data from Hole 865A cover the interval from the bottom of the drill string (102.5 mbsf) to near the base of the hole, at 867 mbsf. All except the geochemical data are of high quality; no valid data were recorded by the GST tool because of mechanical problems with the tool. Hole size is the most important control on accuracy of the logs in Hole 865A. Two caliper logs were obtained on two separate runs: the lithodensity-tool caliper, and the four-arm caliper of the FMS. The two give generally similar results, except that the FMS caliper has a maximum opening of 16 in (40.64 cm), and the lithodensity caliper measures to a maximum of 18 in (45.7 cm). Large hole diameters (>17 in or 43.16 cm) over 20–35 meter intervals account for questionable FMS and density/porosity data from these zones. Most other logs do not require pad contact and therefore are less sensitive to the changes in borehole size.

Some occurrence of either cycle skipping or noise interference can be seen in the sonic velocity log data. The noise problems are predominantly localized to specific depths (191–232, 253–263, and 341–351 mbsf) and we anticipate that many of the problems with noise can be overcome by close examination of sonic waveforms after the cruise.

Each log was shifted in depth, by correlating the gamma-ray logs between runs, to correct for differences in the stretch of the logging cable. All logs were then corrected to the base of the drill pipe by subtracting the depth from rig floor to sea floor (1529 m). These depths should be accurate to within ±2 m.

Depths for the temperature tool were determined using the pressure recorded in the instrument and a depth vs. pressure table derived from pressure readings at depths noted during logging.

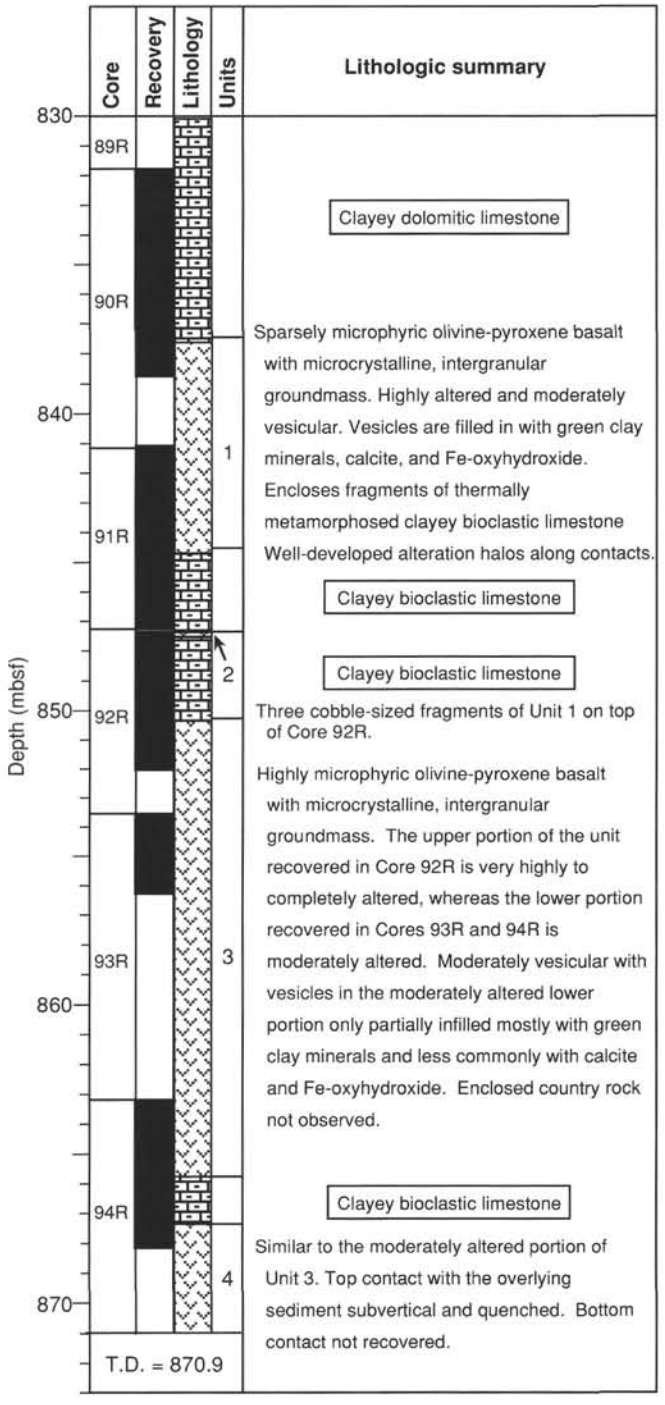

Figure 31. Summary of lithostratigraphy of igneous rocks in Hole 865A.

Velocity, Resistivity, and Density Relationships

Increases in velocity and resistivity with depth do not follow a simple compaction profile (Fig. 47), suggesting that diagenesis and grain-size variation influence porosity much more than does mechanical compaction. Although we were unable to find comparable data for near-reef carbonates, velocity and density values within the open-hole logged interval are much greater than those normally observed in terrigenous or calcareous sediments at comparable depths. Average velocity increases from 1.65–1.7 km/s at 80 mbsf, to 2.8–3.1 km/s at

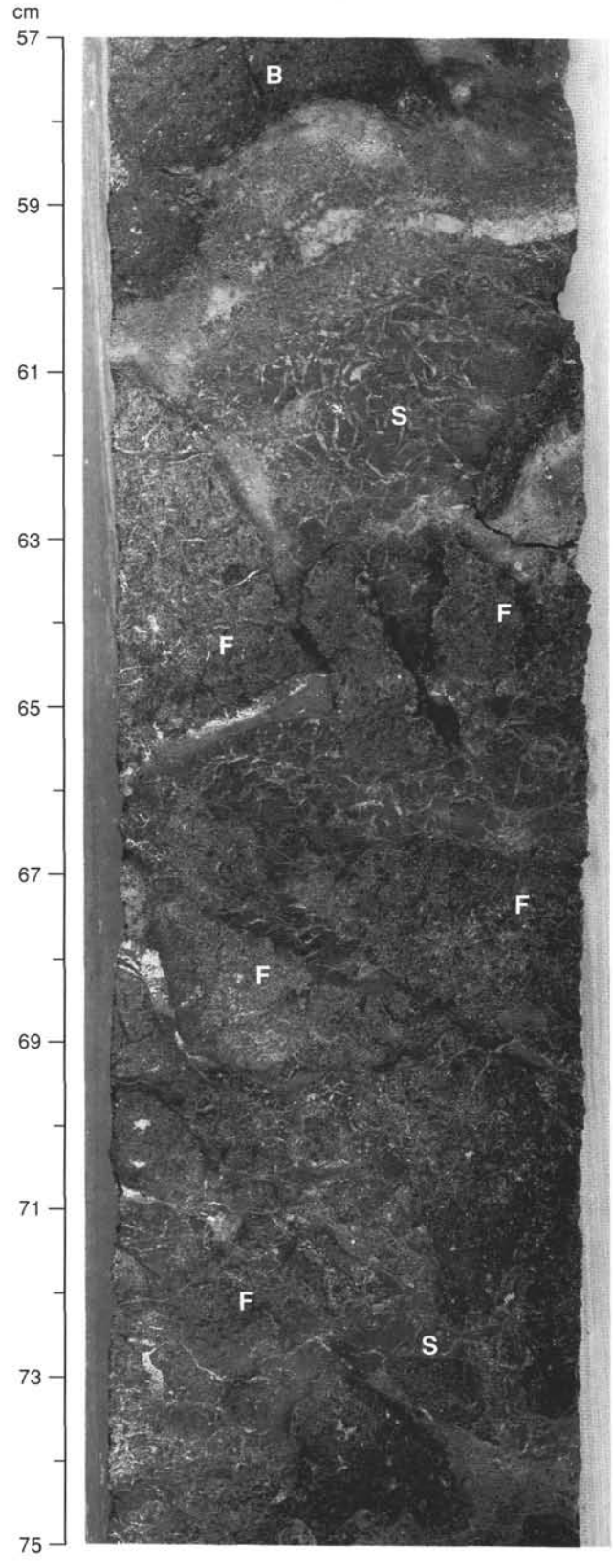

Figure 32. Well-indurated lower portion of the decarbonated, metasomatized clayey dolomitic limestone layer at the top of basalt Unit 1. Highly altered Unit 1 fragments of various sizes and shapes (F; relatively darker shade) are set in the sedimentary matrix of the decarbonated layer (S; lighter shade and with desiccation cracks filled with white, secondary calcite). The quenched, highly irregular margin of Unit 1 (B) is shown at the bottom of the photo (Interval 143-865A-90R-5, 57–75 cm).

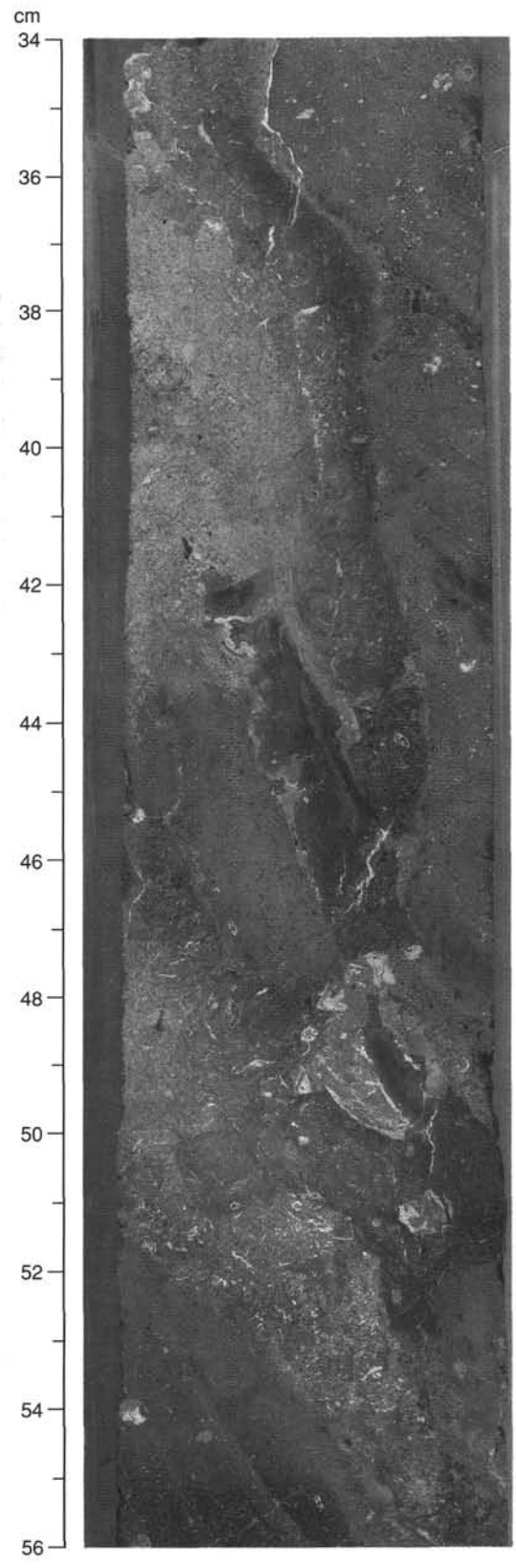

Figure 33. Vertical contact between basalt Unit 4 and the clayey bioclastic limestone showing that Unit 4 sends irregular tongues into the limestone. The margin of Unit 4 is quenched, whereas the portion of the limestone in contact with the basalt is thermally metamorphosed (Interval 143-865A-94R-4, 34–56 cm).

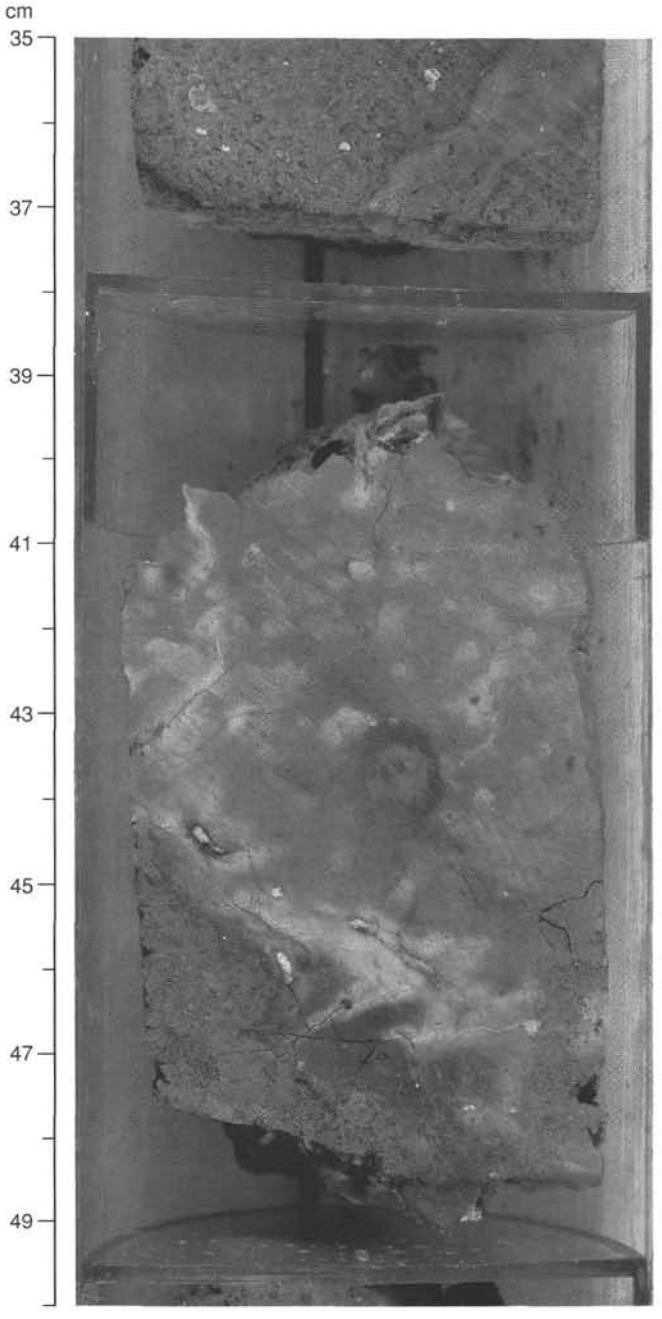

Figure 34. A fragment of clayey bioclastic limestone enclosed in Unit 1 showing relict outlines of fossils and burrows (white, subrounded to elongated areas in the lighter-colored rock). The alteration halo in Unit 1 along the contact is also shown (Interval 143-865A-91R-3, 35–50 cm).

380 mbsf, compared with typical values for these depths of 1.55–1.60 and 1.9–1.95 km/s, respectively (Hamilton, 1979). The Hole 865A velocities may be higher because the reef-derived component adds rigidity to the matrix. Similarly, density increases in a stepwise fashion from 1.45 g/cm^3 at 80 mbsf to about 2.2 to 2.25 g/cm^3 at 380 mbsf, compared to typical values for these depths of about 1.64 and 1.98 g/cm^3 (Hamilton, 1976).

The interval logged below 138 mbsf exhibits a very complex character, apparently with substantial changes involving varying degrees of compaction and cementation in addition to facies changes. Several zones exist in which resistivity and velocity decrease with depth, contrary to the normal compaction profile. This agrees with drilling results, where soft intervals were encountered below hard layers, resulting in poor core recovery.

A detailed investigation of the resistivity data can be made when viewed at a more suitable scale as shown in Figure 48, where the sonde with the shallowest depth of investigation (SFLU) can be seen to have the highest resolution but generally lower values than the medium and deep phasor induction resistivity sondes, which have greater depths of investigation. The differences between the three resistivity log types are attributable to the different depth responses of the three readings. The effect is accentuated by the large hole diameter. Given that the resistivity of formation water is similar to that of seawater, this suggests that resistivity increases with distance away from the borehole sondes because of the large diameter of the borehole. Thus, logs with the most depth of penetration will provide the most reliable data when the beds are thick, but all values are likely to be degraded in the presence of thin beds.

Velocity, resistivity and density logs are moderately well correlated with the gamma-ray log (SGR in Fig. 49). Thin beds occur within the logged interval both as isolated units and as apparent intercalations of high and low resistivity "beds." In the upper portion of the logged hole (100–555 mbsf) sharp maxima in velocity, density and resistivity at 241.7, 303.4, 422.5, and 552.7 mbsf correspond to lows in porosity and gamma, locating what are probably thin, highly dolomitized beds. The FMS has the highest resolution of any resistivity device currently available and is able to delineate these thin beds to a precision of about 10 mm, which is enough to provide reliable geological information regarding structure in addition to qualitative changes in borehole-wall resistivity. The FMS record and expanded log plots in Figure 50 highlight sharply defined bedding that brackets a minor change in lithology within a broad trend. If this is the case, we have an example of a lithologic unit (from about 296–304 mbsf) that has widely varying properties, in this case, mainly cementation variations.

In the lower portion of the hole (below 555 mbsf) gamma-ray maxima correspond to velocity maxima and resistivity and porosity minima, all of which correspond to increased pyrite and/or lignite content in the clays relative to adjacent strata. Gamma-ray counts (Fig. 49) ranging from 3 to more than 40 confirm a pattern of increasing clay content downhole as well as the presence of alternating strata with high and low clay contents. Potassium values decrease downhole, from values in the range of 0.1 to 1%, until basalt was encountered at 842 mbsf. This may indicate the presence of illite (3–8% potassium; Serra, 1986) as a significant constituent of the clays in the upper units. Thorium increases by a factor of two, while the trend follows that of the total gamma-ray counts.

Density values have been slightly degraded by large hole size, which can be seen in the caliper log (Fig. 47); this is unfortunate, but confirms that substantial petrophysical changes occur within this interval. Apparent neutron porosity values, ranging from 1 to 50% (Fig. 51), are also affected by the large changes in borehole size.

The log "Thin Layer Ratio" (Fig. 51) provides a quantitative indicator of the frequency of thin beds. This log delineates thin, resistive layers by taking a ratio of the shallow, high-resolution SFLU and the more deeply penetrating, but lower-resolution induction log. "Thin R" is seen as sensitive to instantaneous changes in resistivity caused by high-contrast thick beds, in addition to thin beds that are outside the resolving power of the measurements. Thin beds are plentiful in the intervals where the borehole diameter is less than 42 cm (16.5 in.) (289 to 370 and 726 to 760 mbsf, and below 837 mbsf).

Temperature

The Lamont temperature tool was run at the bottom of the geophysical tool string to determine equilibrium temperatures in the hole. The temperature data was recorded from sea floor to 869.6 mbsf at a speed of 1400 m/hr in a downhole direction, with one three-minute station

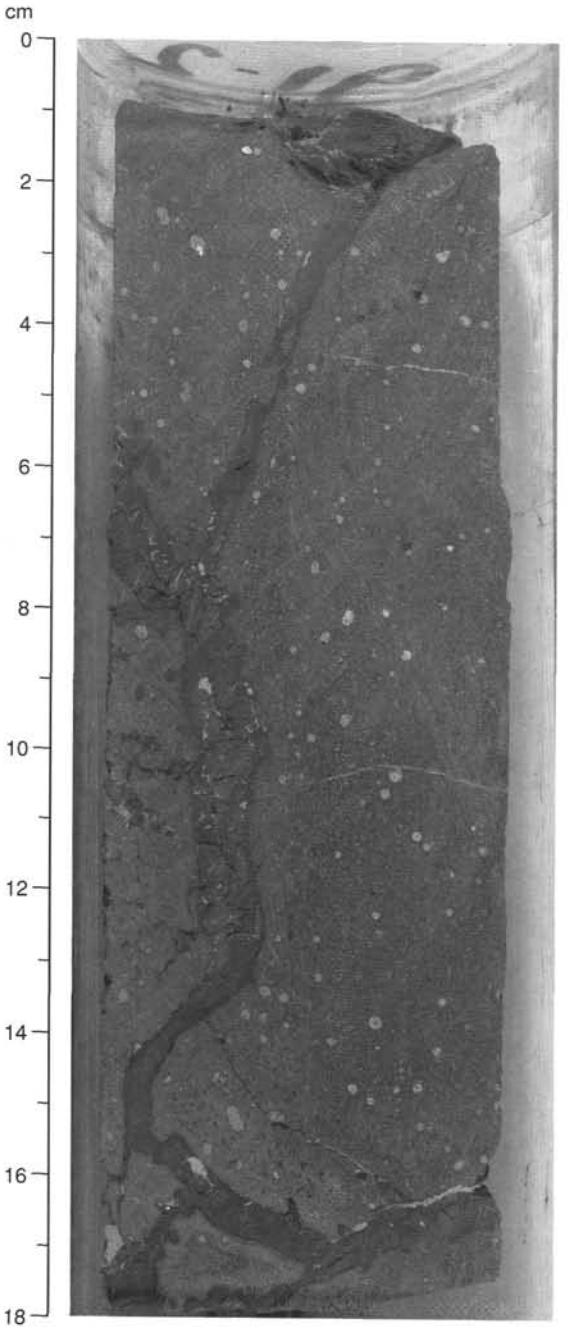

Figure 35. An elongate, highly irregular streak of thermally metamorphosed clayey bioclastic limestone inside Unit 1. This inclusion consists of Fe-oxyhydroxides cemented by quartz and is noncalcareous. Note the absence of alteration halo in the upper part of the inclusion. The typical microcrystalline, amygdaloidal texture of Unit 1 is also shown (Interval 143-865A-91R-2, 0–18 cm).

taken at 821.1 mbsf for reference. The temperature tool measured temperature as a function of pressure. The pressure data were converted to depths, but may be revised by up to 5 m by post-cruise merging of the Schlumberger time/depth data with the temperature-tool time/pressure data. Because the borehole temperatures have been reduced by circulation during coring and by hole conditioning immediately prior to logging, the single temperature run provides only a minimum estimate of the equilibrium temperature profile.

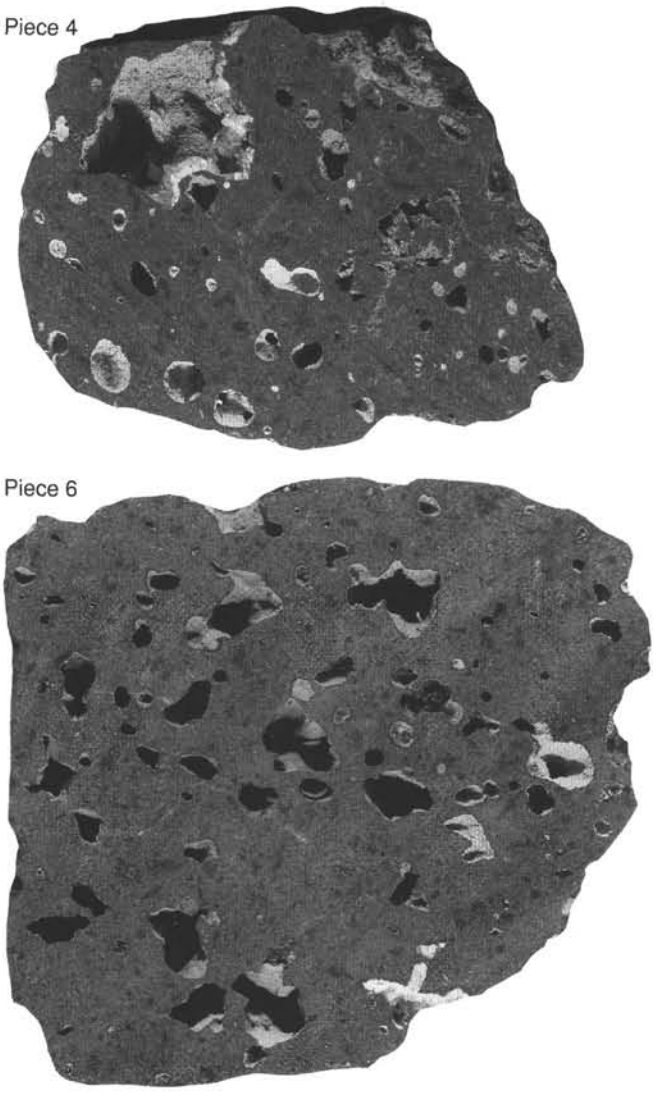

Figure 36. Moderately altered, olivine-pyroxene microphyric basalt having intergranular matrix. Highly vesicular with vesicle walls lined with clays and calcite (Sample 143-865A-93R-2, Pieces 4 and 6).

The temperature profile of Figure 52 is nonlinear and cannot be explained by the circulation history. The entire hole was swept with mud 5 hours prior to logging, which would have suppressed temperatures over the entire borehole. This is not the observed effect. An almost isothermal temperature profile is seen from the base of pipe to about 550 mbsf. These temperatures are approximately equal to bottom-water temperatures and suggest major downflow of water to this depth. Since the pipe was not stopped at this depth during mud circulation, the only plausible explanation for this pattern is fluid flow down into a zone that is drawing water into the formation.

Cyclicity Within Logs

Perhaps the most noteworthy feature of the logs obtained in Hole 865A is their cyclicity in the interval from 206 to 837 mbsf. Four cycles can be seen in this interval spanning the depth ranges: (1) 206–412, (2) 412–495, (3) 495–660, and (4) 660–837 mbsf (Figs. 47 and 49). Each cycle begins with an interval of density, velocity, porosity, and gamma-ray values that oscillate about a fairly constant value. This interval is followed by gradually increasing velocity and

Table 8. Analysis of major and trace elements in Hole 865A basalts.

Site-hole:	143-865A	143-865A	143-865A	143-865A	143-865A	
Core-section:	90R-6	91R-1	93R-2	94R-1	94R-4	
Top-bottom (cm):	105–107	131–133	11–13	89–90	129–130	
Depth (mbsf):	839.18	842.41	855.01	863.99	868.69	
Unit:	1	1	3	3	4	BHVO
Major elements (wt%)						
SiO_2	48.06	45.53	45.05	45.94	47.34	49.94
TiO_2	3.82	3.98	3.73	3.82	3.42	2.75
Al_2O_3	17.91	19	16.69	16.94	16.61	13.62
Fe_2O_3	8.97	10.11	11.24	10.29	9.96	12.21
MnO	0.08	0.12	0.16	0.19	0.13	0.17
MgO	12.39	9.49	8.36	8.16	7.48	7.09
CaO	3.83	6.95	9.16	10.81	9.26	11.41
Na_2O	1.87	2.02	1.77	1.78	2.19	2.95
K_2O	1.69	1.05	2.59	1.15	2.23	0.59
P_2O_5	0.75	0.76	0.77	0.78	0.82	0.28
Total	99.35	99.00	99.50	99.84	99.41	101.00
LOI	9.17	6.57	5.9	4.02	3.11	
Mg#	75.6	67.9	62.6	64.0	62.8	
Trace elements (ppm)						
Ba	626	579	652	727	739	126
Ce	97	111	99	123	106	33
Cr	261	287	216	218	170	291
Cu	51.7	56.6	35.7	52.1	42.5	135.5
Nb	79.7	85.6	69.8	74.8	74.2	18.2
Ni	196	171	125	134	135	122
Rb	16.0	10.1	42.2	11.5	40.2	9.1
Sr	494	793	702	863	782	397
V	282	333	299	299	265	312
Y	26.8	28.3	28.4	30.4	29.4	25.6
Zn	10.7	88.1	73.0	70.5	70.4	108.2
Zr	349	380	354	369	382	173

Notes: Major-element data for each sample represent an average of two analyses; that for BHVO is an average of four. Trace-element data for BHVO are an average of three analyses. LOI was determined gravimetrically. All Fe values are expressed as Fe_2O_3. Mg# = (atomic) $Mg/(Mg+Fe^{2+})$ where Fe_2O_3/FeO is set at 0.15.

gamma-ray counts and decreasing porosity. The cycle ends with decreasing velocity and gamma-ray counts and increasing porosity.

An expanded plot for resistivity, velocity, and gamma rays is shown in Figure 53. The velocity log follows that of the gamma-ray log closely in character; velocity and resistivity correlate only broadly, suggesting that the log response to the cycles is controlled by sedimentary fabric and any associated changes in grain morphology. Changes in grain morphology, distribution of grain sizes, and compaction all may be contributing factors that should be evaluated collectively.

Within the depth ranges 213–247, 388–417, and 680–715 mbsf the velocity is variable but high (2.5–4.7 km/s) when compared to resistivity (1.8–2.9 ohm-m), as would be the case for a highly porous sediment in which the grain contacts had been cemented. In all cases the recovered lithologies exhibit variable degrees of induration; secondary cementation occurs in some material. All three intervals occupy the same relative position within their respective cycles. Similarly, the (depth-wise) lower portion of each cycle shows more thin layers.

The cyclic nature of the caliper and density logs suggests that any decrease in porosity is accompanied by a substantial loss in hole stability. The density log may read too low in these regions.

Cyclicity was identified in visual core descriptions, and shore-based analysis may refine those that were detected by downhole logging.

Downhole Three-component Magnetometer Log

The downhole magnetometer measured three components of the geomagnetic field within Hole 865A from 500 to 865 mbsf. Because the magnetometer measures the signal every 3 s, the sampling interval at the logging cable speed of 1000 m/hr was about 0.9 m. The horizontal and vertical components of the magnetic field inside the hole were calculated from the observed three components of the magnetic field. The orientation of the tool with respect to the present geomagnetic field was also determined from the magnetic field measured by the two orthogonal horizontal axes of the magnetometer. These variations are shown in Figure 54.

Very high-amplitude, sharp decreases in the horizontal magnetic field were recorded above 650 mbsf. These variations were caused by abrupt changes in the tool orientation. The change in tool orientation also affected the vertical magnetic field variations. Vertical magnetic field variations between 650 and 830 mbsf show an almost sinusoidal response curve corresponding to the rotation cycle of the tool. The amplitude of these variations is about 500 nT. This amplitude is equivalent to about 1° dip of the hole.

Variations of horizontal and vertical magnetic field above 830 mbsf are smooth except for those caused by the abrupt change of the tool orientation. Their values are almost the same as the IGRF85 field (IAGA Division I Working Group 1, 1987). This indicates that the surrounding materials above 830 mbsf (mainly limestone) are weakly magnetized. This result is in good agreement with shipboard measurements of weak magnetization of recovered limestone.

Below 830 m, there are three obvious peaks in both the horizontal and vertical magnetic field components at about 840, 845 and 857 mbsf. There is also an obvious peak in the horizontal component, accompanied by an obscure peak of vertical component variation, at about 853 mbsf. These four peaks almost coincide with the basaltic layers. The character of these peaks shows that the magnetization of the basaltic layer has a negative inclination and normal directions of declination which were acquired in the southern hemisphere during

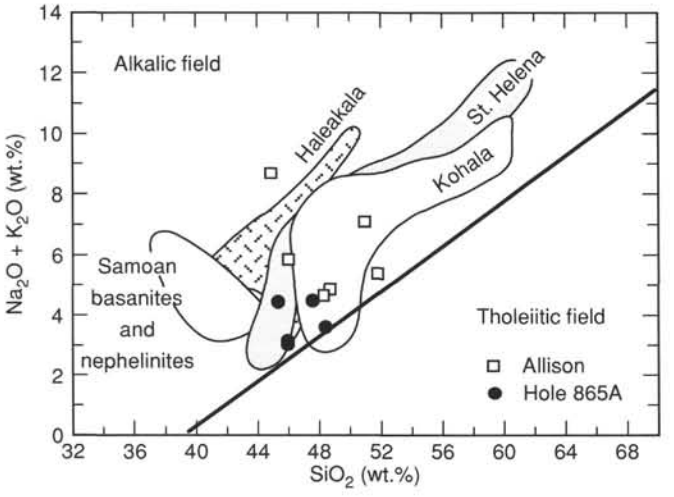

Figure 37. Alkali (wt% $Na_2O + K_2O$) vs. silica (wt% SiO_2) diagram for Hole 865A basalts. Alkalic rocks from Hawaii (Kohala and Haleakala), St. Helena, Samoa, and Allison Guyot dredges are shown for reference.

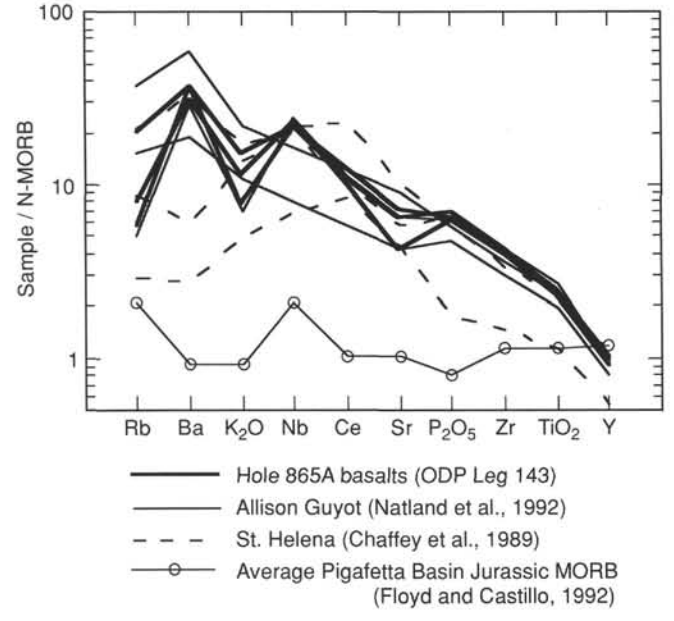

Figure 38. Plot of N-MORB normalized trace elements for Hole 865A basalts. The ranges and average trace element content of basalts (5 wt% MgO) from St. Helena (Chaffey et al., 1989), Allison Guyot dredges, and Pigafetta Basin are shown for comparison. N-MORB normalizing values are from Pearce (1983).

a normal polarity chron. This result is concordant with strong magnetization of recovered basalt samples (12 A/m) as determined by shipboard paleomagnetic studies.

The width of the aforementioned peaks is almost 2–3 m. Assuming a simple cylindrical magnetized block model with horizontal boundaries (Hamano and Kinoshita, 1990), basaltic layers between 830 and 860 mbsf should be divided into four layers with the width of 2-3 m centered on each peak.

The amplitude of the horizontal component variation is different from that of the vertical at each peak. The ratio of the amplitudes of the horizontal and vertical components at each peak ranges from approximately 0.7 to 3.0. The inclination of basalt obtained by paleomagnetic studies ranges from about –29° to –38°. Inclination variations of basalt obtained from shipboard paleomagnetic studies cannot explain these variations of the horizontal to vertical ratio at each peak using a simple cylindrical magnetized block model with horizontal boundaries. However, these variations of the ratio could be explained by a tilting basaltic layer (Hamano and Kinoshita, 1990).

Both the horizontal and the vertical component magnetic field increase below 860 mbsf. This trend is uncertain, because it may result partly from the magnetic field of the drill bit left at the bottom of the hole.

Log-based Units

Seven logging units were identified using the geophysical and spectral gamma-ray logs. The units are defined primarily on the basis of the resistivity, velocity, density, gamma-ray and potassium logs.

Logging Unit 1—Base of Pipe (102.5 mbsf) to 138.5 mbsf

Logging Unit 1 corresponds to the lower portion of lithologic Unit I, a high-porosity foraminiferal sand and foraminiferal-nannofossil ooze. Based on log responses alone, the calcareous oozes of logging Unit 1 are homogeneous. The base of this unit is clearly defined by all geophysical logs. Resistivity values within Unit 1 range from 0.6 to 0.7 ohm-m. Three intervals of uniform velocity are defined: 103 to 122 mbsf (1.6–1.7 km/s), 122 to 129 mbsf (1.5–1.6 km/s), and 129 to 137 mbsf (1.6–1.8 km/s). Density is less than 1.6 g/cm^3 for the entire interval to 141 mbsf. Gamma-ray counts are uniformly 2.5 to 5.0 API units.

Logging Unit 2—138.5 to 197 mbsf

Logging Unit 2 corresponds to lithologic Unit II, a mineralized pelagic and shallow-water limestone. Resistivity increases sharply to 4.0 ohm-m at 136 mbsf, and remains highly variable (2.0–6.0 ohm-m) but generally decreases to 2.0 ohm-m from 173 to 181 mbsf. The sharp increase in resistivity observed at 136 and again at 181 mbsf is accompanied by equally sharp increases in gamma-ray counts. As can be seen from Figure 49, the gamma increase at the upper contact is offset to 138.8 mbsf, whereas the gamma decrease at the base of the unit is offset to 206 mbsf. Furthermore, the lower portion of Unit 2 appears to be enriched in uranium. Downward mobilization of the uranium component may be responsible for the variation in unit boundaries observed on the logs: density, resistivity, porosity, and velocity logs place the lower boundary of Unit 2 at 197 mbsf, the gamma-ray log places it at 206 mbsf.

Density is highly variable, ranging from 2.0 to 2.4 g/cm^3. Velocity values are degraded by cycle skipping in this unit; however, it is evident that velocities in this interval are actually highly variable, ranging from 1.6 to 4.6 k/s. Velocities are higher than can be accounted for by mechanical compaction of fine-grained carbonates, and may be due to in-situ cementation. The broad range of porosities suggests that fresh water may have been present in the formation in the past.

Logging Unit 3—197 to 369 mbsf

Logging Unit 3 corresponds to lithologic Subunit IIIA, a poorly recovered limestone section similar to the facies encountered in Unit II, and the uppermost portion of Subunit IIIB. Wackestones represent the bulk of the recovered core material. Logging Units 3 through 6 represent individual cycles of log response, as explained above. The recovery of cored material that appears to indicate episodic subaerial exposure suggests that these log cycles may correspond to changes in sea level. Poor recovery and sparse paleodates preclude a firm conclusion to that effect at this time.

The overall downhole increase in resistivity values is punctuated by two broad peaks at 238 to 245 and 301 to 307 mbsf, with corresponding highs in density and velocity, and low porosity and gamma-ray counts. The corresponding intervals of high resistivity

Table 9. *P*-wave velocities for pelagic sediments, obtained by digital sound velocimeter (DSV) for Holes 865A and 865B.

Core, section, interval (cm)	Depth (mbsf)	Velocity (km/s)	Core, section, interval (cm)	Depth (mbsf)	Velocity (km/s)
143-865A-			143-865B-		
2R-3, 72	9.55	1.512	4X-5, 84	34.34	1.506
2R-4, 47	10.70	1.506	5X-1, 72	37.72	1.509
3R-2, 18	16.41	1.506	5X-1, 72	37.72	1.466
4R-1, 72	24.95	1.465	5X-2, 116	39.66	1.482
4R-2, 72	26.45	1.499	5X-3, 72	40.72	1.490
4R-3, 52	27.75	1.507	5X-4, 72	42.22	1.499
5R-2, 27	35.00	1.514	5X-5, 47	43.47	1.510
5R-3, 80	36.11	1.509	5X-6, 24	44.24	1.471
5R-4, 47	37.35	1.510	6X-3, 72	50.22	1.476
5R-5, 27	38.08	1.509	6X-4, 47	51.47	1.502
5R-6, 51	37.97	1.517	6X-5, 124	53.74	1.514
6R-1, 38	43.61	1.488	7X-2, 108	58.58	1.523
6R-2, 72	45.52	1.510	7X-3, 40	59.40	1.528
7R-1, 57	53.30	1.514	7X-4, 50	61.00	1.502
7R-2, 47	54.20	1.535	7X-5, 51	62.51	1.488
7R-3, 72	55.02	1.476	7X-6, 25	63.25	1.515
7R-4, 52	56.39	1.512	8X-1, 112	66.62	1.482
7R-5, 34	57.31	1.476	8X-2, 105	68.05	1.512
8R-1, 72	63.05	1.519	8X-3, 100	69.50	1.519
8R-2, 47	64.37	1.528	8X-4, 72	70.72	1.510
9R-1, 66	72.49	1.462	8X-5, 87	72.37	1.474
13R-1, 43	111.26	1.479	8X-6, 54	73.54	1.472
13R-2, 79	113.12	1.479	9X-1, 72	75.72	1.472
14R-1, 79	122.82	1.487	9X-2, 72	77.22	1.474
14R-2, 79	124.32	1.542	9X-3, 73	78.73	1.471
14R-3, 76	125.79	1.540	9X-4, 110	80.60	1.482
14R-4, 78	127.31	1.542	9X-5, 72	81.72	1.472
14R-5, 75	128.78	1.532	9X-6, 79	83.29	1.474
15R-1, 121	131.34	1.543	10X-2, 74	86.74	1.472
15R-2, 121	132.84	1.525	10X-3, 74	88.24	1.512
15R-3, 116	134.29	1.550	10X-4, 38	89.38	1.515
15R-4, 118	135.81	1.525	10X-5, 62	91.12	1.514
15R-5, 81	136.94	1.530	11X-1, 75	94.75	1.472
15R-6, 81	138.64	1.512	11X-2, 75	96.25	1.502
16R-1, 34	135.47	1.507	11X-5, 75	100.75	1.479
16R-3, 75	138.88	1.569	12X-1, 57	104.07	1.471
16R-4, 75	140.38	1.576	12X-2, 72	105.72	1.476
16R-5, 52	141.65	1.530	12X-3, 72	107.22	1.466
			12X-4, 72	108.72	1.514
143-865B-			12X-5, 50	110.00	1.474
			13X-1, 50	113.50	1.479
2H-2, 73	10.73	1.052	13X-2, 40	114.90	1.520
1X-3, 74	3.74	1.369	13X-3, 75	116.75	1.476
2X-4, 74	13.74	1.465	13X-4, 40	117.90	1.520
2X-5, 73	15.23	1.517	13X-5, 59	119.59	1.527
2X-6, 31	16.31	1.515	13X-6, 38	120.88	1.527
3X-1, 75	18.75	1.502	14X-1, 73	123.23	1.477
3X-2, 98	20.48	1.517	14X-2, 73	124.73	1.502
3X-3, 69	21.69	1.502	14X-3, 34	125.84	1.487
3X-4, 109	23.59	1.520	14X-4, 72	127.72	1.514
3X-5, 75	24.75	1.515	14X-5, 72	129.22	1.517
3X-6, 75	26.25	1.509	14X-6, 20	130.20	1.474
3X-7, 22	27.22	1.509	15X-1, 75	132.75	1.472
4X-1, 84	28.34	1.496	15X-2, 75	134.25	1.519
4X-4, 69	32.69	1.466	15X-3, 17	135.17	1.523

were located on the FMS at 237.1 to 243.3 and 301 to 308.4 mbsf (Cores 143-865A-28R and -34R, respectively). Their mottled appearance on the FMS image is consistent with the recovered lithologies, in both cases primarily wackestone with moldic porosity.

The gamma-ray, density, and velocity logs correlate well in this interval. Values oscillate about a constant value to a depth of about 270 mbsf, increase gradually over the next 100 m and then decrease to a value only slightly higher than that of the upper part of the cycle.

Logging Unit 4—369 to 494 mbsf

Logging Unit 4 corresponds to the upper portion of lithologic Subunit IIIB. Lithologies are similar to those of Subunit IIIA, with the appearance of some mudstones and grainstones. Gamma-ray counts are higher, and more variable than those logged in Unit 3. Resistivity is moderately variable over the upper part of logging Unit 4, averaging 3.0 ohm-m and decreasing downhole to 2.0 ohm-m.

Velocity exhibits considerable variation throughout the unit. From 388–417 mbsf, velocities are high (up to 3.5 km/s) but resistivity is low, indicating a highly porous interval with well cemented grain contacts. Three velocity intervals of 3.1, 3.6, and 3.2 km/s span the depth range 388–403 mbsf. This is followed by a series of rhythmic variations in velocity from about 2.9 to 5.1 km/s, and then a homogeneous zone (2.8 km/s). The remainder of the unit consists of alternating intervals of rhythmic variations in velocity and homogeneous zones (2.9–3.0 km/s).

The character of the velocity, density and gamma logs indicates the presence of many thin layers in the lower halves of Log Units 4, 5, 6 and 7. This is confirmed by the FMS scan showing numerous thin layers of alternating high and low resistivity, some as thin as 1 cm. Recovery was extremely poor to zero throughout Unit III, hence the corresponding lithologies cannot be confirmed. Nevertheless, recovered lithologies were consistently fine-grained and well-indurated (wackestones, mudstones, and chalks) with rare pebbles of more porous material (chalky limestone).

Logging Subunits 5a (494–560 mbsf) and 5b (560–660 mbsf)

Logging Unit 5 corresponds to the lower portion of lithologic Subunits IIIB and IVA. This unit is subdivided because the cycle unit appears to have been interrupted. The base of Subunit 5a is defined by broad maxima in the resistivity, density, velocity, and gamma logs, from 550 to 560 mbsf. The interval from 551.9 to 554.8 mbsf on the FMS log shows a mottled pattern characteristic of vuggy porosity; the materials recovered in Core 143-865A-60R are calcite-cemented mudstones exhibiting moldic porosity. Resistivity, velocity, density, and gamma-ray counts decrease with depth in Subunit 5b.

Logging Subunits 6a (660–745 mbsf) and 6b (745–837 mbsf)

Logging Unit 6 corresponds to lithologic Subunits IVB and IVC. This unit is subdivided because there is some indication in the resistivity (745 mbsf, defining the base of Subunit 6a) and gamma-ray logs (780 mbsf) that the cycle unit was interrupted. The decreasing resistivity values in the interval from 740 to 827 mbsf reflect the increasing presence of lignite and the highly conductive mineral pyrite that was observed in the cores. At the base of Subunit 6a, resistivity logs show a series of peaked excursions to very high (>100 ohm-m) resistivity, and broad excursions to lower values (2.5 ohm-m); these are echoed by the density logs almost peak-for-peak; a distinct anti-correlation with the velocity log indicates that clay content, not porosity, controls the velocity response in this lower portion of the hole. Gamma-ray peaks are roughly coincident with highs in resistivity and density.

Logging Unit 7 (837–861 mbsf)

Logging Unit 7 corresponds to lithologic Subunit IVD, a series of basalt sills intruded into calcareous sediments. Resistivity logs show a broad, flat high (>10 ohm-m), followed by sharp decrease to 0.9 ohm-m at 839 mbsf and a high (>10 ohm-m) at 842 mbsf. This unit is well defined by all logs, including the downhole magnetometer.

Summary

Logging in Hole 865A has contributed significantly to our efforts to refine the stratigraphy and structure of Allison Guyot. The geophysical and spectral gamma-ray logs have demonstrated the existence of several intervals of rhythmic variation in lithology that would not have been revealed otherwise because of poor core recovery. The FMS logs were essential for verifying the depth positions of strata exhibiting moldic, vuggy, and clear horizontal banding. The FMS logs

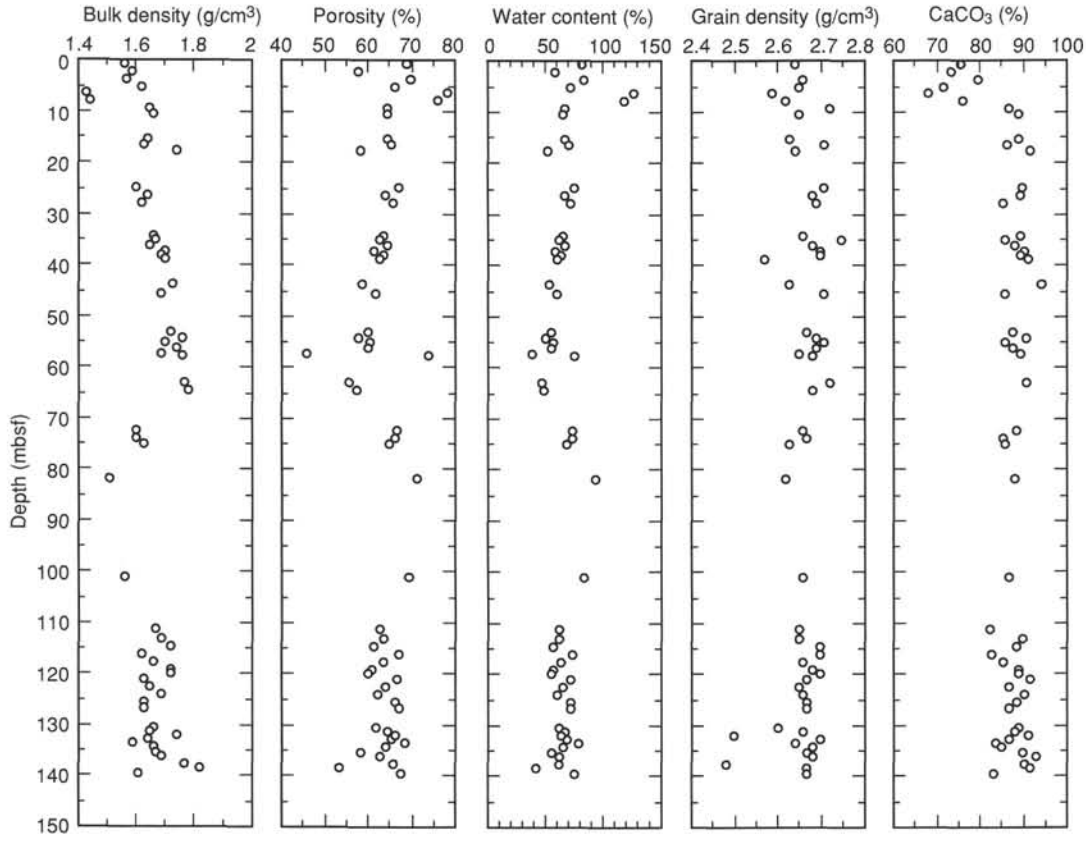

Figure 39. Index properties and carbonate content for pelagic sediments in Hole 865A.

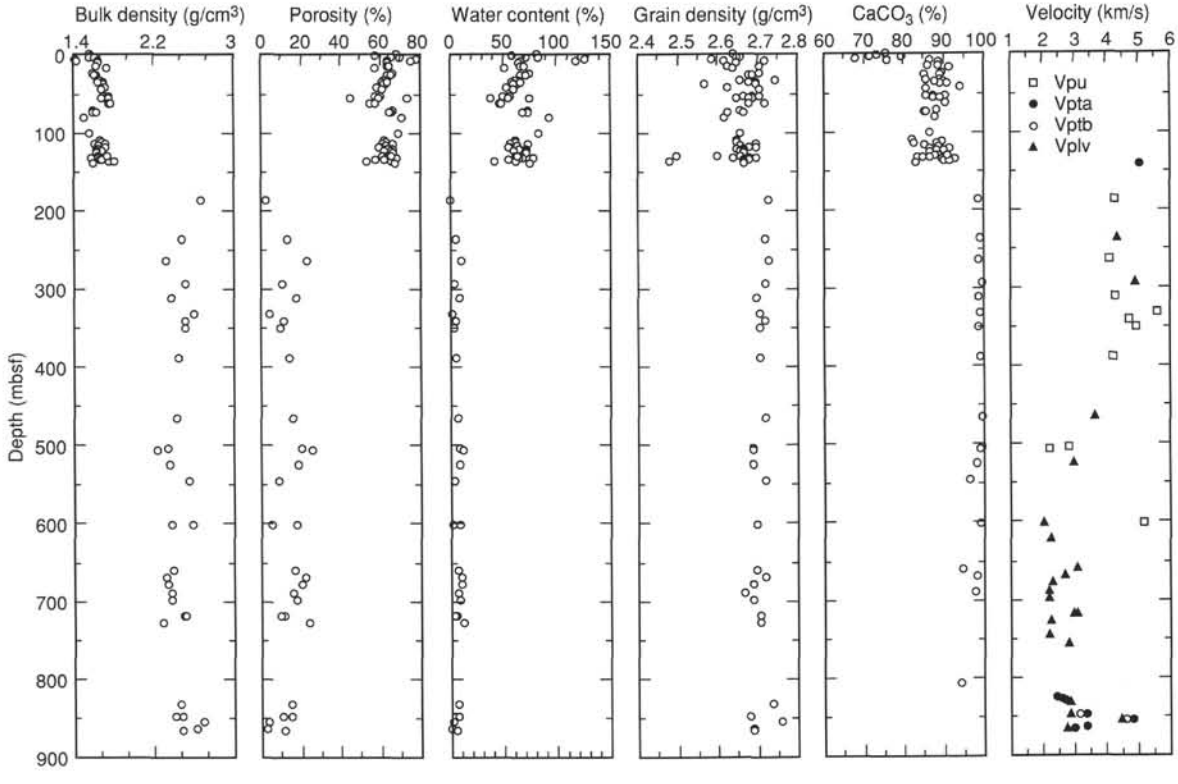

Figure 40. Index properties, acoustic velocity, and carbonate content for both pelagics and lithified shallow-water platform carbonates and mixed carbonates-basalts in Hole 865A. Measurements of *P*-wave velocity are discriminated for direction: *Vpu* is unoriented; *Vpta* is transverse (horizontal); *Vpl* is longitudinal (parallel core axis).

Table 10. Sonic velocity, index properties, carbonate content and anisotropy, Hole 865A.

Core, section, interval (cm)	Depth (mbsf)	$V_{pta\ (cu)}$ (km/s)	$V_{ptb\ (cu)}$ (km/s)	$V_{pl\ (cu)}$ (km/s)	$V_{pa\ (mc)}$ (km/s)	$V_{pt\ (mc)}$ (km/s)	$V_{pl\ (mc)}$ (km/s)	Anisotropy (cu) (%)	Water content (%)	Bulk density (g/cm^3)	Grain density (g/cm^3)	Porosity (%)	$CaCO_3$ (%)
143-865A-													
1R-1, 79–80	0.79								82.80	1.56	2.64	68.90	75.64
1R-2, 79–80	2.29								59.20	1.59	2.87	57.80	73.64
1R-3, 75–76	3.75								84.30	1.57	2.66	70.10	79.63
1R-4, 60–61	5.10								72.40	1.62	2.65	66.20	71.63
2R-1, 77–78	6.47								127.60	1.43	2.59	78.30	68.30
2R-2, 77–78	7.97								119.00	1.44	2.62	76.10	76.09
2R-3, 77–78	9.47								66.70	1.65	2.72	64.50	86.96
2R-4, 49–50	10.69								65.80	1.66	2.65	64.40	88.88
3R-1, 76–77	15.46								67.90	1.64	2.63	64.70	89.05
3R-2, 23–24	16.43								70.00	1.63	2.71	65.50	86.30
3R-CC, 5–6	17.75								52.00	1.74	2.64	58.20	91.71
4R-1, 76–77	24.96								75.80	1.60	2.71	67.30	89.96
4R-2, 76–77	26.46								67.10	1.64	2.68	64.20	89.63
4R-3, 56–57	27.76								71.90	1.62	2.69	66.00	85.55
5R-1, 51–52	34.21								65.30	1.66	2.66	63.90	89.38
5R-2, 31–32	35.01								62.60	1.67	2.75	62.60	85.96
5R-3, 83–83	36.11								67.00	1.65	2.68	64.50	88.30
5R-4, 49–50	37.34								58.40	1.70	2.70	61.30	90.46
5R-5, 31–32	38.16								63.20	1.69	2.70	63.70	89.30
5R-6, 55–56	38.98								61.10	1.70	2.57	62.80	91.05
6R-1, 41–42	43.61								53.70	1.73	2.63	58.90	94.54
6R-2, 75–76	45.52								60.20	1.69	2.71	61.80	85.80
7R-1, 61–62	53.31								56.00	1.72	2.67	60.30	87.80
7R-2, 51–52	54.21								50.60	1.76	2.69	57.90	90.79
7R-3, 75–76	55.20								57.50	1.70	2.71	60.70	86.13
7R-4, 55–56	56.39								55.10	1.74	2.69	60.20	87.79
7R-5, 37–38	57.31								38.70	1.69	2.65	46.00	89.46
7R-CC, 5–6	57.72								75.40	1.76	2.68	73.90	
8R-1, 76–77	63.06								47.70	1.77	2.72	55.80	90.71
8R-2, 51–52	64.38								49.60	1.78	2.68	57.70	
9R-1, 70–71	72.50								74.70	1.60	2.66	66.90	88.80
9R-2, 84–85	74.14								73.50	1.60	2.67	66.30	85.30
9R-3, 19–20	74.99								68.60	1.63	2.63	64.90	86.05
10R-CC, 8–9	81.88								93.40	1.51	2.62	71.30	88.05
12R-CC, 8–9	101.28								83.70	1.56	2.66	69.30	86.80
13R-1, 44–45	111.24								62.20	1.67	2.65	62.70	82.21
13R-2, 81–82	113.11								62.50	1.69	2.65	63.50	89.76
13R-3, 76–77	114.56								58.00	1.72	2.70	61.70	88.80
13R-4, 76–77	116.06								73.90	1.62	2.70	67.10	82.63
13R-5, 76–77	117.56								64.50	1.66	2.66	63.70	85.38
13R-6, 76–77	119.06								57.00	1.72	2.68	60.90	89.13
13R-CC, 26–27	120.06								55.80	1.72	2.70	60.20	89.21
14R-1, 76–77	121.26								72.10	1.63	2.67	66.60	91.63
14R-2, 79–80	122.79								66.00	1.65	2.65	64.10	86.88
14R-3, 79–80	124.19								61.30	1.69	2.66	62.50	90.54
14R-4, 79–80	125.59								71.50	1.63	2.67	66.40	88.63
14R-5, 78–79	126.98								72.70	1.63	2.67	67.10	86.71
15R-1, 123–124	130.71								61.60	1.66	2.60	61.90	88.96
15R-2, 125–126	131.50								67.10	1.65	2.66	64.60	88.30
15R-3, 119–120	132.21								64.30	1.74	2.50	66.50	91.13
15R-4, 121–122	132.96								69.40	1.64	2.70	65.40	86.88
15R-5, 81–82	133.51								79.10	1.59	2.64	68.40	83.71
15R-6, 82–83	134.26								65.50	1.66	2.68	64.00	85.05
16R-1, 76–77	135.61								55.90	1.67	2.67	58.30	89.88
16R-2, 41–42	136.37								61.70	1.69	2.68	62.80	92.96
16R-3, 76–77	137.61								61.60	1.77	2.48	65.80	90.54
16R-4, 76–77	138.61								43.00	1.82	2.67	53.50	91.71
16R-5, 55–65	139.47								75.60	1.61	2.67	67.70	83.38
23R-CC, 3–6	188.10				4.314				1.06	2.68	2.73	2.81	98.79
28R-1, 91–94	237.29						4.435		5.62	2.49	2.72	13.26	99.37
31R-CC, 14–17	265.32				4.116				11.05	2.33	2.73	23.14	98.87
34R-1, 32–35	294.50						4.989		4.63	2.53	2.72	11.18	99.62
36R-CC, 29–32	313.37				4.320				8.28	2.39	2.70	18.27	98.79
38R-CC, 6–9	332.44				5.618				1.92	2.62	2.71	4.94	99.10
39R-CC, 34–37	342.22				4.761				4.90	2.52	2.72	11.76	
40R-CC, 4–7	351.62				4.972				4.18	2.53	2.71	10.15	98.96
44R-CC, 3–6	390.11				4.227				6.30	2.46	2.71	14.57	99.04
52R-CC, 3–6	467.31						3.684		7.17	2.44	2.72	16.34	99.87
56R-CC, 3–6	505.91				2.846				9.50	2.35	2.69	20.34	99.71
56R-CC, 37–40	506.26				2.248				12.91	2.25	2.69	25.77	99.29
58R-CC, 3–6	525.21						2.997		8.50	2.37	2.69	18.61	98.22
60R-CC, 7–10	544.57								3.80	2.56	2.72	9.35	96.71
66R-CC, 4–7	602.51						2.050		8.08	2.39	2.70	17.90	99.29
66R-CC, 11–14	602.60				5.170				2.35	2.60	2.70	5.97	99.46
68R-CC, 4–7	621.91						2.281						

Table 10 (continued).

Core, section, interval (cm)	Depth (mbsf)	$V_{pta\,(cu)}$ (km/s)	$V_{ptb\,(cu)}$ (km/s)	$V_{pl\,(cu)}$ (km/s)	$V_{pu\,(mc)}$ (km/s)	$V_{pt\,(mc)}$ (km/s)	$V_{pl\,(mc)}$ (km/s)	Anisotropy (cu) (%)	Water content (%)	Bulk density (g/cm^3)	Grain density (g/cm^3)	Porosity (%)	$CaCO_3$ (%)
143-865A-													
72R-CC, 27–30	660.65						3.139		7.69	2.41	2.70	17.19	94.71
73R-1, 58–61	670.66						2.720		10.77	2.33	2.72	22.64	98.29
74R-1, 34–37	680.03						2.371		9.74	2.34	2.69	20.73	
75R-1, 64–67	690.02						2.262		7.44	2.39	2.67	16.57	98.04
76R-1, 55–58	699.63						2.264		8.25	2.38	2.69	18.16	
78R-1, 75–78	719.04						3.012		4.93	2.51	2.71	11.78	
78R-1, 75–78	719.04						3.139		4.29	2.53	2.71	10.42	
79R-1, 36–39	728.45						2.269		12.10	2.29	2.71	24.67	
81R-1, 63–66	748.01						2.264						
82R-1, 28–31	757.36						2.840						
82R-1, 76–79	757.85												
87R-2, 52–55	807.32												94.29
89R-1, 99–102	825.78					2.440							
89R-3, 90–93	828.42					2.630							
89R-5, 16–19	830.34					2.760							
90R-5, 107–110	832.84						2.882		6.48	2.48	2.74	15.07	
92R-1, 112–115	848.31					3.429			4.66	2.49	2.68	11.10	
92R-1, 126–129	848.52	3.406	3.169	2.928				11.570	6.93	2.42	2.68	15.66	
93R-3, 45–48	856.74	4.854	4.646	4.491				5.610	1.43	2.70	2.76	3.80	
94R-2, 62–65	865.18					3.397			1.24	2.63	2.69	3.22	
94R-3, 47–50	866.00	3.011	3.016	2.796				7.500	4.80	2.49	2.69	11.43	
143-865B-													
17X-CC, 5–10	141.77					5.062							

Note: Measurements of *P*-wave velocity from one single lithified carbonate sample of Hole 865B are included. Measurements are labeled for direction and sample shape: $V_{pta\,(cu)}$, $V_{ptb\,(cu)}$ are from unoriented cubes (transverse or horizontal); $V_{pl\,(cu)}$ is longitudinal (parallel core-axis) from a cube; $V_{pu\,(mc)}$ is from an unoriented minicore; $V_{pt\,(mc)}$ is transverse from a minicore; $V_{pl\,(mc)}$ is longitudinal from a minicore.

also helped to distinguish between very dense beds that are too thin to resolve using the resistivity sondes and thicker, less dense beds.

Based on log responses alone, the calcareous oozes (see "Lithostratigraphy" section, this chapter) of logging Unit 1 are homogeneous. Logging Unit 2 includes lithologies that are nearly identical with logging Unit 3, but it consists of many thin (<5 m) beds that are highly cemented and phosphatized. These thin beds appear to be important permeability barriers to compaction, as no evidence for a carbonate compaction trend is seen. Porosity decreases in a stepwise fashion downhole; however, the log response is dominated by numerous thin beds of low porosity. These thin and very dense beds might be either dolomite or calcite wackestones and mudstones; they are certainly diagenetic in origin. Some of the less dense beds may be rich in bioclasts, which are more lithified than the surrounding matrix.

SEISMIC STRATIGRAPHY

The seismic reflection profile across Site 865, taken from the Scripps Institution of Oceanography research vessel *Thomas Washington* during Leg 10 of the Roundabout Expedition (Fig. 55; see also Fig. 4), shows a series of prominent reflectors both within the pelagic cap and within the lagoonal sediments. Many of the reflectors have continuity across the entire lagoon, over a distance of about 20 km.

The reflectors within the pelagic cap are nearly flat and have been truncated by erosion at their outside edges (Fig. 56). The reflector that nearly crops out at Site 865 is overlain by a cover of sediment about 50 m thick (assuming a velocity of about 1.7 km/s), and this reflector rests on an unconformity, plausibly located at about 25 mbsf at Site 865, between upper and middle Eocene pelagic oozes.

The prominent reflector at the top of the Cretaceous shallow-water limestone shows local relief on the order of 20 m over distances of 1 km (using a velocity of 1.7 km/s in the pelagic cap). The reflector appears to arch upward gently, but this effect is almost entirely owing to the difference between the velocity of sound in water and in the lens-shaped pelagic cap. This surface is not entirely flat: a broad sag of about 25 m is seen in the surface of the lagoonal sediments between the center of the guyot and the perimeter reef. This may be the result of original lagoonal topography.

In Table 13, the strongest of these reflectors are listed in order of their two-way reflection times. The reflectors have been assigned labels (SF, K_1, etc.), used in both Table 13 and in Figure 55.

The positions of the seafloor (SF), the top of the Cretaceous lagoonal limestone (K_1), and the top of the basalt (B) are simple to place: they are unequivocal in the drilling records, in the lithologic samples, and in the downhole logs. The other reflectors are at less certain depths. The method used for estimating the depths was iterative: by taking the average sonic log velocities and the interval reflection time between pairs of reflectors, a trial depth was picked, and the velocity and density logs searched for changes that result in a significant change in acoustic impedance. The record of drilling characteristics, as given in the "Geolograph" recorder on the derrick floor, was studied for changes in drilling behavior that might be associated with real changes in the rocks, not merely changes in drilling technique (rotation rate, weight on bit, pumping rates, etc.). Finally, the lithologic content of the recovered core material was considered.

Reflector B, at the top of the basalt at 840 mbsf, can be traced almost to the edge of the guyot. In the profile in Figure 55, the reflector has been obscured by the incoherent reflectors beneath the perimeter reef, but in the profile of Figure 7, taken from the *JOIDES Resolution*, reflector B is traceable beneath the reef to within about 500 m of the south-facing outer slope of the guyot. The extrapolated point of emergence of the reflector is at about 3.1 s of reflection time in water, or about 2325 m. The depth to reflector B beneath Hole 865A is 2369 m.

Traced northward, toward the interior of the guyot, reflector B arches over a central broad ridge (Fig. 4), which appears to trend about WNW, judging by the location of the arch in other profiles across the guyot taken by the *Thomas Washington*. The relief on reflector B over

this ridge is about 0.11 s of two-way reflection time, which translates to about 175 m, using the interval sound velocity given in Table 13.

The broad sag seen in reflector K1 beneath Site 865 is mimicked by reflectors K2 through K5. This probably partly results from the original topographic relief on the basalt, enhanced by greater compaction of sediments beneath Site 865 than those sediments deposited over the buried hill of basalt. There does not appear to be any onlap of limestones onto basalt toward the hill.

Beneath reflector B at Site 865, a series of discontinuous reflectors is visible down to a level about 0.2 s deeper than the basalt (Figs. 55 and 4). Traced toward the buried hill, these sub-B reflectors fade into incoherent hyperbolas; but beyond the hill, in the broad sag on the north side of the guyot, sub-B reflectors are again discernable, down to about 0.4 s under reflector B (Fig. 4). Whether these reflectors represent more sediments like those in the deeper parts of Hole 865A, perhaps interlayered with basalt, is moot: too many plausible possibilities exist to control speculation. Using the sonic velocities derived for the overlying section, the minimum additional depth to the deepest visible sub-B reflectors would be about 300 m.

REFERENCES*

Baker, I., 1969. Petrology of the volcanic rocks of St. Helena Island, south Atlantic. *Geol. Soc. Am. Bull.,* 80:1283–1310.

Berggren, W.A., Kent, D.V., Flynn, J.J., and Van Couvering, J.A., 1985. Cenozoic geochronology. *Geol. Soc. Am. Bull.,* 96:1407–1418.

Bralower, T.J., and Siesser, W.G., 1992. Cretaceous calcareous nannofossil biostratigraphy of Sites 761, 762, and 763, Exmouth and Wombat Plateaus, northwest Australia. *In* von Rad, U., Haq, B.U., et al., *Proc. ODP, Sci. Results,* 122: College Station, TX (Ocean Drilling Program), 529–556.

Bukry, D., 1973. Low-latitude coccolith biostratigraphic zonation. *In* Edgar, N.T., Saunders, J.B., et al., *Init. Repts. DSDP,* 15: Washington (U.S. Govt. Printing Office), 685–703.

Chaffey, D.J., Cliff, R.A., and Wilson, B.M., 1989. Characterization of the St. Helena magma source. *In* Saunders, A.D., and Norry, M.J. (Eds.), *Magmatism in the Ocean Basins.* Geol. Soc. Spec. Publ. London, 42:257–276.

Darwin, C., 1842. *The Structure and Distribution of Coral Reefs:* London, (John Murray).

Floyd, P.A., and Castillo, P.R., in press. Geochemistry and petrogenesis of Jurassic of Jurassic ocean crust basalts, ODP Leg 129, Site 801. *In* Larson, R.L., Lancelot, Y., et al., *Proc. ODP, Sci. Results,* 129: College Station, TX (Ocean Drilling Program).

Grow, J.A., Lee, M.W., Miller, J.J., Agena, W.F., Hampson, J.C., Foster, D.S., and Woellner, R.A., 1986. Multichannel seismic reflection survey of KOA and OAK craters. *In* Folger, D.W. (Ed.), *Sea-floor Observations and Subbottom Seismic Characteristics of OAK and KOA Craters, Enewetak Atoll, Marshall Islands.* U.S. Geol. Surv. Bull., 1678-D:D1–D46.

Hamano, Y., and Kinoshita, H., 1990. Magnetization of the oceanic crust inferred from magnetic logging in Hole 395A. *In* Detrick, R., Honnorez, J., Bryan, W.B., Juteau, T., et al. *Proc. ODP, Sci. Results,* 106/109: College Station, TX (Ocean Drilling Program), 223–229.

Hamilton, E.L., 1956. Sunken islands of the Mid-Pacific Mountains. *Mem.—Geol. Soc. Am.,* 64.

————, 1976. Variations of density and porosity with depth in deep-sea sediments. *J. Sediment. Petrol.,* 46:280–300.

————, 1979. Sound velocity gradients in marine sediments. *J. Acoust. Soc. Am.,* 65:909–922.

Hancock, J.M., and Kauffman, E.G., 1979. The great trangressions of the Late Cretaceous. *J. Geol. Soc. London,* 136:175–186.

Heezen, B.C., Matthews, J.L., Catalano, R., Natland, J., Coogan, A., Tharp, M., and Rawson, M., 1973. Western Pacific guyots. *In* Heezen, B.C., MacGregor, I.D., et al., *Init. Repts. DSDP,* 20: Washington (U.S. Govt. Printing Office), 653–723.

Honnorez, J., Laverne, C., Hubberten, H.-W., Emmermann, R., and Muehlenbachs, K., 1983. Alteration processes in layer 2 basalts from Deep Sea Drilling Project Hole 504B, Costa Rica Rift. *In* Cann, J.R., Langseth, M.G., Honnorez, J., Von Herzen, R.P., White, S.M., et al., *Init. Repts. DSDP,* 69: Washington (U.S. Govt. Printing Office), 509–546.

IAGA Division I Working Group I, 1987. International Geomagnetic Reference Field revision 1987. *J. Geomagn. Geoelectr.,* 39:773–779.

Johnson, C.C., Collins, L.S., and Kauffman, E.G., 1986. Rudistid biofacies across the El Abra Formation (Late Albian(?)/Early-middle Cenomanian), Northeastern Mexico. *Trans. 11th Caribbean Geol. Conf., Barbados,* 1–11.

Lincoln, J.M., and Schlanger, S.O., 1990. Atoll stratigraphy as a record of sea level change-problems and prospects. *J. Geophys. Res.,* 96:6727–6752.

MacDonald, G.A., 1968. Composition and origin of Hawaiian lavas. *In* Coats, R.R., Hay, R.L., and Anderson, C.A. (Eds.), *Studies in Volcanology: A Memoir in Honor of Howel Williams.* Mem.—Geol. Soc. Am., 116:477–522.

Martini, E., 1971. Standard Tertiary and Quaternary calcareous nannoplankton zonation. *In* Farinacci, A. (Ed.), *Proc. 2nd Int. Conf. Planktonic Microfossils Roma:* Rome (Ed. Tecnosci.), 2:739–785.

McFadden, P.L., and Reid, A.B., 1982. Analysis of paleomagnetic inclination data. *Geophys. J. R. Astron. Soc.,* 69:307–319.

Natland, J.H., Dieu, J.J., and Wright, E., in press. Petrology of volcanic rocks dredged from Cretaceous guyots of the central and western Pacific. *In* Pringle, M., Sager, W., Sliter, W., and Stein, C. (Eds.), *Mesozoic Pacific.* Am. Geophys. Union, Geophys. Monogr.

Nemoto, K., and Kroenke, L.W., 1985. Sio guyot: a complex volcanic edifice in the western Mid-Pac Mountains. *Geo-Mar. Lett.,* 5:83–89.

Palmer, R.H., 1928. The rudistids of Southern Mexico. *Occas. Pap. Calif. Acad. Sci.,* 14:1–132.

Parker, R.L., Shure, L., and Hildebrand, J.A., 1987. The application of inverse theory to seamount magnetism. *Rev. Geophys.,* 25:17–40.

Pearce, J.A., 1983. Role of the sub-continental lithosphere in magma genesis at active continental margins. *In* Hawkesworth, C.J., and Norry, M.J. (Eds), *Continental Basalts and Mantle Xenoliths:* Nantwich (Shiva Publ.), 230–249.

Perch-Nielsen, K., 1985. Mesozoic calcareous nannofossils. *In* Bolli, H.M., Saunders, J.B., and Perch-Nielsen, K. (Eds.), *Plankton Stratigraphy:* Cambridge (Cambridge Univ. Press), 329–426.

Roth, P.H., 1978. Cretaceous nannoplankton biostratigraphy and oceanography of the northwestern Atlantic Ocean. *In* Benson, W.E., Sheridan, R.E., et al., *Init. Repts. DSDP,* 44: Washington (U.S. Govt. Printing Office), 731–760.

Sager, W.W., 1986. Magnetic-susceptibility measurements of metal contaminants in ODP Leg 101 cores. *In* Austin, J.A., Jr., Schlager, W., et al., *Proc. ODP, Init. Repts.,* 101: College Station, TX (Ocean Drilling Program), 39–46.

————, 1988. Paleomagnetism of Ocean Drilling Program Leg 101 Sediments: magnetostratigraphy, magnetic diagenesis, and paleolatitudes. *In* Austin, J.A., Jr., Schlager, W., et al., *Proc. ODP, Sci. Results,* 101: College Station, TX (Ocean Drilling Program), 327–360.

————, 1992. Seamount age estimates from paleomagnetism and their implications for the history of volcanism on the Pacific Plate. *In* Keating, B.H., and Bolton, B. (Eds.), *Geology and Offshore Mineral Resources of the Central Pacific Basin.* Circum.-Pac. Counc. Energy Miner. Resourc., Earth Sci. Ser., 14: New York (Springer-Verlag), 21–37.

Sager, W.W., Duncan, R.A., and Handschumacher, D.W., in press. Paleomagnetism of the Japanese and Marcus-Wake seamounts, Western Pacific Ocean. *In* Pringle, M.S., Sager, W.W., Sliter, W.V., and Stein, S. (Eds.), *The Mesozoic Pacific.* Am. Geophys. Union, Geophys. Monogr. Ser.

Schlanger, S.O., 1963. Subsurface geology of Eniwetok Atoll. *Geol. Surv. Prof. Pap. U.S.,* 260-BB:991–1066.

————, 1986. High frequency sea-level fluctuations in Cretaceous time: an emerging geophysical problem. *In* Hsü, K.J. (Ed.), *Mesozoic and Cenozoic Oceans.* Am. Geophys. Union, 61–74.

Sissingh, W., 1977. Biostratigraphy of Cretaceous calcareous nannoplankton. *Geol. Mijnbouw,* 56:37–65.

Suess, E., 1906. *The Face of the Earth* (Vol. 2): Oxford (Clarendon Press).

Tarduno, J.A., Mayer, L.A., Musgrave, R., and Shipboard Scientific Party, 1991. High-resolution, whole-core magnetic susceptibility data from Leg 130, Ontong Java Plateau. *In* Kroenke, L.W., Berger, W.H., Janecek, T.R., et al., *Proc. ODP, Init. Repts.,* 130: College Station, TX (Ocean Drilling Program), 541–548.

Thierstein, H.R., 1976. Mesozoic calcareous nannoplankton biostratigraphy of marine sediments. *Mar. Micropaleontol.,* 1:325–362.

van Waasbergen, R.J., and Winterer, E.L., in press. Summit geomorphology of Western Pacific guyots. *In* Pringle, M.S., Sager, W.W., Sliter, W.V., and Stein, S. (Eds.), *The Mesozoic Pacific.* Am. Geophys. Union, Geophys. Monogr. Ser.

* Abbreviations for names of organizations and publication titles in ODP reference lists follow the style given in *Chemical Abstracts Service Source Index* (published by American Chemical Society).

Vogt, P.R., and Smoot, N.C., 1984. The Geisha Guyots: multibeam bathymetry and morphometric interpretation. *J. Geophys. Res.*, 89:11085–11107.

Winterer, E.L., Duncan, R.A., McNutt, M.K., Natland, J.H., Premoli Silva, I., Sager, W.W., Sliter, W.V., van Waasbergen, R.J., and Wolfe, C.J., in press. Cretaceous guyots in the northwest Pacific: an overview of their geology and geophysics. *In* Pringle, M.S., Sager, W.W., Sliter, W.V., and Stein, S. (Eds.), *The Mesozoic Pacific.* Am. Geophys. Union, Geophys. Monogr. Ser.

Winterer, E.L., Ewing, J.I., et al., 1973. *Init. Repts. DSDP,* 17: Washington (U.S. Govt. Printing Office).

Winterer, E.L., and Metzler, C.V., 1984. Origin and subsidence of guyots in Mid-Pacific Mountains. *J. Geophys. Res.*, 89:9969–9979.

Ms143IR-106

NOTE: For all sites drilled, core-description forms ("barrel sheets") and core photographs have been reproduced on coated paper and can be found in Section 3, beginning on page 381. Forms containing smear-slide data can be found in Section 4, beginning on page 691. Thin-section data are given in Section 5, beginning on page 709. Conventional-log, FMS, and dipmeter data can be found in CD-ROM form (back pocket).

Table 11. Index properties and carbonate content data for pelagic sediments, Hole 865B.

Core, section, interval (cm)	Depth (mbsf)	Water content (%)	Bulk density (g/cm^3)	Grain density (g/cm^3)	Porosity (%)	$CaCO_3$ (%)
143-865B-						
1H-1, 74–75	0.73	125.20	1.44	2.76	77.90	
1H-1, 75–76	0.74	129.00	1.41	2.70	77.30	
1H-2, 76–77	2.25	132.40	1.41	2.60	78.30	93.20
1H-3, 76–77	3.75	128.40	1.41	2.67	77.60	
1H-4, 76–77	5.25	121.10	1.44	2.66	77.00	93.20
1H-5, 76–77	6.75	126.10	1.44	2.66	78.40	
1H-6, 34–35	7.83	39.50	1.88	2.72	52.00	95.90
2H-2, 74–75	10.73	112.40	1.48	2.65	76.50	94.50
2H-3, 74–75	12.23	97.60	1.52	2.69	73.40	
2H-4, 76–77	13.74	96.70	1.51	2.56	72.40	94.80
2H-5, 74–75	15.23	64.20	1.66	2.66	63.20	
2H-6, 34–36	16.33	61.00	1.68	2.69	62.00	96.90
3H-1, 78–79	18.77	71.80	1.61	2.64	65.70	95.40
3H-2, 97–98	20.46	68.10	1.64	2.70	64.90	
3H-3, 71–72	21.70	73.30	1.61	2.65	66.30	95.60
3H-4, 110–112	23.59	56.90	1.71	2.68	60.70	
3H-5, 78–79	24.76	62.20	1.68	2.69	63.00	96.30
3H-6, 78–79	26.26	65.10	1.66	2.64	63.70	98.50
3H-7, 24–25	27.23	64.90	1.66	2.67	63.70	96.90
3H-CC, 18–19	27.69	56.90	1.70	2.65	60.20	
4H-1, 88–89	28.37	71.30	1.64	2.61	66.50	96.30
4H-2, 76–77	29.75	71.40	1.65	2.69	67.00	
4H-3, 78–79	31.26	72.20	1.63	2.64	66.90	96.00
4H-4, 77–78	32.76	75.30	1.63	2.65	68.20	
4H-5, 88–89	34.36	66.40	1.66	2.72	64.60	96.00
4H-6, 13–14	35.12	72.90	1.61	2.67	66.10	
4H-CC, 29–30	35.54	57.20	1.71	2.68	60.90	
5H-1, 78–79	37.77	70.60	1.63	2.64	65.80	
5H-2, 118–119	39.68	60.00	1.68	2.67	61.60	96.40
5H-3, 76–77	40.75	53.00	1.74	2.68	58.80	
5H-4, 76–77	42.25	65.70	1.65	2.65	64.00	96.50
5H-5, 50–51	43.49	62.80	1.70	2.62	63.90	
5H-6, 27–28	44.26	66.20	1.66	2.65	64.70	95.70
6H-1, 135–137	47.84	61.20	1.68	2.68	62.30	
6H-2, 71–72	48.70	56.40	1.71	2.65	60.20	96.70
6H-3, 75–76	50.24	67.30	1.66	2.67	65.20	95.50
6H-4, 52–53	51.51	59.70	1.71	2.71	62.30	96.80
6H-5, 129–130	53.78	57.40	1.71	2.68	61.00	96.50
7H-1, 108–109	57.07	55.40	1.72	2.71	60.00	
7H-2, 112–113	58.61	52.50	1.75	2.70	58.80	97.10
7H-3, 42–43	59.41	52.60	1.75	2.70	58.90	
7H-4, 54–55	61.03	53.30	1.74	2.70	59.20	97.00
7H-5, 55–56	62.54	58.50	1.71	2.68	61.50	
7H-6, 29–30	63.28	54.80	1.75	2.69	60.40	
7H-CC, 37–38	64.20	54.40	1.75	2.68	60.00	
143-865B-						
8H-1, 117–118	66.66	56.30	1.73	2.67	60.70	97.50
8H-2, 108–109	68.07	62.30	1.66	2.69	62.20	
8H-3, 114–115	69.63	53.50	1.74	2.66	59.40	96.70
8H-4, 75–76	70.74	56.50	1.72	2.70	60.60	
8H-5, 90–91	72.39	63.60	1.68	2.65	63.70	96.00
8H-6, 57–58	73.56	66.60	1.66	2.63	64.70	
9H-1, 77–78	75.76	64.00	1.65	2.64	63.00	96.80
9H-2, 75–76	77.24	61.30	1.68	2.68	62.40	
9H-3, 75–76	78.74	71.10	1.63	2.68	66.20	95.80
9H-4, 113–114	80.62	61.10	1.68	2.66	62.30	
9H-5, 76–77	81.75	69.90	1.60	2.66	64.40	96.40
9H-6, 83–84	83.32	65.90	1.66	2.68	64.20	
10H-1, 76–77	85.25	96.30	1.52	2.61	72.70	
10H-2, 79–80	86.78	86.70	1.57	2.68	71.10	93.40
10H-3, 76–77	88.25	80.10	1.54	2.38	66.70	
10H-4, 33–34	89.32	64.20	1.57	2.64	59.90	96.80
10H-5, 66–67	91.15	82.90	1.58	2.64	69.70	
11H-1, 79–80	94.78	67.70	1.68	2.69	66.20	95.90
11H-2, 79–80	96.28	69.20	1.64	2.67	65.30	
11H-3, 79–80	97.78	81.10	1.56	2.60	68.20	92.50
11H-4, 79–80	99.28	77.50	1.59	2.66	67.70	
11H-5, 79–80	100.78	88.10	1.56	2.63	71.20	94.30
11H-6, 51–52	102.00	112.80	1.54	2.31	79.60	
12H-1, 59–60	104.08	75.20	1.60	2.69	66.90	95.80
12H-2, 75–76	105.74	81.00	1.58	2.65	69.20	
12H-3, 76–77	107.25	67.50	1.67	2.67	65.60	96.50
12H-4, 75–76	108.74	60.70	1.69	2.68	62.40	
12H-5, 54–55	110.03	66.30	1.63	2.67	63.40	96.10
12H-6, 63–64	111.62	73.30	1.62	2.68	66.80	
13H-1, 55–56	113.54	77.20	1.58	2.63	67.30	95.60
13H-2, 44–45	114.93	66.10	1.65	2.71	64.00	
13H-3, 78–79	116.77	66.20	1.65	2.66	64.00	97.40
13H-4, 44–45	117.93	72.70	1.62	2.67	66.60	
13H-5, 62–63	119.62	65.20	1.67	2.66	64.40	96.60
13H-6, 43–44	120.92	67.90	1.65	2.72	65.00	
14H-1, 76–77	123.25	61.60	1.68	2.69	62.70	
14H-2, 76–77	124.75	44.80	1.81	2.68	54.70	95.50
14H-3, 36–37	125.84	60.20	1.69	2.68	62.00	
14H-4, 74–75	127.73	58.00	1.71	2.68	61.20	95.20
14H-5, 74–75	129.23	65.70	1.67	2.66	64.60	
14H-6, 23–24	130.22	63.40	1.68	2.67	63.50	96.00
15X-1, 77–78	132.76	69.80	1.64	2.64	65.70	
15X-2, 77–78	134.26	56.90	1.73	2.69	61.10	95.80
15X-3, 19–20	135.18	56.40	1.75	2.67	61.40	

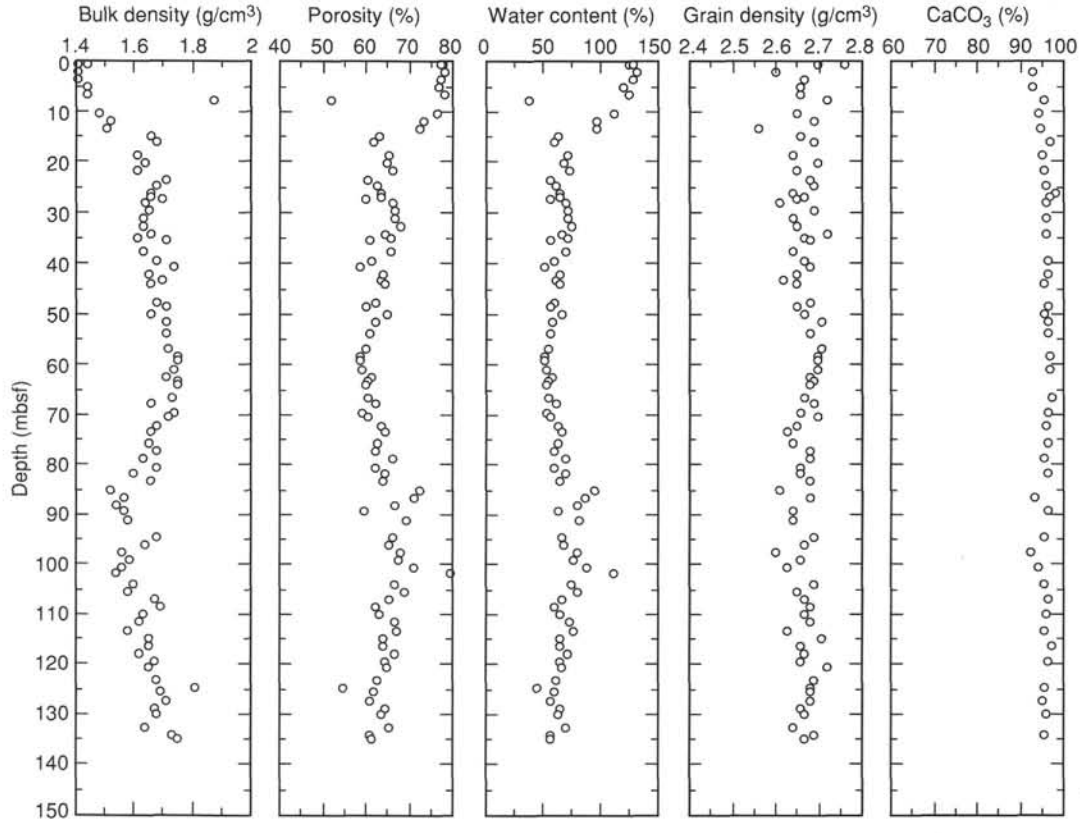

Figure 41. Index properties and carbonate content for pelagic sediments in Hole 865B.

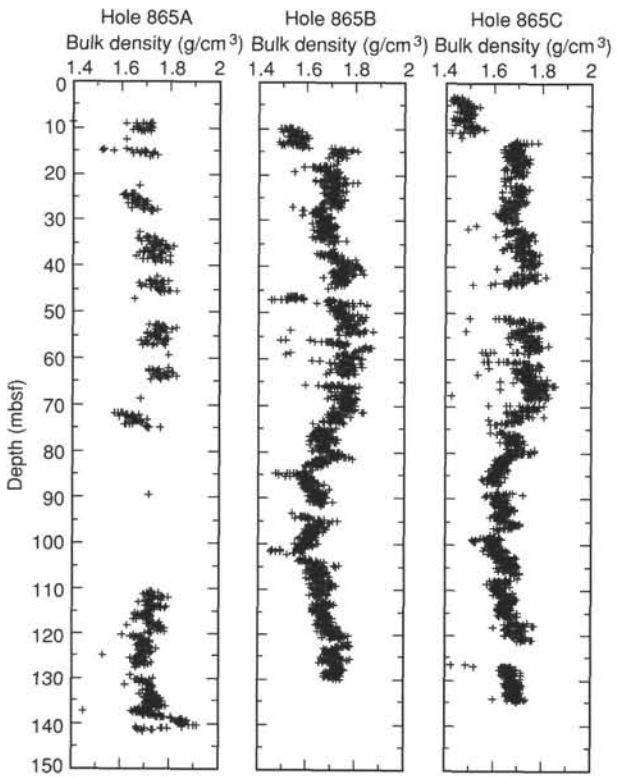

Figure 42. GRAPE density logs for pelagic sediments in Holes 865A, 865B and 865C. The GRAPE data sets have been reduced in size by applying a "sliding average" whereby every five successive data points were averaged for depth and GRAPE density.

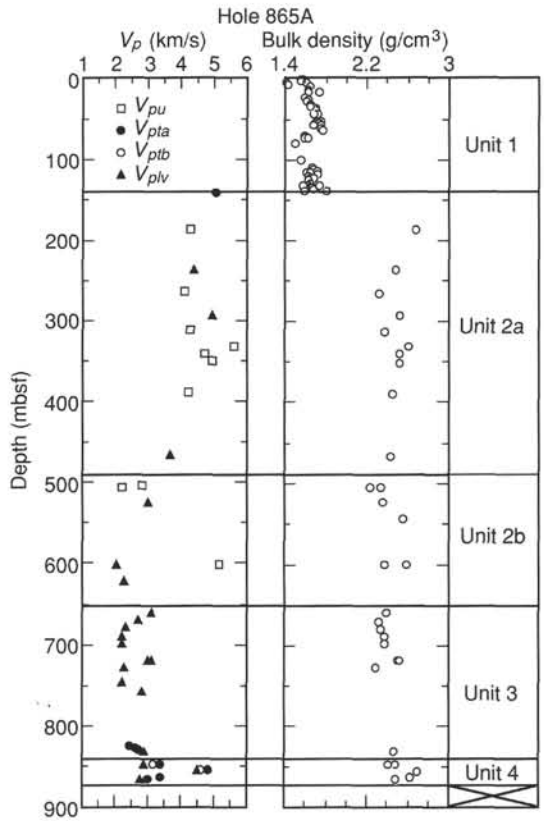

Figure 43. PP units for Site 865 based on variation in acoustic velocity and bulk density. Velocity symbols as in Figure 40.

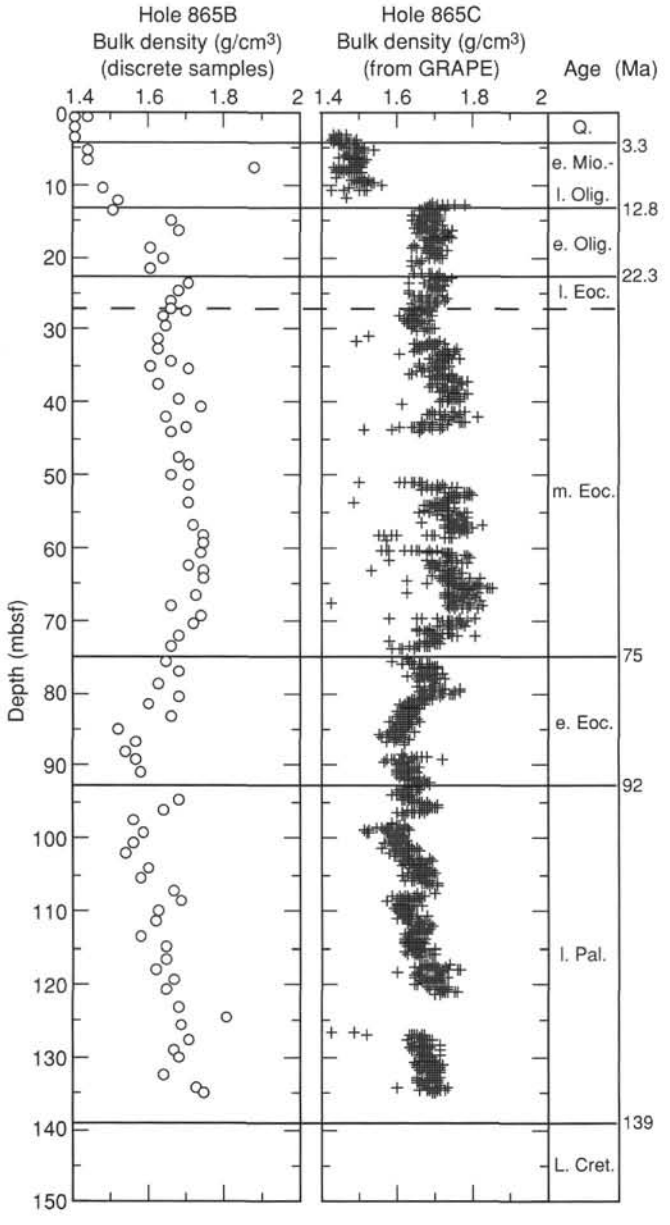

Figure 44. Correlation between GRAPE density (Hole 865C), bulk density from discrete measurements (Hole 865B), and depositional age in pelagic sediments from Site 865. The GRAPE data set has been reduced by applying a sliding average correction (see Fig. 42 caption).

Table 12. Thermal conductivity for pelagic sediments, Holes 865A and 865B.

Core, section, interval (cm)	Depth (mbsf)	Thermal conductivity (W/m · K)
143-865A-		
4R-1, 75	24.95	1.194
4R-2, 72	26.42	1.160
4R-2, 75	26.45	1.098
4R-3, 72	27.92	1.115
5R-4, 50	37.35	1.213
6R-2, 75	45.45	1.188
7R-3, 75	55.02	1.182
7R-4, 55	56.34	1.329
7R-5, 36	57.25	1.257
8R-1, 75	63.05	1.214
8R-2, 50	64.30	1.309
9R-2, 75	74.05	1.128
9R-3, 26	75.06	1.138
13R-3, 75	114.55	1.177
13R-6, 75	119.05	1.237
14R-2, 75	122.75	1.169
14R-3, 75	124.25	1.117
14R-4, 75	125.75	1.131
14R-5, 52	127.02	1.202
15R-3, 75	133.85	1.160
15R-4, 75	135.35	1.101
15R-5, 67	136.77	1.081
15R-6, 75	138.35	1.071
15R-7, 25	139.35	1.267
143-865B-		
2H-5, 113	15.63	1.206
2X-6, 50	16.50	1.115
3X-3, 123	22.23	1.090
3X-4, 123	23.73	1.111
4X-3, 120	31.70	1.213
5X-3, 120	41.20	1.238
5X-4, 120	42.70	1.071
5X-5, 62	43.62	1.142
8X-1, 75	66.25	1.119
8X-2, 75	67.75	1.371
8X-3, 75	69.25	1.165
8X-4, 75	70.75	1.188
8X-5, 75	72.25	1.135
9X-6, 92	83.42	1.113
10X-3, 100	88.50	0.970
10X-5, 100	91.50	1.154
13X-3, 100	117.00	1.046
13X-4, 100	118.50	0.991
13X-5, 100	120.00	0.984
13X-6, 80	121.30	1.053

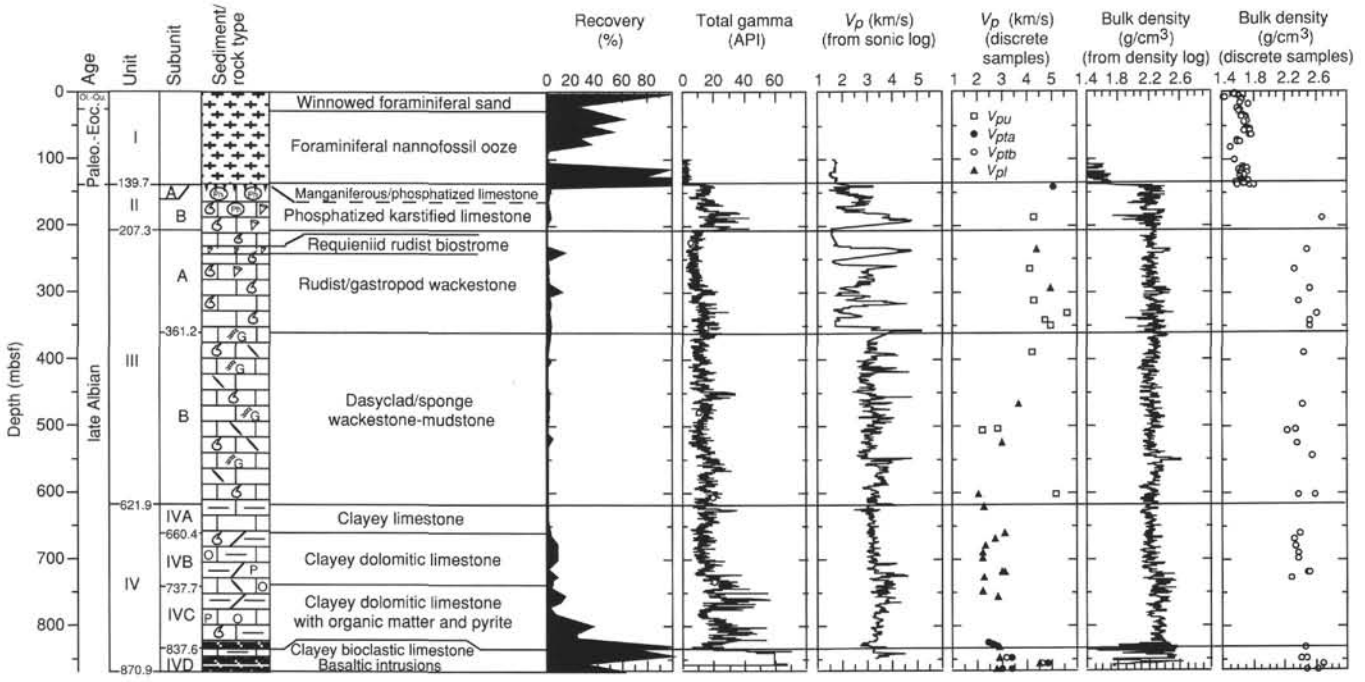

Figure 45. Correlation between recovery, discrete measurements of acoustic velocity and bulk density, well-log sonic velocity and bulk density, total gamma-ray, and lithologic units. Velocity symbols as in Figure 40.

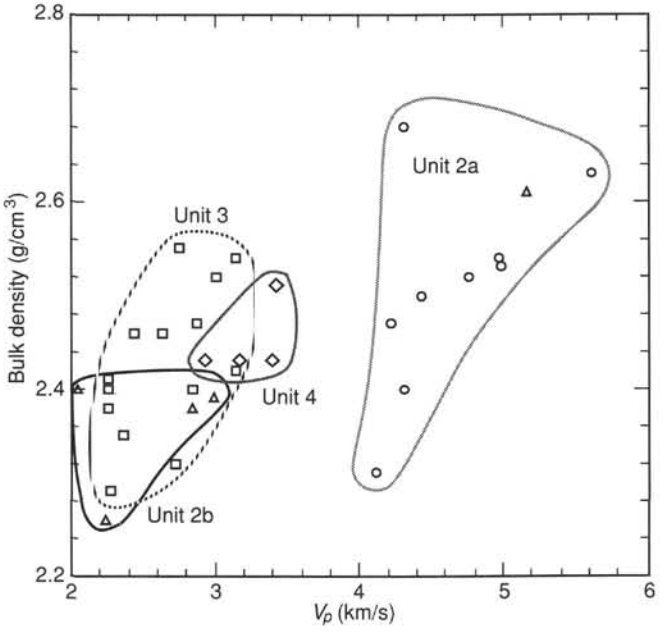

Figure 46. Cross plot of bulk density and acoustic velocity measured in discrete samples from the shallow-water platform sediments in Hole 865A (139.7–870.9 mbsf). Measurements of *P*-wave velocity are discriminated for PP units.

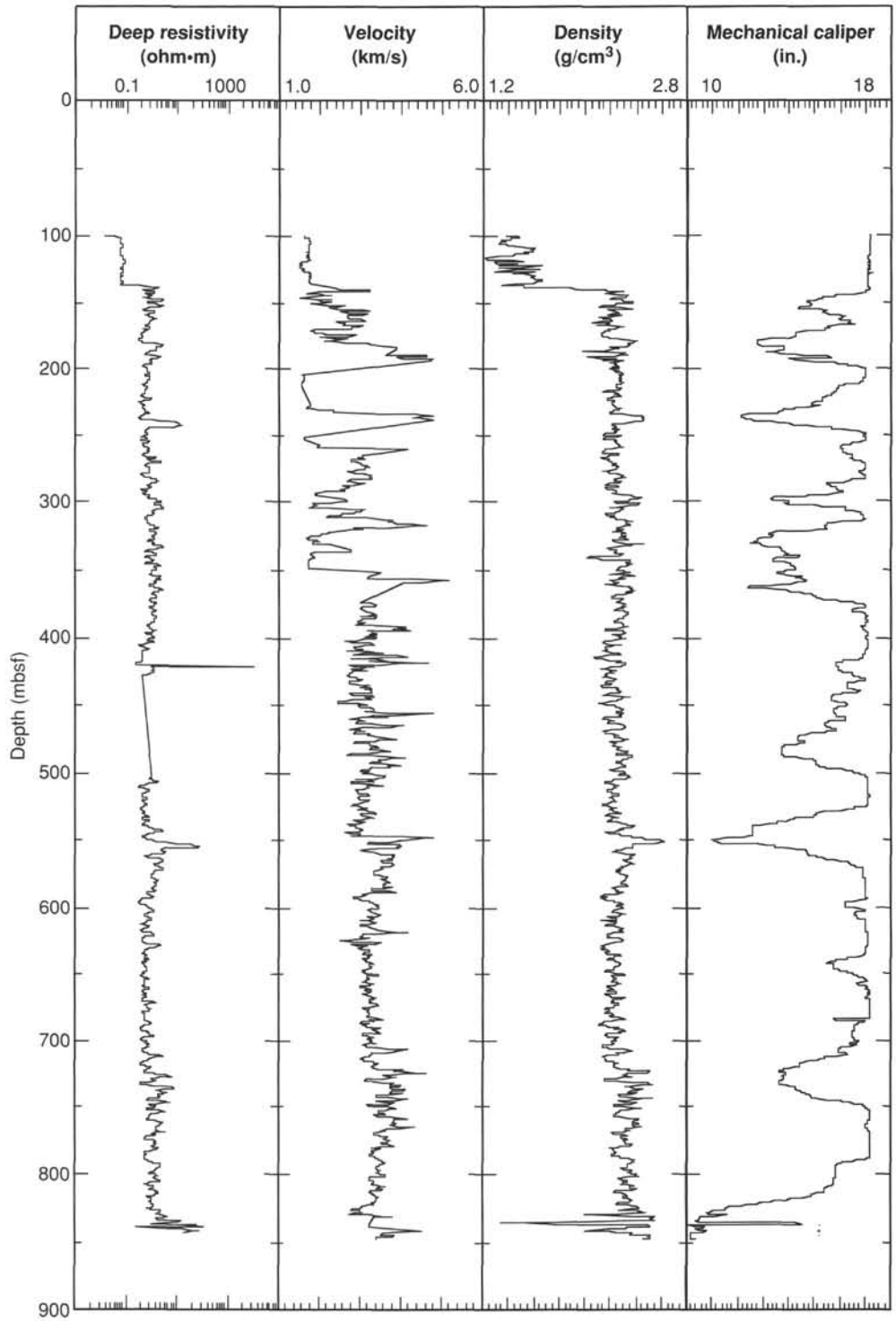

Figure 47. Primary porosity logs used for determining lithologies in Hole 865A.

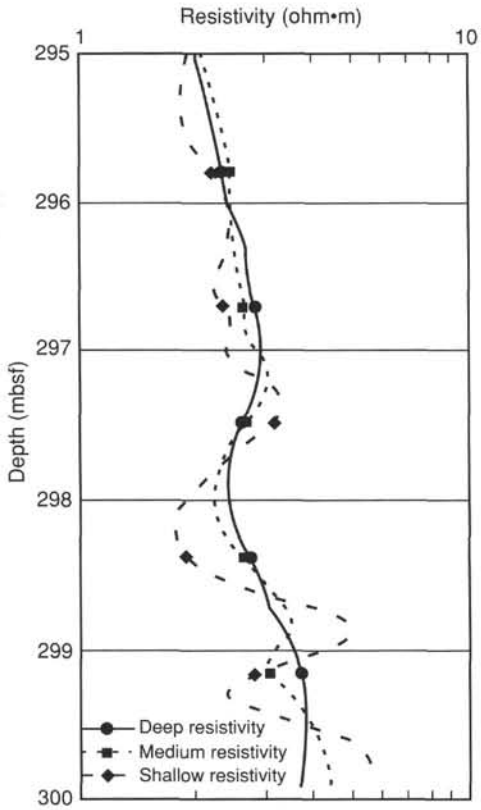

Figure 48. Comparison of the responses of the deep, medium, and shallow resistivity measurements.

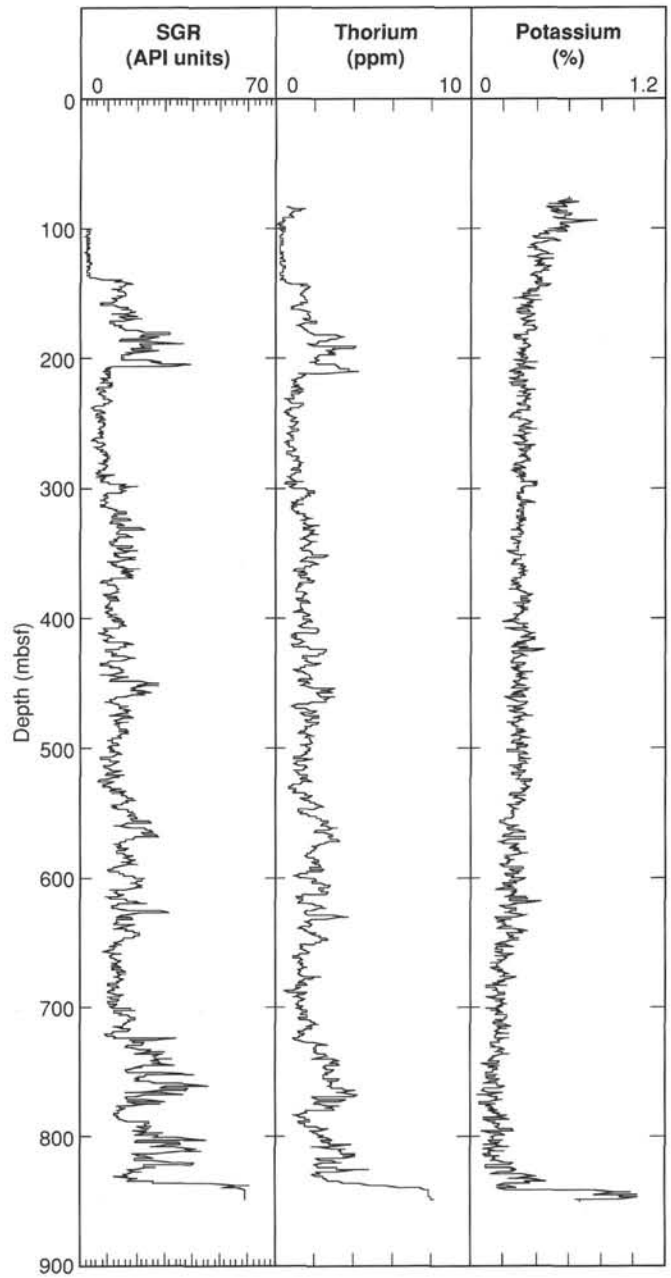

Figure 49. Primary NGT logs used for determining lithologies in Hole 865A.

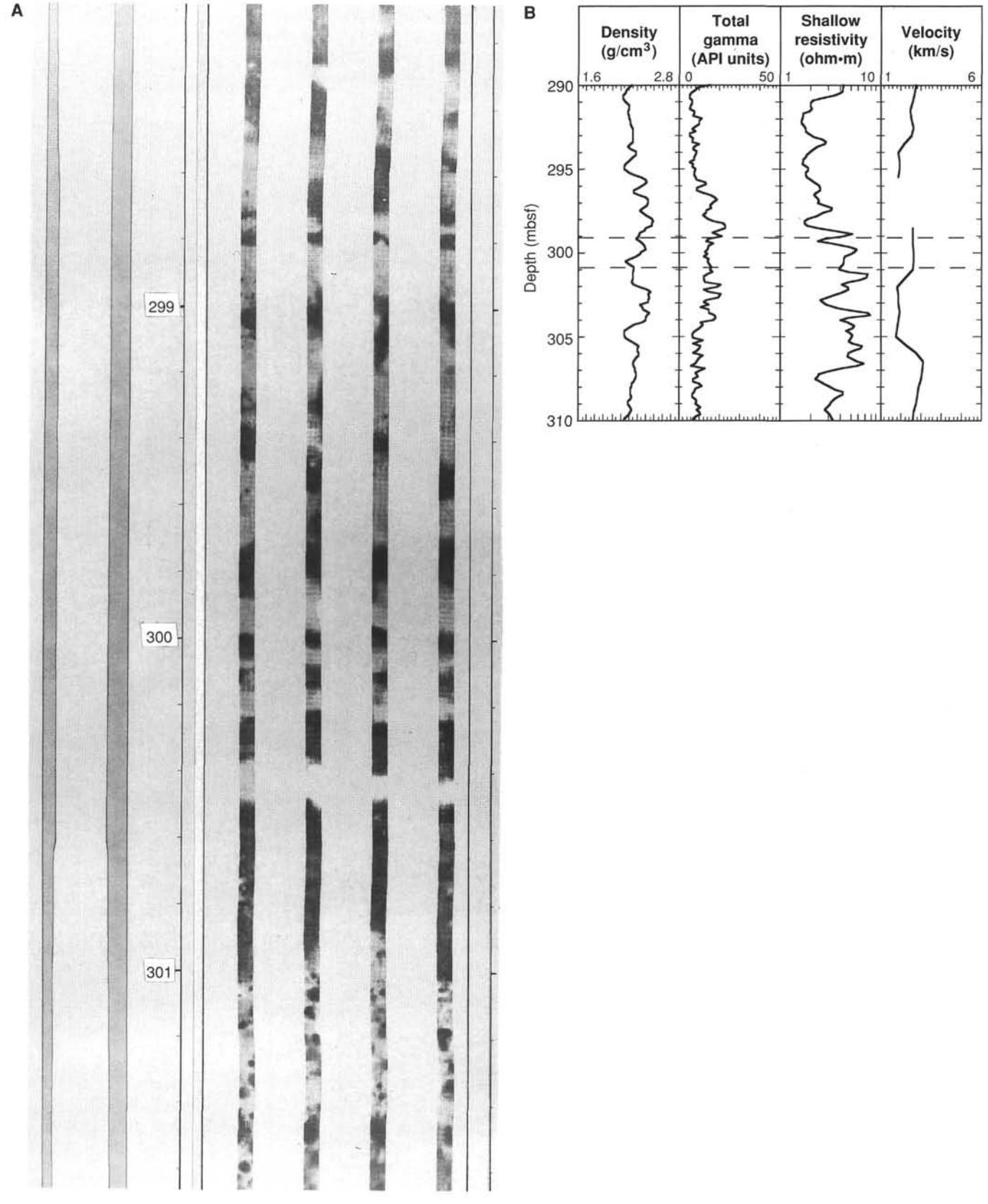

Figure 50. **A.** FMS image of porosity variations for the interval at 299–301 mbsf. **B.** Expanded-scale plot of conventional logs bracketing that interval. Horizontal, dashed lines in B show position of FMS image.

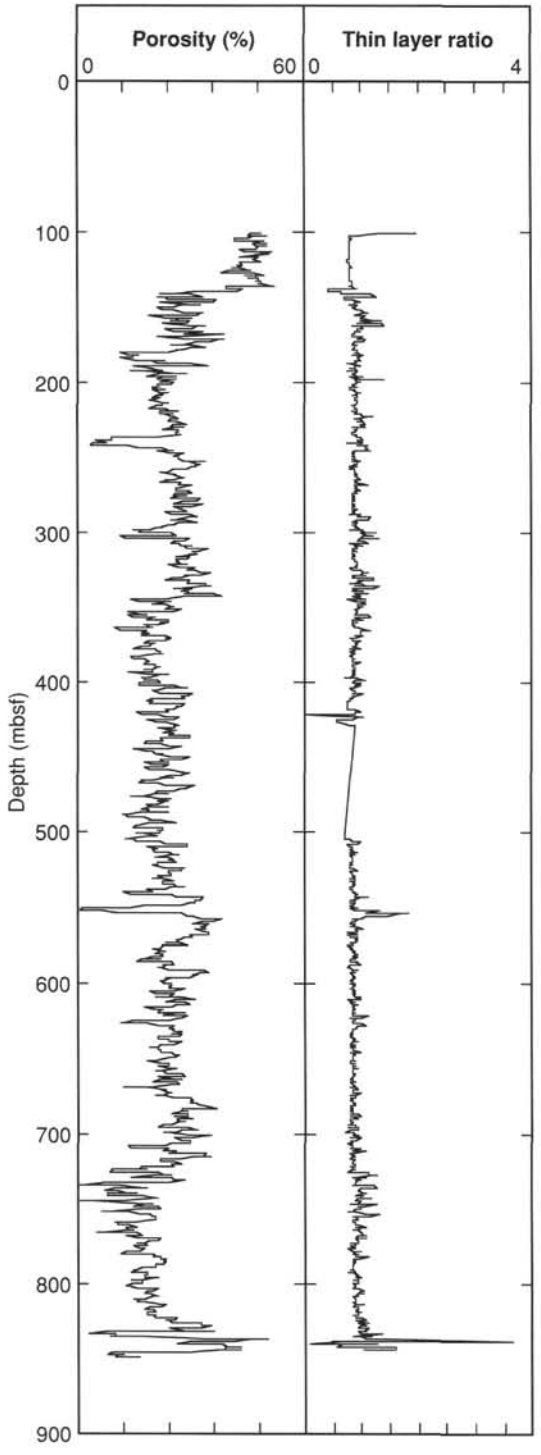

Figure 51. Porosity and calculated Thin Layer Ratio.

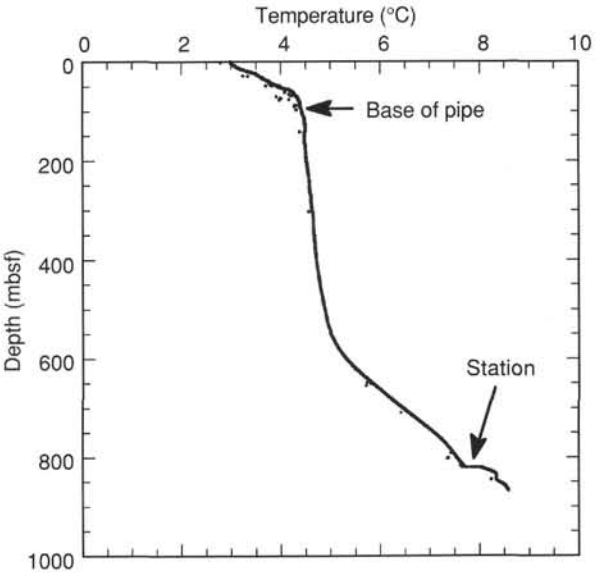

Figure 52. Temperature profile for Hole 865A.

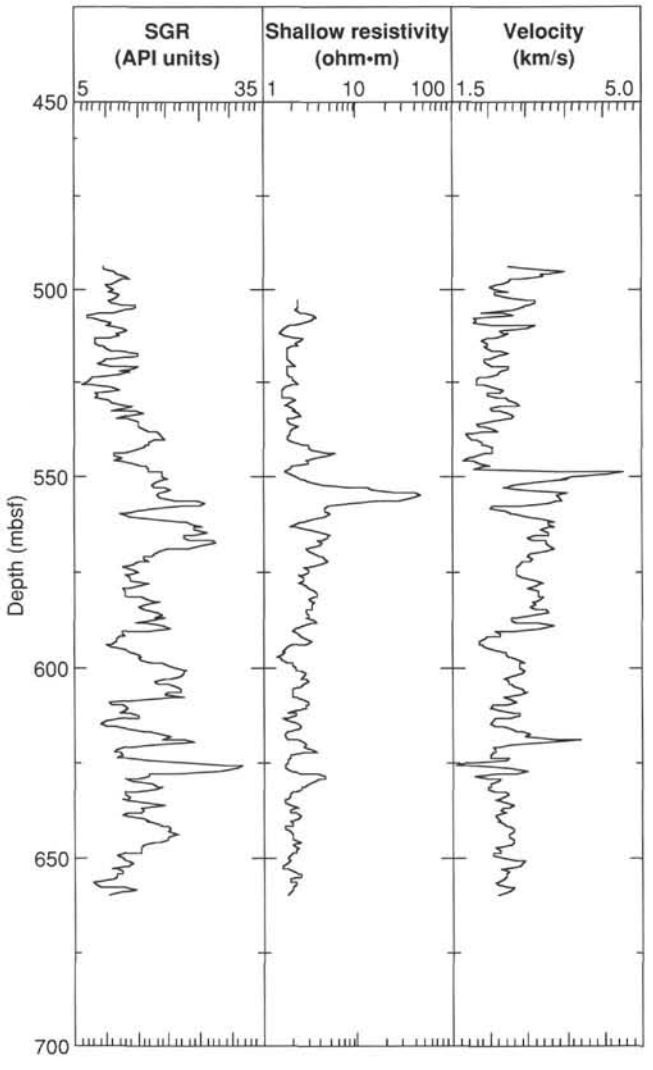

Figure 53. Expanded plot of gamma-ray count, resistivity, and velocity for logging Unit 5.

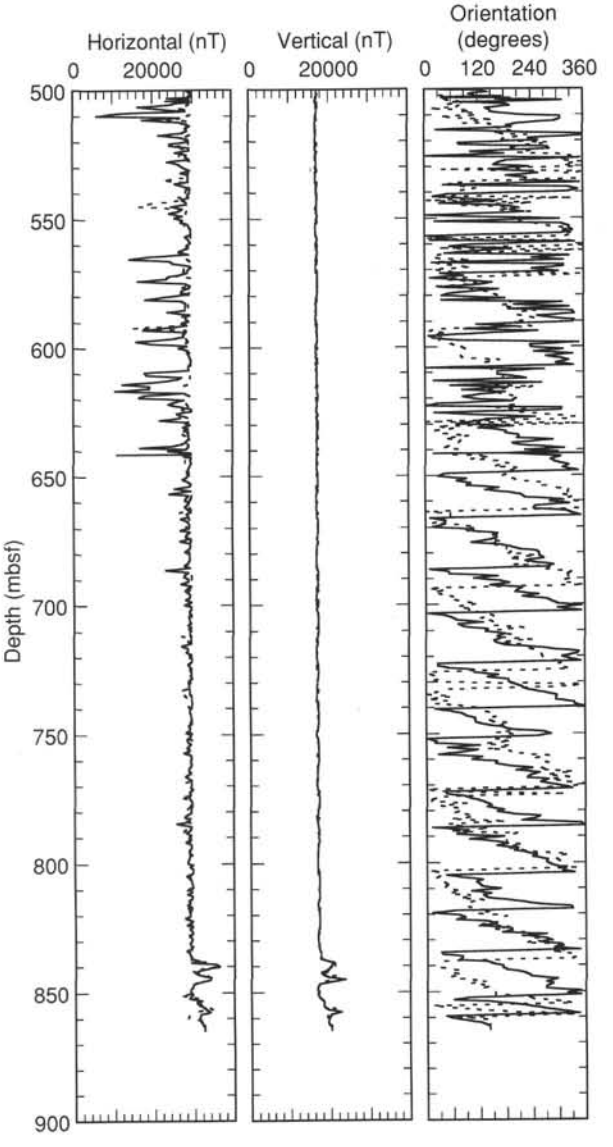

Figure 54. Variations in horizontal and vertical components of the geomagnetic field and the orientation of the tool with respect to the present geomagnetic field within Hole 865A from 500 to 865 mbsf. Solid and dashed lines show down- and up-going logs, respectively.

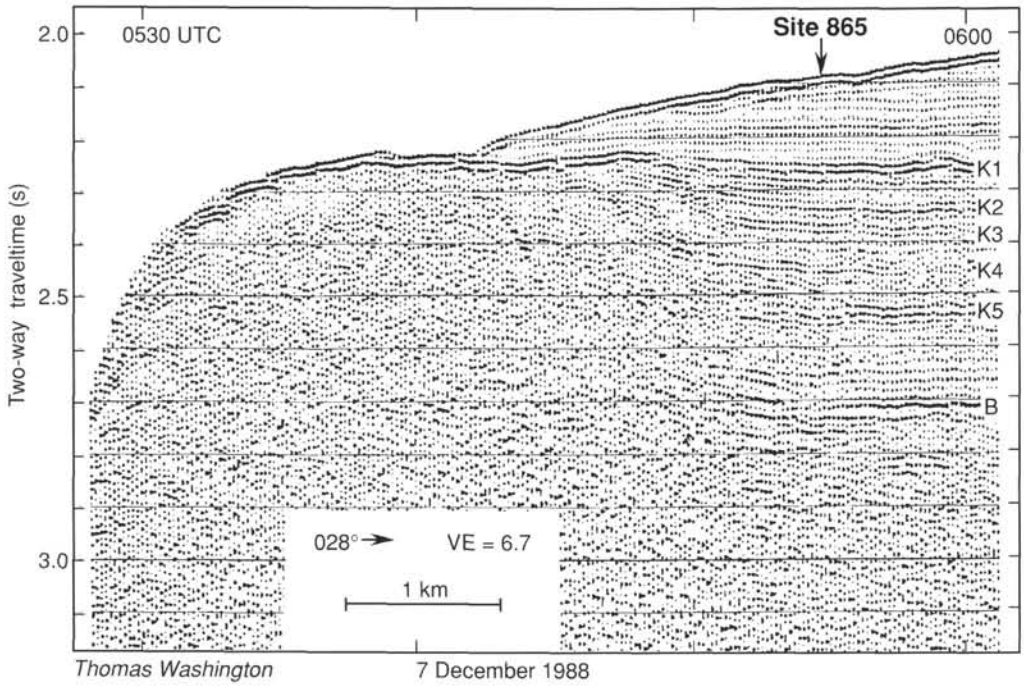

Figure 55. Seismic reflection profile through Site 865, taken from *Thomas Washington* (Scripps Institution of Oceanography), during Leg 10 of the Roundabout Expedition, 7 December 1988. The principal reflectors, listed in Table 13, have been labeled. This profile is an enlargement of the complete guyot-crossing displayed in Figure 4.

Table 13. Principal seismic reflectors at Site 865, showing estimated depth beneath the seafloor and calculated sonic velocities.

Reflector	Time bsl (ms)	Time bsf (ms)	Depth (mbsf)	Ave. vel. (m/s)	Int. vel. (m/s)	Ave. vel. ls (m/s)
SF	2083	0	0	1500	1500	
K1	2250	167	138	1653	1653	
K2	2324	241	236	1959	2649	2649
K3	2380	297	314	2115	2786	2708
K4	2445	362	412	2276	3015	2810
K5	2525	442	536	2425	3100	2895
B	2716	633	840	2654	3183	3013

Note: Average velocities from the seafloor to each reflector are given in Column 5, interval velocities between successive reflectors in Column 6, and average velocities from the top of the Cretaceous limestone in the last column. Vel = velocity; ls = in limestone section; bsl = below sea level; bsf = below seafloor.

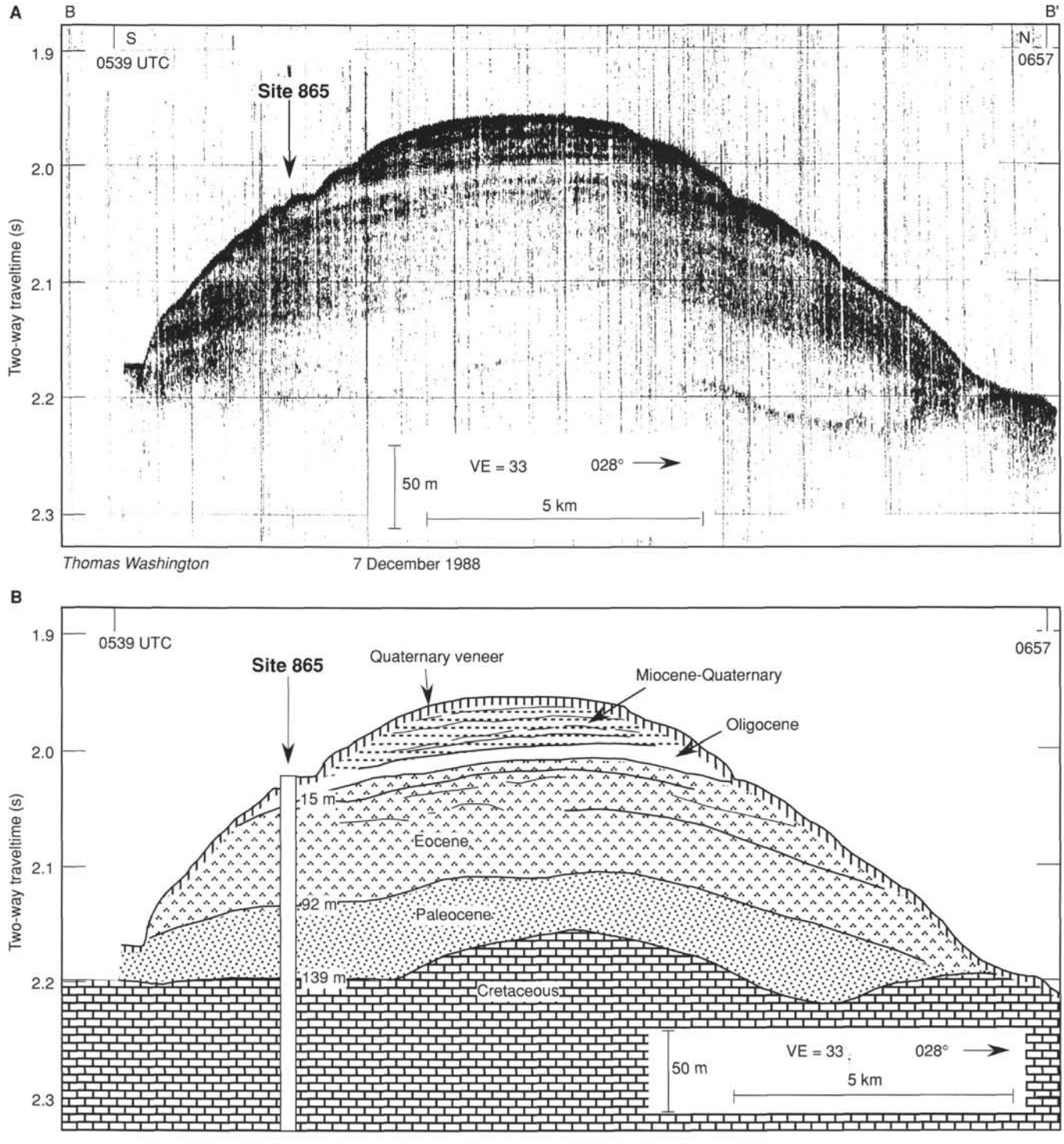

Figure 56. **A.** A 3.5-kHz echo-sounder profile of the pelagic cap at Site 865, taken from the *Thomas Washington* during Leg 10 of the Roundabout Expedition, 7 December 1988. **B.** Interpretation of acoustic reflection character of the pelagic cap. Ages and layer thicknesses were correlated with the drilling results of Holes 865B and 865C. For location, see Figure 2.

Hole 865A: Resistivity-Sonic-Natural Gamma Ray Log Summary

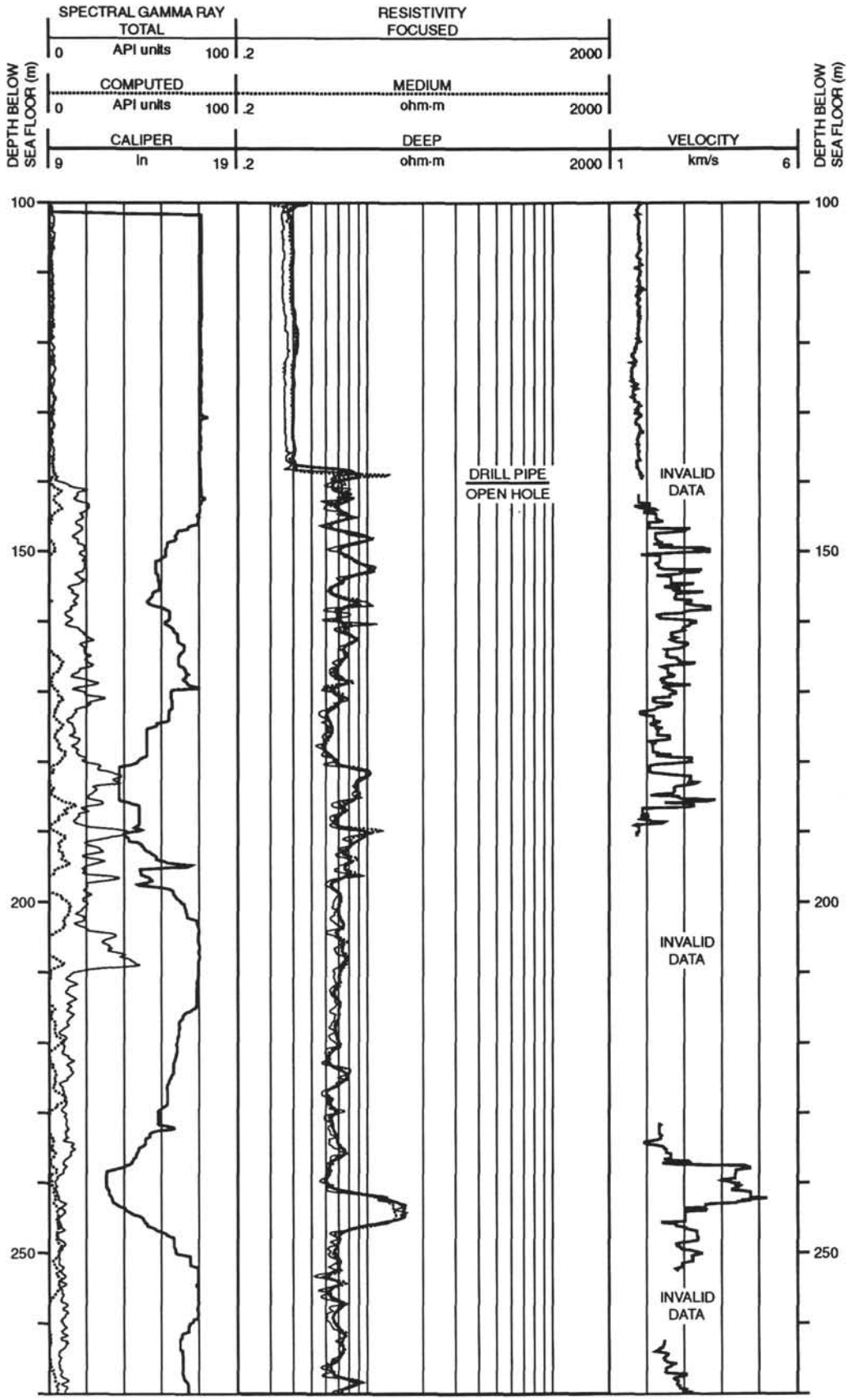

Hole 865A: Resistivity-Sonic-Natural Gamma Ray Log Summary (continued)

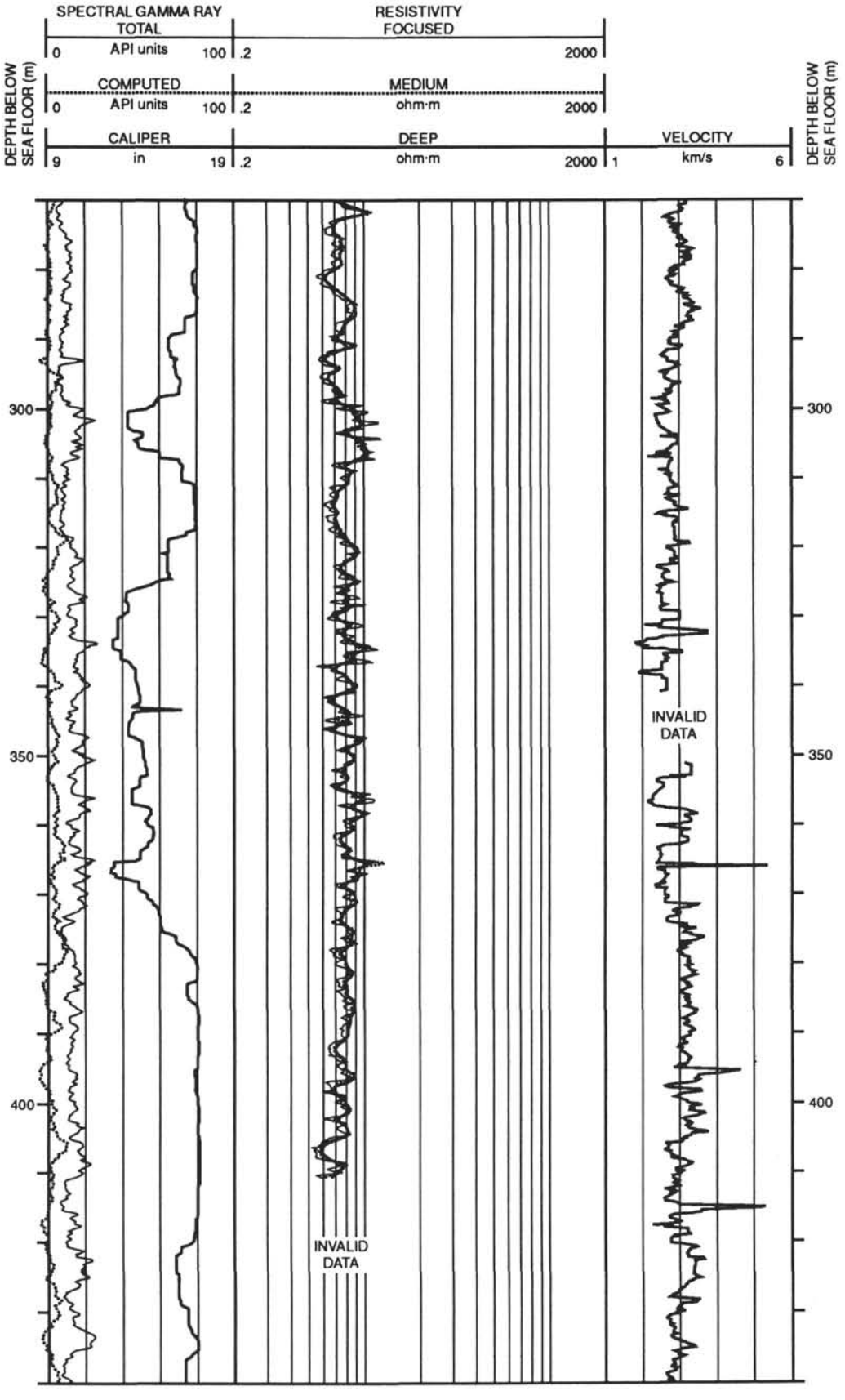

Hole 865A: Resistivity-Sonic-Natural Gamma Ray Log Summary (continued)

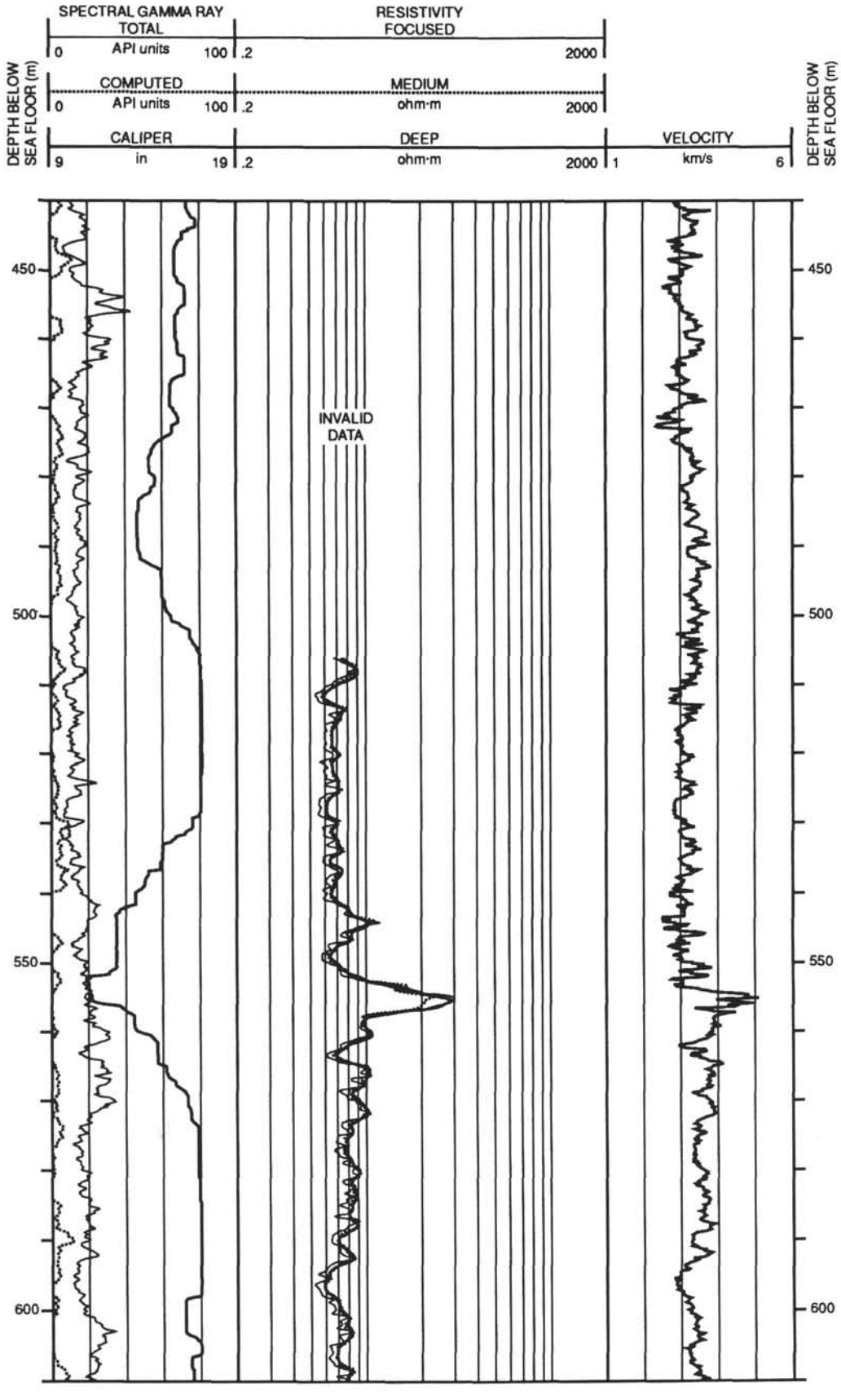

Hole 865A: Resistivity-Sonic-Natural Gamma Ray Log Summary (continued)

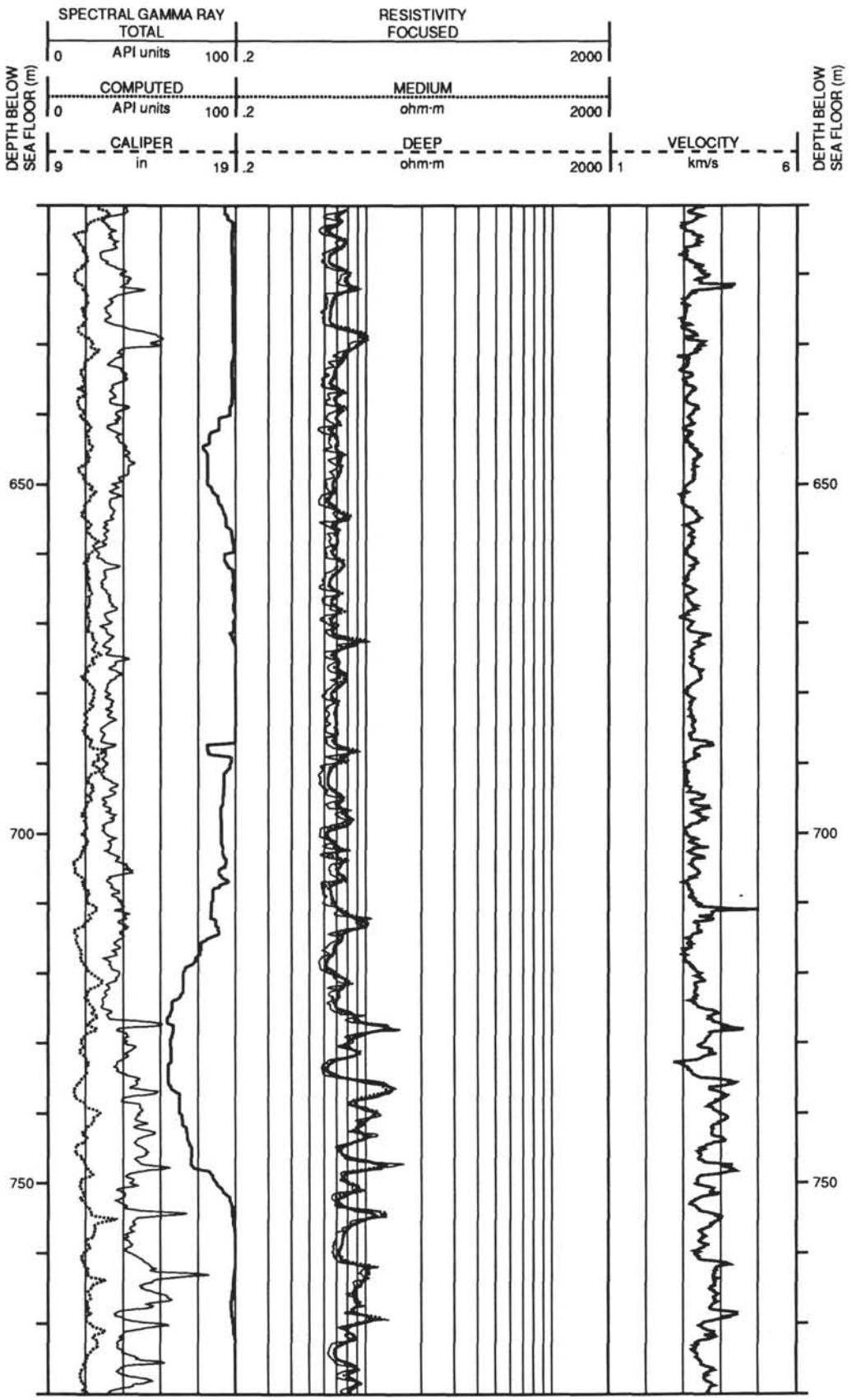

Hole 865A: Resistivity-Sonic-Natural Gamma Ray Log Summary (continued)

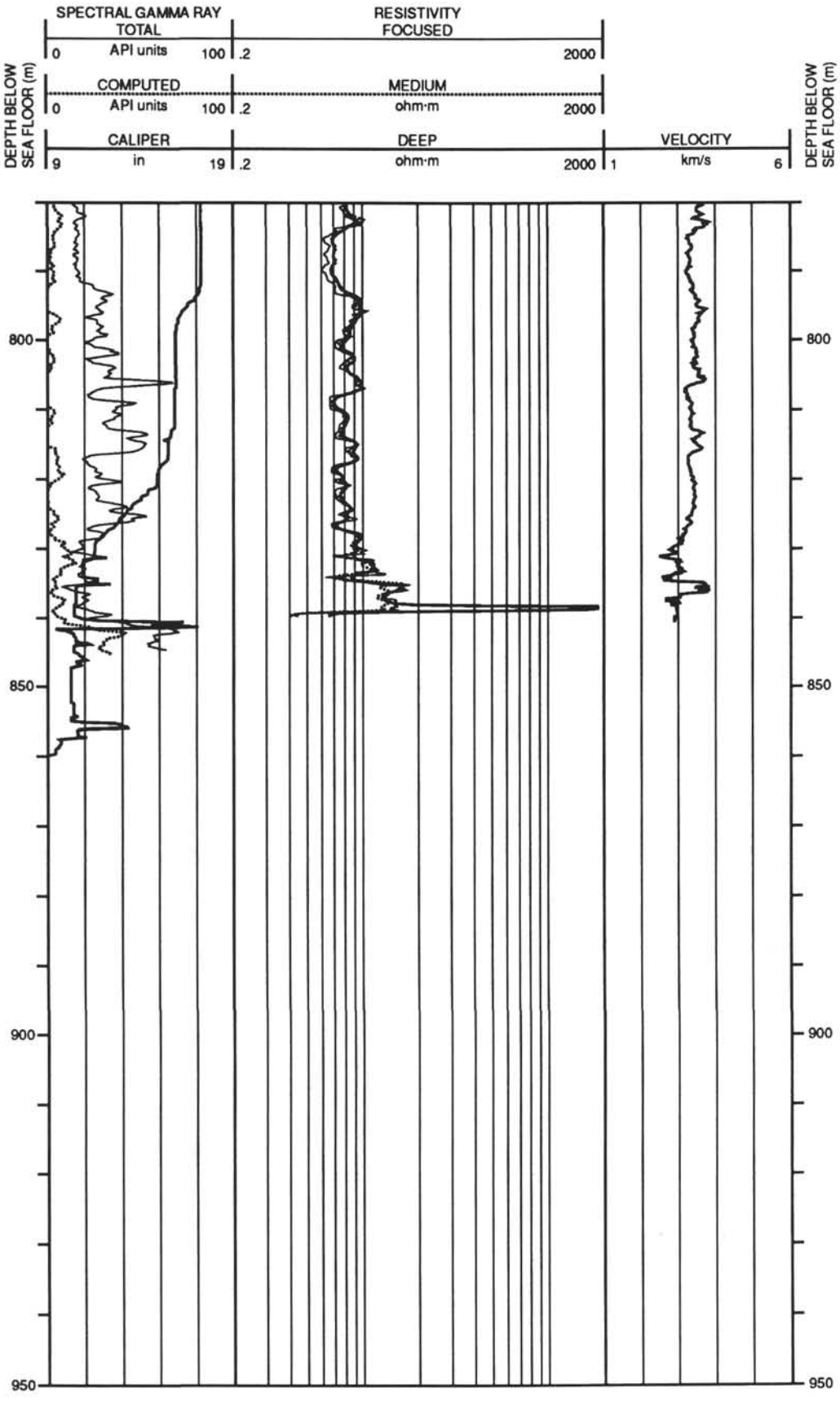

Hole 865A: Density-Porosity-Natural Gamma Ray Log Summary

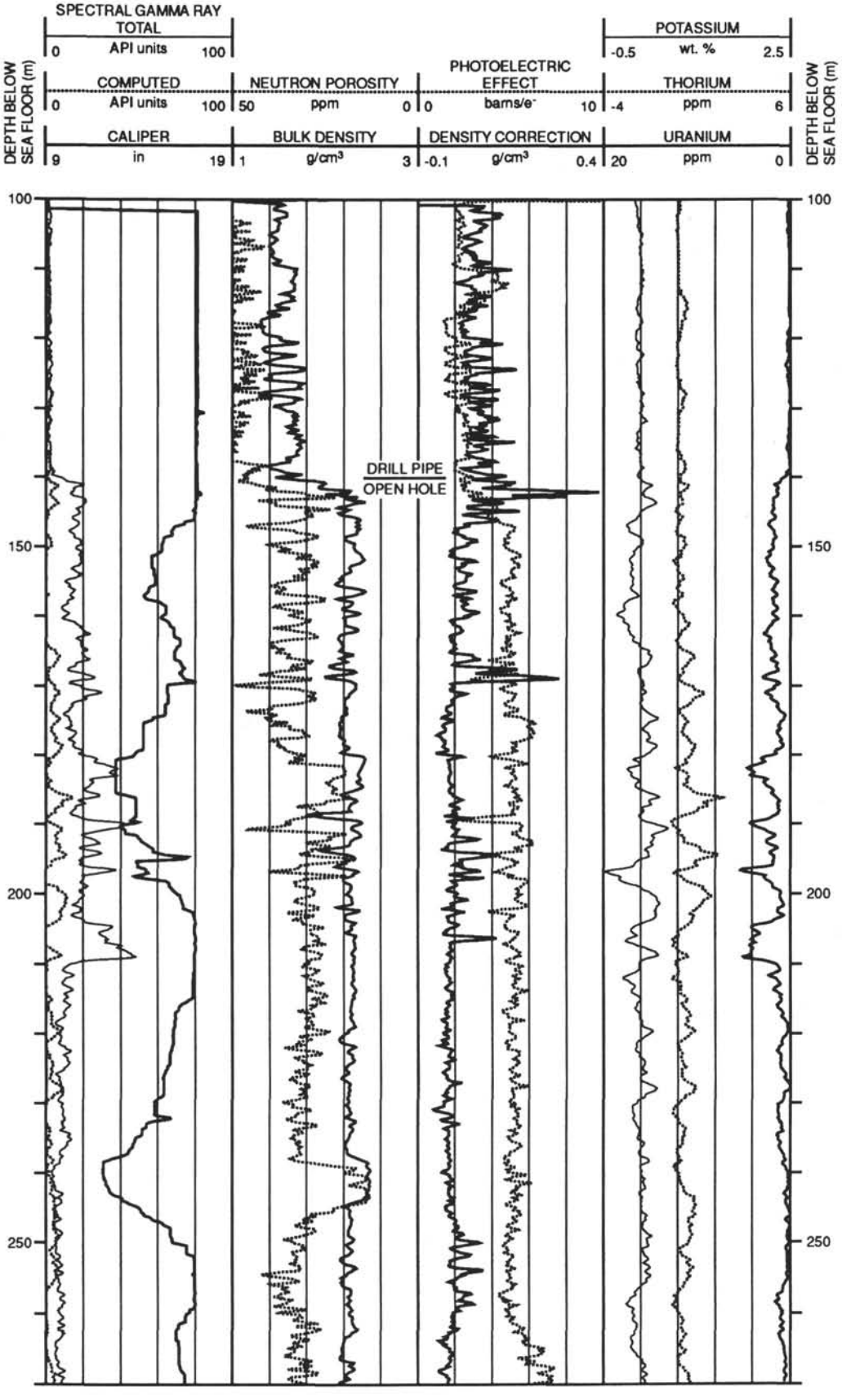

Hole 865A: Density-Porosity-Natural Gamma Ray Log Summary (continued)

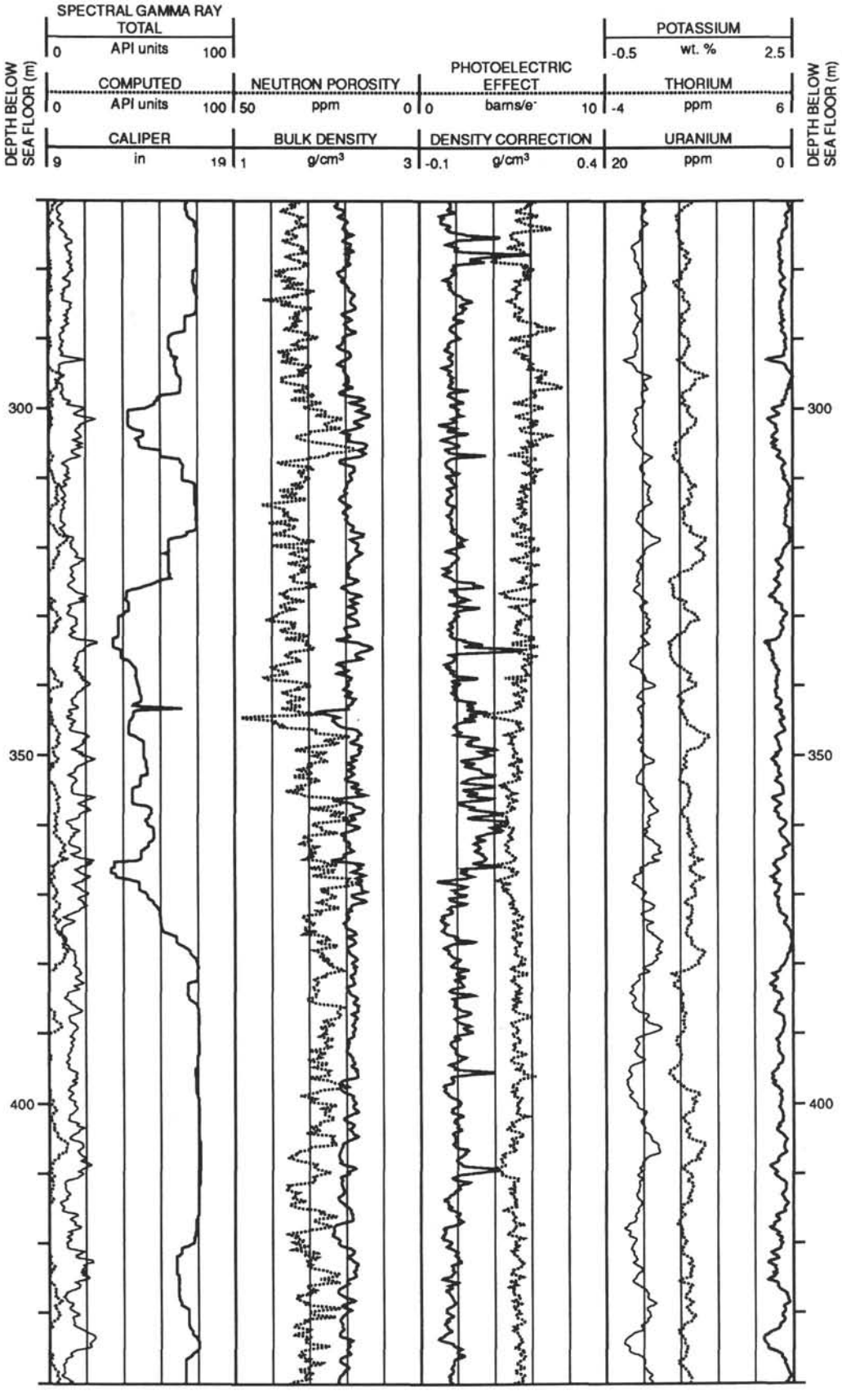

Hole 865A: Density-Porosity-Natural Gamma Ray Log Summary (continued)

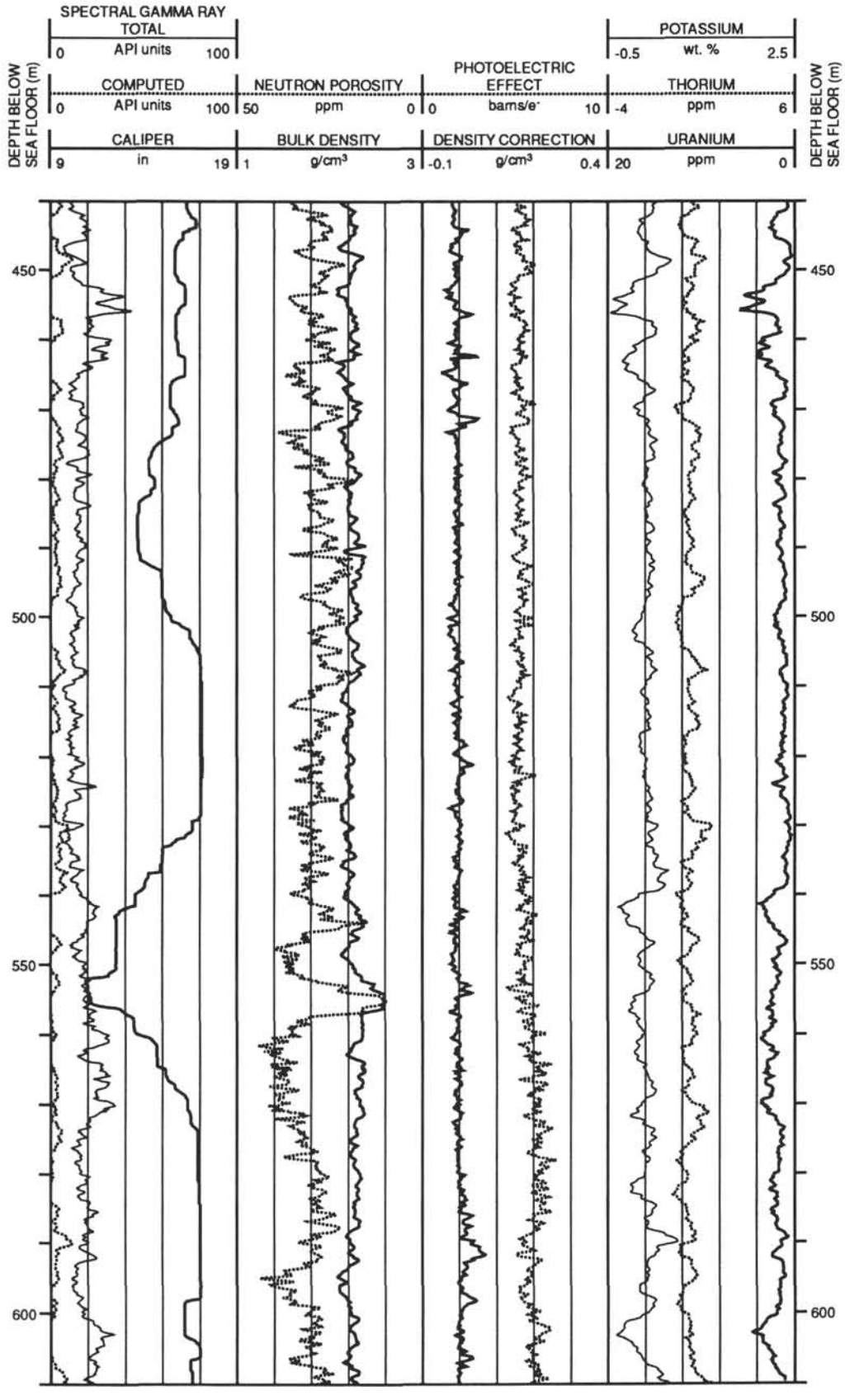

Hole 865A: Density-Porosity-Natural Gamma Ray Log Summary (continued)

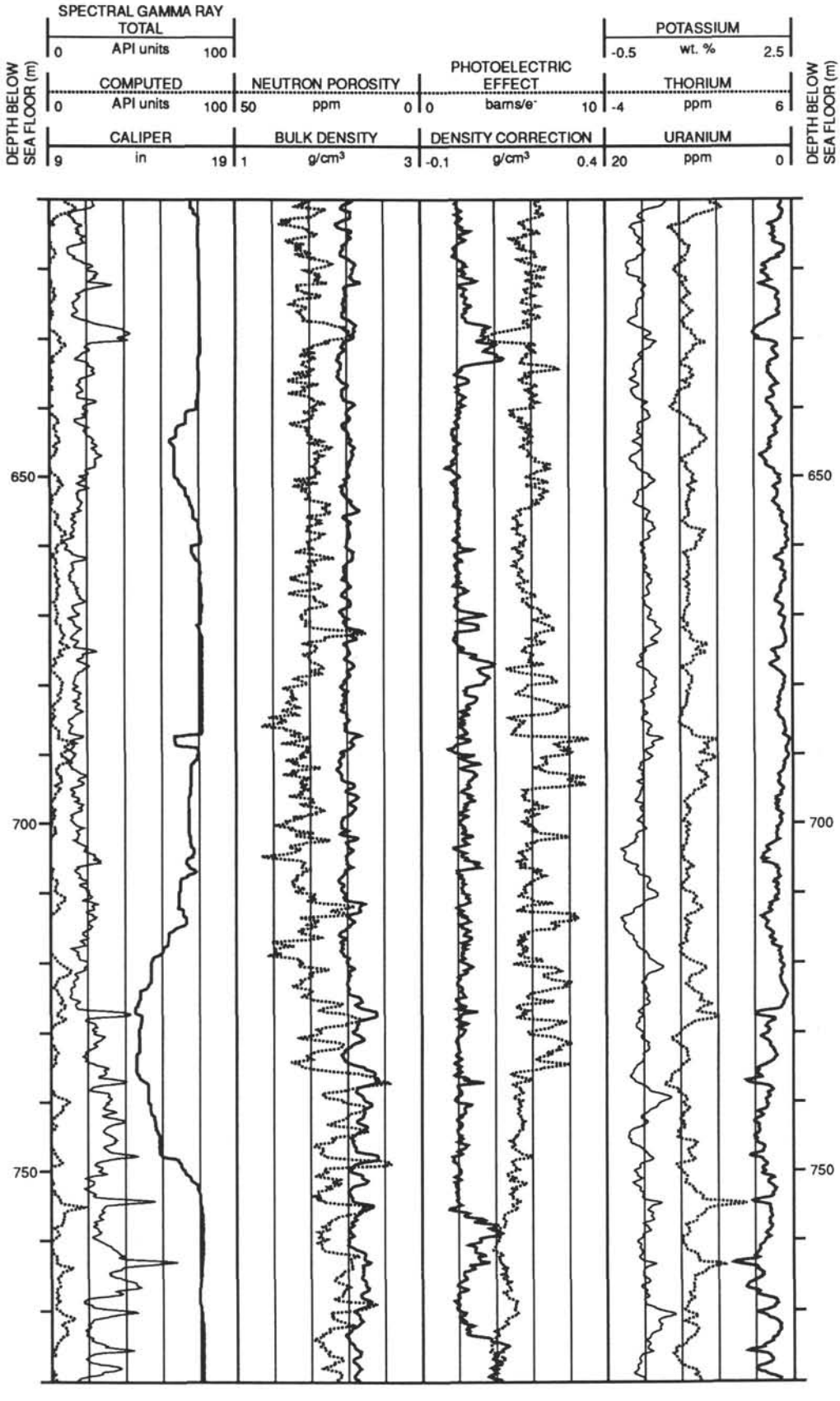

Hole 865A: Density-Porosity-Natural Gamma Ray Log Summary (continued)